ABSTRACT

A MINIATURE NANOSECOND SPARK SOURCE FOR FLUORESCENCE LIFETIME DETERMINATIONS AND FOR TIME-RESOLVED EMISSION SPECTROCHEMICAL ANALYSIS

By

Jacob Zynger

A high power, low duty cycle source is described for fluorescence lifetime measurements. Light pulses with a time constant of 7 to 15 nsec are produced by a coaxial capacitor, air discharge. The radiant emittance observed is approximately 10^6 W cm^{-2}. The spectral distribution of the source radiation can be shifted from the ultraviolet to the visible region by adjusting the gap length. Equations are derived to predict the light output energy and the time constant of the discharge as a function of gap length. The fluorescence lifetime of a 10^{-5} M solution of quinine sulfate was measured to demonstrate the usefulness of the source.

The spark source described above was used as an excitation source for solution analysis by emission spectroscopy. Samples are introduced into the spark source as dry salt particles which are formed by solution nebulization into a heated desolvation chamber. The spark is formed through a stream of argon that

transports the desolvated aerosol. The emitted radiation is detected with a photoelectric, time-resolved detection system which employs a gated, synchronous integrator that is controlled by a digital timing and sequencing system. The time-resolved spectral characteristics of the spark source are presented. The spark plasma is also characterized according to its electron density, the processes that govern the continuum emission, and its spectroscopic and ionization temperatures. The spark source is applied to the spectrochemical determination of Si, Mo, C, Ca, B, P, Cu, and Al. Working curves and detection limits are presented, for these eight elements, obtained using time-slicing and time-resolution. It is shown that time resolution enhances the sensitivity. The detection limits obtained are critically compared to the sensitivities obtained by other spectrochemical techniques. The detection limits obtained are all in the sub-PPM range.

A MINIATURE, NANOSECOND SPARK SOURCE FOR FLUORESCENCE LIFETIME DETERMINATIONS AND FOR TIME-RESOLVED EMISSION SPECTROCHEMICAL ANALYSIS

By

Jacob Zynger

A THESIS

Submitted to
Michigan State University
in partial fulfillment of the requirements
for the degree of

DOCTOR OF PHILOSOPHY

Department of Chemistry

1973

To my wife Doris and
two daughters Karen
and Linda

ACKNOWLEDGMENTS

The author would like to begin by expressing his gratitude to Michigan State University for providing him with financial aid, in the form of teaching and research assistantships, and laboratory facilities. He would like to acknowledge the excellent technical assistance given him by Mr. Charles Hacker of the Chemistry Department's Machine Shop, and Mr. Martin Rabb and Mr. Ron Hass of the Chemistry Department's Electronic Shop.

He would also like to express his gratitude to the members of his research group. To Dr. Gene Palermo for being the marvelous guy that he is, to Ed Glass for continuing the work that I have started with the same enthusiasm, and to the entire group, past and present, for providing much helpful discussion and many good times.

To Dr. Stan Crouch, the author would like to express his sincerest thanks, for his guidance and for the confidence he instilled in the author. Thanks also go to Dr. Andy Timnick for acting as the dilligent second reader of this work.

He would also like to thank his wife for "typing"? this work and putting up with the author's absence night after night.

TABLE OF CONTENTS

LIST OF TABLES

LIST OF FIGURES

Figure Page

PART I

VERSATILE, HIGH INTENSITY, NANOSECOND LIGHT SOURCE FOR FLUORESCENCE LIFETIME MEASUREMENTS

I. INTRODUCTION

A knowledge of the transition probability for electronic transitions of atoms and molecules is of great importance in analytical chemistry. When a species in state 1 is illuminated with a pulse of radiation, the species is excited to state 2 and may then decay back to state 1 with the emission of radiation. The decay process can be expressed for a simple exponential decay as:

$$N_t = N_0 \exp(-t/\tau) \qquad (1)$$

where N_t and N_0 are the excited state populations at time t and 0, respectively, and τ is the mean lifetime of the excited state. The decay time (τ) is, therefore, the time required for N_t to equal N_0/e. The transition probability $A_{2\rightarrow1}$ for this process is then the reciprocal of the decay time.

The transition probability or the fluorescence lifetime can be used to predict the absorption coefficient of a sample of interest. Throughout the years, τ has been used for the study of quenching effects, self-absorption of radiation, and quantum efficiency determinations. The decay time has also been used by many workers to correlate theoretical calculations with experimental observations.

Experimenters have, however, been hampered in the application of lifetime data because lifetimes, particularly those of atoms,

are generally known to an accuracy of only about 50%. The major limitation, in the accurate determination of fluorescence decay times, until recently, was that instrumentation with the required resolution time on the order of one nanosecond (nsec) was not available. The other limitation has been in the availability of an excitation source which was capable of producing reproducible, intense and fast light pulses.

Within the last ten years, the problem of the availability of fast instrumentation has been overcome with the development of accurate, and relatively inexpensive sampling oscilloscopes. However, the sampling oscilloscopes require input currents in the range of 1 - 100 mA. If reasonably high gain photomultiplier tubes are to be used as radiation transducers and if a wavelength dispersing device must be used, the fluorophor will have to emit intense radiation if the fluorescence decay is to be observed on the sampling oscilloscope. Since the emission intensity by the sample is directly related to the intensity of the excitation source, over the absorption band of the sample, intense, reproducible, and fast light sources are needed for precise and accurate measurements.

Excitation sources which are used for lifetime determinations have been described in the literature. However, many of the sources previously described have associated with them the drawbacks of low radiant powers, sometimes as low as a few watts, relatively long pulse durations, often 20 nsec or longer, or the generation of radio frequency noise by the discharge itself. This latter disadvantage may prevent the use of electronic circuitry

for data acquisition and processing in the immediate vicinity of the source, unless extensive shielding steps are taken.

To overcome the aforementioned problems, a new, high intensity, nsec light source has been developed. The source is an air spark discharge which produces pulses of continuous radiation over the wavelength range 200 to 500 nm. The output pulse decays approximately exponentially with a time constant which can be varied from 7 to 15 nsec. The radiant power of the source is on the order of 10^4 watts per flash.

The usefulness of the source is further enhanced because the light can be easily collimated, being localized over a luminous area of 10^{-2} cm^2. Hence, a radiant emittance on the order of 10^6 $W\,cm^{-2}$ is observed. The lamp is designed for maximum versatility. The electrodes are removable and can be replaced in a few minutes when necessary. The gap spacing is variable within limits, which gives some control over the breakdown voltage and the time constant. The lamp is designed to produce minimal r.f. noise, and electronic circuits can consequently be operated only a few feet away.

The source can be characterized by a mathematical expression relating discharge current to electrical parameters. Electrical characteristics of the source were measured and are described.

To gain a better understanding of the performance, so that operating conditions for the spark source could logically be optimized, the spectral characteristics both by time-integrated and time-resolved methods of observation were obtained and are described.

II. HISTORICAL

A. Introduction

Einstein (1) in 1917 derived the fundamental equations describing the transition probabilities for induced absorption and emission and that for spontaneous emission of radiation. Using the notation of Mitchell and Zemansky (2), we can describe the probability $A_{2\rightarrow 1}$ of spontaneous emission (fluorescence), from an upper state 2 to a lower state 1, by:

$$A_{2\rightarrow 1} = \frac{1}{\tau} = \frac{8\pi g_1}{\lambda_0^2 g_2 N} \int K_\nu \, d_\nu \qquad (2)$$

where τ is the decay time, g_1 and g_2 are the statistical weights of states 1 and 2, respectively, λ_0 is the wavelength of maximum absorption, $\int K_\nu \, d_\nu$ is the integrated absorption coefficient over all wavelengths, and N is the number of atoms per cc. Equation 2 is valid only when the refractive index (n) of the medium is unity. Lewis and Kasha (3) modified Equation 2, to account for the refractive index of the medium, which surrounds the absorbing atoms or molecules. For refractive indices different from unity, the right hand side of Equation 2 is multiplied by n^2. In the derivation of Equation 2 it was assumed that the absorption band was sharp, and that the fluorescence occurs at the same wavelength as the

absorption. This means, in general, that the equation is strictly applicable only to atomic transitions.

Strickler and Berg (4) modified Einstein's equation and obtained a relationship which was valid for broad molecular bands when transitions were strongly allowed. They evaluated the theoretical relationship by comparison of calculated decay times to experimentally determined decay times for a series of aromatic compounds.

B. Analytical Utility of the Fluorescence Decay Time

The accurate determination of the fluorescence lifetime of atoms and molecules is of fundamental importance in analytical chemistry. The decay time (τ) through the use of Equation 2, relates directly to the absorption coefficient of a sample and hence to the absorption intensity of a measurement. Also, one of the easiest methods of obtaining information regarding the effect of quenching of foreign species upon the fluorescence radiation, is to monitor the decay time as a function of foreign gas concentration. Brus (5) using this approach, studied the effect of halogen pressure on the lifetime of the Na(3^2P) state produced by far-u.v. photodissociation of NaI. He was able to derive empirical relationships for the quenching reactions of I_2 and Br_2 on the emission from Na. His calculations were based, however, on a knowledge of the natural radiative lifetime of the Na(3^2P) state, which he obtained from the measurements of Kibble, et al. (6) who had

studied the effect of self-absorption of Na. Kibble and co-workers were able to show, by monitoring the decay times for various concentrations of Na, produced by a Na vapor lamp, that the experimental data agreed quite well with Milne's (7) theory of radiation trapping. They also showed that at concentrations of Na below about 10^{11} atoms/cc no self-absorption was observed. Under these conditions, a constant natural radiative lifetime (τ) of 16.3 nsec was determined. At higher concentrations, self-absorption led to a rapid increase in the measured decay time. Hence, by measuring decay times, one can study the extent of self-absorption through the application of Milne's theory.

Another example of the necessity for accurate fluorescence lifetime data arises from the work done by Winefordner and Vickers (8) who placed atomic absorption spectroscopy on a mathematical basis. Their calculated limits of detection require a knowledge of the transition probabilities of the excited atomic states. Parsons and McElfresh (9) attempted to correlate experimentally observed detection limits to the theoretical limits of detection by solving the equations proposed by Winefordner and Vickers (8). This comparison was, however, greatly hampered by the inaccuracies in the transition probabilities. These were obtained from tables of Corliss and Bozman (10), who reported that the transition probabilities could have uncertainties of 50% or more.

Few workers have recognized the possibility of using the decay time, which is a fundamental property of each compound, as a "handle" for qualitative identification. Winefordner and co-workers

(11, 12) have already demonstrated the analytical utility of obtaining the phosphorescence lifetimes of structurally similar molecules which possess identical excitation and emission spectra. They were able to detect individual components in a mixture of halogenated biphenyls down to 10 ng, and they showed that not only could one obtain quantitative information, but also it was possible to identify components with the assistance of the species phosphorescence lifetime. Similarly, Birks, et al. (13) have shown that a series of mono-methyl-1, 2-benzanthracene compounds possessed radically different fluorescent decay times. It would, therefore, seem quite possible to obtain qualitative information for a series of structurally similar compounds based on fluorescence lifetimes. Quantitatively, Struder, et al. (14) were able to obtain reproducible decay times and to detect quinine sulfate at concentrations as low as 5×10^{-9} M.

Analytical applications of fluorescence lifetimes have, however, been quite limited. This is due in part to the difficulty inherent in the instrumentation which is required to measure decay times on the order of 100 nsec or less. And, since the fluorescence intensity is linearly related to the excitation intensity, the major difficulty has been the lack of a high power, short duration light pulse with which to excite the sample.

C. Methods for Obtaining the Fluorescence Decay Time

There are three basic methods used for the measurement of the fluorescence decay time. The first method is basically an

indirect approach where one obtains the decay time by measuring something other than τ, while the other two are direct methods.

1. Indirect Methods

Füchtbaüer and co-workers (15), who were the first to use the indirect approach, obtained τ for Hg by measuring the integral of the absorption coefficient as a function of frequency. The decay time τ was then obtained by applying Equation 2. The authors placed Hg in a cell maintained at 18°C and then exposed the vapor to a continuum source from which the Hg vapor absorbed the 253.7 nm radiation. The transmitted radiation was then observed by a spectrograph. The major difficulty associated with this method of measuring τ is the narrowness of most resonance lines (16, 17). It is obvious that, if one is to obtain the true shape of the absorption line, the bandpass of the spectrograph must be smaller than the absorption line half-width. Füchtbaüer and co-workers found, therefore, that it was necessary to work only with very broad absorption lines which were obtained by introducing a foreign gas at very high pressure into the Hg absorption cell. The high pressure, foreign gas caused Lorentz broadening. Data were obtained as a function of foreign gas pressure and extrapolated to zero pressure. In this manner a value of τ equal to 1.0×10^{-7} sec was obtained for the 253.7 nm Hg line. The main error in this method, which is otherwise simple, is the need for extrapolation to zero foreign gas pressure. Also, this method seems applicable only to fairly volatile elements.

Another early method used for involatile elements consists of measuring the intensity of the resonance emission by aspiration of a salt of the element of interest into a flame. Assuming that thermodynamic equilibrium exists, and then combining Boltzmann's distribution with Equation 2, one can obtain the decay time from the following equation:

$$I = \frac{Nhcg_1}{\lambda_0 \tau g_2} \exp(-E/kT) \qquad (3)$$

where I is the absolute emission intensity, h is Planck's constant, c is the speed of light, k is Boltzmann's constant, T is the temperature, E is the energy difference between the ground and excited state, and N is the population of ground states atoms. Van der Held and Ornstein (18) used this method to obtain a decay time of 1.6×10^{-8} sec for the Na doublet.

The major limitation in the resonance emission method is that it requires an absolute measurement. Therefore, the experimenter is required to know both I and N accurately. This assumes that he knows both the degree of vaporization and the extent of atomization of the salt solution in the flame. These values are known only to an accuracy of 50% (9), which would, therefore, limit the accuracy of τ to the same uncertainty. Another limitation of this method, is the assumption that thermodynamic equilibrium exists in the flame. Workers (19) have found that complete thermodynamic equilibrium does not exist and, therefore, one cannot characterize the flame by a single temperature. As discussed above, absolute

indirect methods used for obtaining τ can lead to quite large inaccuracies.

Corliss and Bozman (10) used a relative, indirect method for tabulating the transition probabilities of 70 elements. They obtained line intensities for a large number of spectra, all measured under the same conditions with the same source, a 10 A, 220 V DC arc between copper electrodes. They, also, made use of Equation 3. However, since N was not known on an absolute basis, a calibration was made with "known" values of τ. The calibration procedure involved careful selection of τ values that had been reported in the literature. A comparison was then made for 37 determinations obtained in the arc against absolute data obtained by various authors. Having performed this laborious procedure, the authors obtained transition probabilities for 25,000 lines with an accuracy of 10% to 100%.

Because indirect methods do not yield decay time data with the degree of accuracy that is desirable, direct methods for determining τ have gained in popularity. These methods are discussed in the section that follows.

2. Direct Methods

a. Modulation fluorometry

Two direct techniques are used for the measurement of τ. The first method, introduced by Gaviola (20) in 1926, is that of modulation fluorometry. The fluorescence is excited by continuous uv-visible radiation whose amplitude modulates a high frequency

carrier. The fluorescence waveform is compared with the waveform of the radiation and the decay time is then obtained directly.

The earliest method of modulation was introduced by Gaviola (21). In his instrument, modulation of a carrier by the source was achieved by allowing linearly polarized light to pass through a Kerr cell. The intensity of the light transmitted was then only a function of the voltage applied to the Kerr cell, and, therefore, the Kerr cell acted as a fast optical shutter.

Over the years, improvements have been made on the original system (6, 21). The apparatus is restricted in its usefulness, however, by the properties of the Kerr cell. Suitable cell materials (e.g., nitrobenzene) with a high Kerr constant limit excitation and observation to the visible region since most such materials absorb strongly in the ultraviolet. Kerr cells also possess low optical speeds with switching times of typically 20 nsec.

Improved electro-optical modulators have been developed using the Pockels effect. Müller, et al. (22) described a fluorometer which employed a Pockels cell for modulation. The spectral range of the modulated radiation was between 200 to 1000 nm with little jitter in the switching times. However, they found a crucial dependence of the degree of modulation on the frequency of the incident radiation.

Another method of modulation involves the application of the Debye-Sears effect (23) wherein a series of ultrasonic standing waves is produced in a liquid such as water. When excited at about

10^6 Hz, the change in refractive index due to the waves in the liquid causes it to behave like an optical diffraction grating, since the stationary wavelength is about 10^{-4} cm. A modulated signal is then observed in its zeroth or higher order. Maercks (24) designed a fluorometer wherein the periodic build up and collapse of the standing wave pattern in a water-filled cell, was controlled by a quartz crystal oscillator. Light in the zeroth order was found to modulate the wave by about 80%.

The detection system commonly used with the ultrasonic modulator is quite complex. It involves allowing the radiation to fall on two sample cells, one containing a reflecting material and the other containing either a reflecting material or a fluorescent substance. Two photomultipliers are used to detect the radiation from the two cells. The radiation from the fluorescent substance is at the same frequency as the reflecting radiation, but is shifted in phase because of the exponential decay of the fluorescence. Thus, the detection system measures the phase difference between the two light beams. The phase shift can be readily related to the decay time (25). Using this procedure, Bailey and Rollefson (26) found the decay time of quinine sulfate to be 22.8 nsec.

The ultrasonic modulation technique, although accurate (Butler and Norris (27) claim time resolutions of 0.2 nsec and a 15% error), is severly limited in that the fluorescence decay must be a simple exponential function. This would lead to large inaccuracies if a complex mixture were to be analyzed by means of decay times. Another potential source of error, which must be borne in

mind, is that the emission lines used for excitation may themselves differ in phase. Also, the method is particularly sensitive to the presence of scattered light, which reduces the apparent lifetime. Other disadvantages of the system include, the high cost, the necessity for multiple detection systems, and the requirement of very careful standardization of the timing and demodulation systems.

b. Plused fluorometry

In the pulsed fluorometric technique, the sample is excited by intermittent energy pulses of short duration, and the fluorescence decay is observed directly during the intervals between the excitation pulses. This method requires a high power pulsed source which cuts off in a time shorter than the fluorescence lifetime and a detection system with a fast rise time.

The first direct observations of fluorescence decay in the nsec region used pulsed electron beams for excitation (28). The procedure uses a short duration pulse of low energy electrons to excite gaseous atoms.

Since the work of Heron, et al. (28), various radioactive emission sources have been used for scintillation and fluorescence lifetime determinations. Falk and Katz (29) used alpha particles and x-rays for the study of the scintillation behavior of stilbene and anthracene. Carlo, et al. (30) used a unique excitation source which consisted of ^{252}Cf undergoing spontaneous fission. They were able to obtain fluorescence decay times for the nitrogen first negative group and the nitrogen second positive group.

The major problem with using radioactive sources is their nonspecificity. Therefore, a large amount of energy is given to the sample that could produce ionization or dissociation of the sample. Another problem associated with radioactive sources is the randomness with which the sample is excited, due to the randomness of the radioactive process. Because of the nonspecificity and the randomness associated with radioactive sources, workers have used them quite infrequently. The most common means of excitation is the pulsed light source whose time of emission is electronically controlled.

The existing sources which emit short duration pulses in the uv-visible region can be divided into the following categories: (1) flash tubes, (2) p-n junctions pulsed by reverse current, (3) lasers, (4) discharge lamps, and (5) spark gaps. Flash tubes, while capable of emitting up to 5 megawatts of radiant power, are severely limited in their use as an excitation source for fluorescence lifetime determinations because the time constant of the discharge circuit is on the order of 1-10 μsec.

Whetstone (31) studied the radiation emitted by a reversed biased silicon p-n junction. He found that the junction emitted about 45,000 photons over the wavelength range of 250-700 nm, when it was pulsed with a 9 A current pulse of short duration. His value corresponds to about 1 μW of radiant power emitted per pulse, with an on-time of less than 2 nsec. The junction is, therefore, at the other extreme relative to the flash lamp. It has a very short on-time but very low intensity. Since fluorescence intensity is

directly related to excitation intensity, the p-n junction can hardly be used as an excitation source.

Broida and co-workers (32, 33) were the first workers to apply a pulsed laser as an excitation source for fluorescence lifetime measurements. They studied the lifetimes of the vibrational levels of I_2 and formaldehyde. Excitation was with a tunable dye laser pumped with a pulsed N_2 laser. The dye solutions emitted powers on the order of 1-5 kW, over a 10-50 nm spectral bandwidth, with a pulse length of about 10 nsec full width at half-height (FWHH).

There are two serious problems associated with using a laser as an excitation source. The first is that, at present, the output pulses are not reproducible to better than 5%. This can, however, be overcome by selecting only those pulses which fall within some preselected intensity range. The second serious problem is the large amount of electrical noise that is generated by the pulsed laser. This latter problem cannot be overcome and it necessitated that Broida and co-workers move the laser to a room adjacent to and electrically shielded from the fluorescence cell and the detection apparatus. The problems mentioned above, coupled with the high cost of the excitation system, makes the laser unattractive at present as an excitation tool.

One of the most common excitation sources is the discharge lamp. It was introduced by Malmberg (34) and first used as an excitation source for the fluorescence lifetime determination of chloropyll by Brody (35). Malmberg's source basically consists of a pyrex tube

filled with H_2 at a pressure of 10 torr. Enclosed within the tube are two needle shaped tungsten electrodes pointing toward each other. The distributed capacitance, which is simply the stray capacitance between the two electrodes, is charged from a high voltage DC power supply (2-4 kV) through a current limiting resistor, whereupon the lamp flashes. The process is then repeated at a repetition rate, determined by the power supply and the resistor, typically 10 kHz. Light flashes are then obtained with a FWHH of less than 1 nsec. Brody's fluorometer consisted of the H_2 lamp for excitation, an emission filter for wavelength isolation and a photomultiplier tube connected to a traveling wave oscilloscope, which was triggered by the light from the lamp, for detection. He then obtained the fluorescence decay time directly from the oscilloscope display.

Berlman, et al. (36) studied H_2 and D_2 lamps in greater detail and found that about 4×10^8 photons were emitted per flash. Both Berlman and Brody studied the spectral distribution of the lamp and found that the source emitted a broad continuum extending from the ultraviolet to the infrared regions of the spectrum. They also observed considerable intensity contributions from singly and doubly ionized hydrogen molecules as well as emission from hydrogen atoms.

Various improvements have been made on the original Malmberg design. D'Alessio and co-workers (37, 38) placed H_2 in a cell at a high pressure of 18 atm and improved the lifetime and stability of the lamp by wetting the electrode with Hg. They were able to increase the radiant output slightly to about 4×10^9 photons per

pulse with a pulse width of about 0.5 nsec FWHH. The firing system that they employed was similar to that used by Malmberg in that the lamp, in combination with the current limiting resistor and its stray capacitance, formed a relaxation oscillator. The lamp designed by the above authors was used by McIntosh (37) for the determination of the fluorescence lifetime of perylene and rubene.

Yguerabide (40) studied nanosecond lamps designed along the lines proposed by D'Alessio. He found that light pulses of less than 1 nsec FWHH could be obtained for an H_2 lamp at a pressure above 10 atm and they seemed to be unaffected by variations in gap width between 0.1-0.6 mm. The radiant power was found to increase both with gap width and pressure due to the higher breakdown voltage, which caused a larger amount of energy to be stored in the stray capacitance. He also found that lamps filled with a variety of different gases could be made to produce radiant energy with a FWHH of less than 1 nsec. He concluded that in a relaxation firing circuit, the lamp must be operated at high pressure and with a minimum of capacitance to obtain short pulses.

Pollack and co-workers (41) increased the radiant output from the Malmberg type Lamps by applying a voltage greater than the breakdown voltage of the lamp through a thyratron controlling switch. They were able to increase the radiant output to a few watts. However, it was found that the pulse width increased. They were able to vary the on-time simply by varying the distance between the electrodes.

Workers, using either the free running or the gated flash lamp as an excitation source, have been forced, due to the very low intensity of the incident radiation, to use a detection system based on single-photon counting. The underlying principle of the single-photon technique for decay time measurements is basically statistical sampling (42). Excited samples have decay-time spectra that closely resemble an exponential function. Hence, the highest probability of emission, or the highest observed rate of emitted photons, will occur immediately after the sample has been excited by a source whose on-time is much smaller than the sample's decay time. Thereafter, the probability of emission will decrease exponentially with time.

The unique feature of the single-photon technique is the measurement of the time of emission of individual fluorescence photons with the reference time zero being the initial rise time of the flash lamp. To accomplish this, the fluorescence intensity must be kept low so that individual photons do not overlap. Photon counting rates should not exceed 1% of the firing rate (43) so that only one photon is probable for every 100 lamp firings. The time of arrival of each photon, referenced to time zero, is measured electronically by a time-to-amplitude converter and the resultant height information is stored in a multichannel pulse height analyzer. Hence, the time of arrival is encoded by the signal height, while the intensity emitted at a particular time is encoded by the number of pulses of a given height. Therefore, from a plot of the number of occurrences vs. height, the decay time can be determined.

This method, also known as the delayed-coincidence technique, has been used by a variety of authors (6, 44-46), and is quite useful for samples with decay times on the order of 2-20 nsec. Samples with longer decay times are inherently weaker emitters in time, and hence the single-photon technique can take hours and sometimes days to accumulate enough photoelectron pulses for a statistically significant decay curve. Also, since the intensity of fluorescence is directly related to the incident intensity, an excitation source capable of yielding greater radiant power would be preferable. The popularity of the delayed-coincidence technique can be partly attributed to the fact that commercially available instrumentation exists (47).

With a more intense source, the experimenter would not be required to use the delayed-coincidence method. He would then be able to use a direct observation system such as a sampling oscilloscope. And, higher signal-to-noise ratios would be obtained because it would not be necessary to mask the fluorescence signal to the point at which only one photon is probable out of every 100 incident flashes.

The need for a more intense nsec light source has prompted workers to study the usefulness of the spark discharge. Sparks have been used for the production of light flashes of a few μsec duration to study rapidly moving objects by high speed photography since 1852 (48). More recently, Beams, et al. (49) designed a spark source which was capable of producing radiant energy pulses of 100 nsec duration. The source consists of a conventional spark gap operating

in air at atmospheric pressure. The source is driven by a pulsing circuit capable of supplying high currents for a short time. The on-time of the radiant output pulse was determined by the length of the transmission line which acted to charge the spark gap.

McMahon and co-workers (50) designed a spark source with an intensity of 10^5 W over the wavelength range 220-700 nm. Their spark was formed between two pointed tungsten electrodes operated in a variety of gases, usually N_2, with a fixed gap spacing of about 2 mm. To obtain the high intensity, an energy storage capacitor was placed directly across the spark gap. The capacitor and the stray capacitance of the gap were charged from a high voltage DC power supply through a current limiting resistor. When spark breakdown occurred, the capacitor discharged and gave rise to the large pulse of radiant energy observed. However, because of the large inductance associated with the external capacitor, the half-widths of the output pulses which depend on the capacitance and the inductance, were on the order of 20-350 nsec. The authors showed, that to obtain radiant powers which were four or more orders of magnitude greater than that from conventional flash lamps, an external capacitor was needed.

It is well known that the maximum energy with the shortest pulse length is delivered into a spark gap from a capacitor discharge when the inductance of the circuit is a minimum. Equally well known is the fact that the maximum energy storage coupled with the minimum inductance is achieved in a capacitor of coaxial design. Hence, the

major disadvantage of the light source designed by McMahon and co-workers (50), the long pulse length, could be easily overcome by using a coaxial capacitor for energy storage.

III. SPARK SOURCE DESCRIPTION

The usefulness of the spark as an excitation source arises not only from its increased brightness, but also from the fact that the light emanates from a small point-like volume. This then makes it rather simple to collimate the emitted radiant and hence to increase the amount of light reaching the sample. On combining all the facts presented, it would appear that a coaxial, spark-lamp (51) would represent the most reasonable choice of an excitation source for fluorescence lifetime measurements if the pulse duration could be made less than about 10 nsec. In the sections to follow, the design considerations and the experimental design for the source developed in this work are presented along with a theoretical description of the source characteristics.

A. Design Considerations

Physically, the excitation source should be designed for maximum versatility. The electrodes should be easily removable and replaceable in a few minutes when necessary. Also, the gap spacing should be made variable which would give the experimenter some control over the breakdown voltage. When these requirements are met, he would be able to control the time constant and the emission intensity of the discharge.

The lamp should be designed so as to produce a minimum of r.f. interference and also give reproducible light pulses so that the major problems associated with using a laser would be overcome. To meet these specifications, none of which have been met previously by other sources, the lamp described in the next section was constructed.

B. Physical Design

The heart of the lamp, of which a cutaway view is shown in Figure 1, is a Teflon or polyethylene tube of 0.5 mm uniform thickness extending from the BNC connection to the end of the aluminum bar. Teflon was chosen originally as the dielectric material because of its high dielectric constant (2.0), its ease of machinability, and its high breakdown voltage. It was found, however, that commercially available electrical grade Teflon, could be obtained to a purity of only 95%. Although satisfactory for initial studies, Teflon often produced lamps with irreproducible firing characteristics. Since the impurities in the Teflon caused the tube to break down at the point of the impurities, high molecular weight polyethylene (HMW-1900, Cadillac Plastics), a purer material with only slightly poorer properties, was chosen.

Polyethylene possesses a dielectric constant of 2.3, is machinable, and is available in about 99.9% purity. The breakdown characteristics of polyethylene are only slightly lower than that of Teflon.

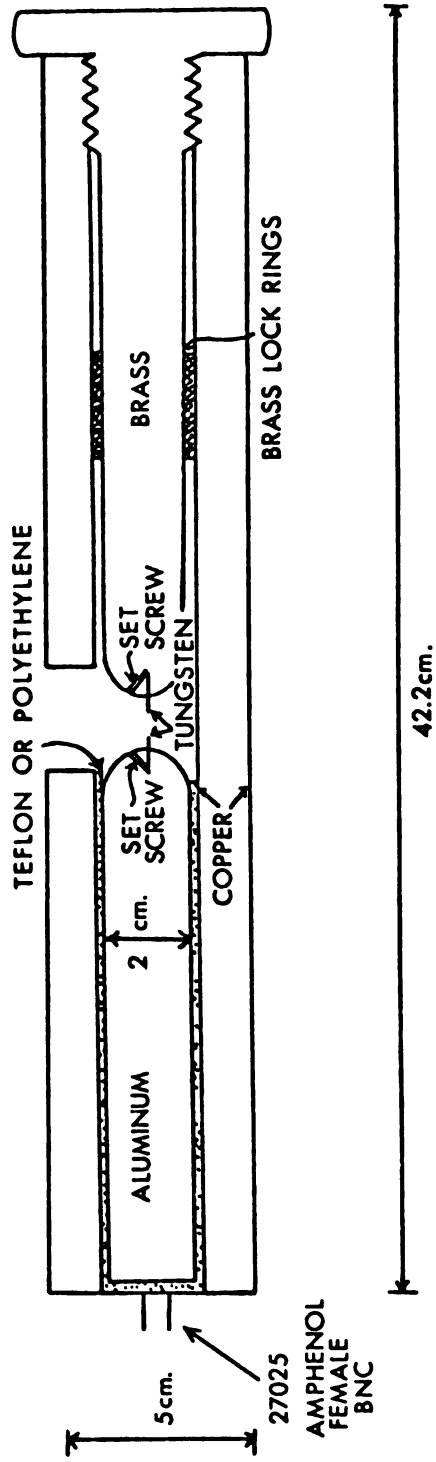

Figure 1. Original design of nanosecond spark source.

The high voltage BNC connector is threaded into the aluminum bar through a hole in the polyethylene tube. Epoxy resin was used to join components of the assembly. The polythylene forms a coaxial capacitor with the inner copper tube and the aluminum bar. The breakdown voltage of the polyethylene tube is about 13 kV. A 0.5 mm rod of tungsten, which has been ground to a point, is connected by a set screw to the aluminum bar. The spark is formed between this point and a similar piece of tungsten connected to the threaded brass rod by another set screw. After about 500,000 firings, the tungsten electrodes become pitted and must be reground and replaced. The brass is connected to the grounded copper tube by means of a variable lock-nut brass connector.

The variable lock-nut arrangement was designed to make it possible to vary both the inductance and the resistance of the spark discharge circuit and could, hence, serve as an electrical vernier. It was later found, however, that the resistance and inductance offered by the spark itself greatly outweighed the slight tuning effect obtained by moving the brass lock rings.

The metals were basically chosen for their electrical properties. Copper was chosen for its low electrical resistivity, while brass was chosen for its high resistivity. Aluminum was chosen basically because of its light weight. The outer five cm diameter copper pipe provides a very effective shield against any r.f. interference generated by the spark discharge.

The lamp is designed to have coaxial geometry for maximum energy storage with a minimum of inductance, and also for minimum

power loss in transmission. The design also allows for eacy replacement of all components in the system and for varying the spark gap length by turning the end knob shown in Figure 1. By changing the gap length, the experimenter can vary the inductance and resistance of the spark discharge and can, therefore, control the spectral output and the decay time of the light pulse. When operated within the limits of gap length to be described in the next section, a constant firing rate is obtained, and the audible noise generated is in the form of a hum. As the gap length approaches either of the limits, the discharge becomes erratic, which can easily be detected by the ear.

C. Theory of Operation

An electrical diagram of the lamp and its associated charging circuitry is shown in Figure 2. The lamp can be considered as a coaxial line capacitor C_L, which is in parallel with the spark gap. Both C_L and the spark gap capacitance C_G are charged through the resistance R_L and the inductance L_L of the line from a pulsed high voltage power supply until the voltage on both capacitors reaches the breakdown voltage V_B of the spark gap. Similarly, the capacitance of the transmission cable C_C (not shown in Figure 2) is charged to the same voltage. Conditions are arranged so that the breakdown voltage of the gap is much less than the breakdown voltage of charging capacitor C_L. Since $C_L > C_C >> C_G$ all the charge may be assumed to be stored in C_L.

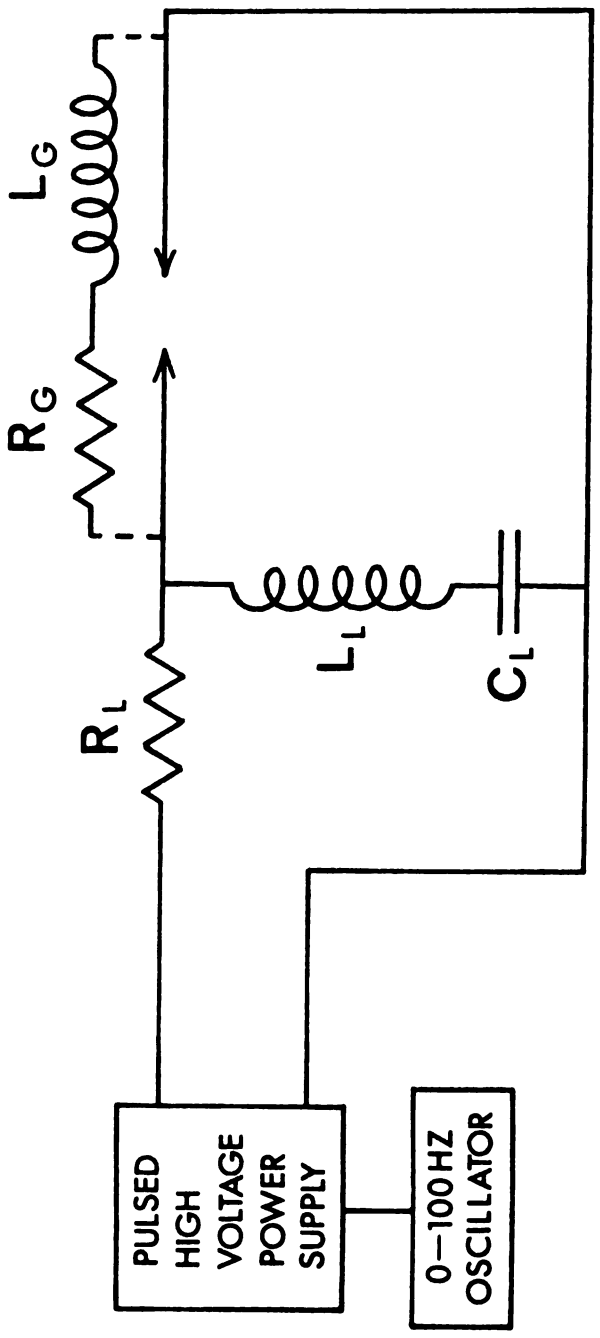

Figure 2. Simplified electrical schematic of the firing circuit.

When the breakdown voltage of the spark gap is reached, the dotted lines shown in Figure 2 represent the electrical characteristics of the spark. When the spark is formed, all the capacitors discharge through the inductance L_G and resistance R_G of the spark gap. The discharge current excites and dissociates the molecular filler gas and hence produces fast, intense light pulses. D'Alessio, et al. (37) have shown that the intensity-time profile of the light pulses produced by such discharges, in the early stages (1-10 nsec) of breakdown, is nearly identical to the discharge current-time profile. Therefore, an equation for discharge current as a function of time is used here to describe the light intensity as a function of time.

To characterize the discharge current mathematically, it is necessary to simplify the circuit shown in Figure 2. The capacitance of both the transmission cable and the spark gap can be neglected relative to C_L. Also, the individual inductances can be assumed not to interact, and can, therefore, be lumped together into an equivalent inductance L for the circuit. Equation 4 results from applying Kirchoff's voltage law to the simplified, closed-loop discharge circuit.

$$iR_G + \frac{Q}{C} + L\frac{di}{dt} = 0 \qquad (4)$$

where i is the discharge current. Differentiating Equation 4 with respect to time, dividing by L, and recognizing that dQ/dt = i, we find:

$$\frac{d^2i}{dt^2} + \frac{R_G}{L}\frac{di}{dt} + \frac{1}{C_L L} i = 0 . \qquad (5)$$

Equation 5 has the auxiliary solution

$$D = \frac{-R_G}{2L} \pm \left(\frac{R_G^2}{L^2} - \frac{4}{LC_L} \right)^{1/2} , \qquad (6)$$

where $D = {}^{di}/_{dt}$. There are three possible solutions to the auxiliary equation. The roots are either real and unequal, real and equal, or unreal. Since real and unequal roots produce rather long discharges and real and equal roots are practically impossible to obtain, this work will only deal with the solution for unreal roots, which yield results consistant with the experimental observations and which are justified later.

To solve Equation 5, the following boundary conditions are set:

a) $\int_0^\infty i\,dt = Q_{C_L} = V_B C_L$

b) at time $t = 0$, $i = 0$ and $Q_{C_L} = V_B C_L$

where Q_{C_L} is the total charge stored on C_L.
The first condition basically means that the average current during some time interval is equal to the charge stored on the capacitor divided by that time interval. The second condition simply serves as a reference for the equation, in that it specifies that at time $t = 0$, the current has not begun in the gap, while at the same time, the capacitor is fully charged.

The general solution to Equation 5 is of the form:

$$i = A \exp(\gamma_1 t) + B \exp(\gamma_2 t) \tag{7}$$

where γ_1 and γ_2 are the roots of D in Equation 6 and A and B are constants which can be evaluated from the boundary conditions. By a change of variables, it can be shown (52) that Equation 7 can be represented by:

$$i = e^{\alpha t} (C_1 \sin(\beta t) + C_2 \cos(\beta t)), \tag{8}$$

where C_1 and C_2 represent new constants introduced by the change of variables, $\alpha = (R_G/2L)$, and $\beta = \left((R_G^2 - 4L/C_L)^{1/2}/2L\right)$. If boundary condition "b" ($i = 0$ at $t = 0$) is substituted into Equation 8, it is found that $C_2 = 0$. Hence, Equation 8 becomes:

$$i = e^{\alpha t} C_1 \sin(\beta t) . \tag{9}$$

Boundary condition "a" can be used to solve for C_1 according to:

$$\int_0^\infty i\,dt = \frac{V_B C_L}{C_1} = \int_0^\infty e^{-\alpha_1 t} \sin(\beta t)\,dt \tag{10}$$

where $\alpha_1 = -\alpha$. The solution to an equation of the form of

$$\int_0^\infty e^{-ax} \sin(mX)\,dx \tag{11}$$

is given (53) as $\frac{m}{a^2 + m^2}$ for $a > 0$. Since $\alpha_1 = -\alpha$, and $\alpha = -R_G/2L$, this means that $\alpha_1 = R_G/2L$. Both R_G and L are positive values and,

therefore, $\alpha_1 > 0$, implying that the solution given for Equation 11 can be applied here. Therefore,

$$\frac{V_B C_L}{C_1} = \frac{4L^2\beta}{R_G^2 + 4L^2\beta} \quad . \tag{12}$$

Solving for C_1 yields:

$$C_1 = \frac{(4L^2\beta + R_G^2)\ V_\beta C_1}{4L^2\beta} \quad . \tag{13}$$

The solution to Equation 5 is given then by the combination of Equations 9 and 13, and is as follows:

$$i = \left(\frac{4L^2\beta + R_G^2}{4L^2\beta}\right) V_B C_L \sin(\beta t) \exp(-R_G t/2L) \ . \tag{14}$$

In general, R_G is on the order of a few ohms, L is on the order of 10^{-9} H, and C_L is order of 10^{-9} F. Hence, $\beta \sim 10^9$ and $L^2 \sim 10^{-18}$. Therefore $4L^2\beta$ is about 10^{-9}, which is much less than R_G^2. Equation 14 can thus be simplified to:

$$i = \frac{R_G^2 V_B C_L}{4L^2\beta} \sin(\beta t) \exp\left(-\frac{R_G t}{2L}\right) \ . \tag{15}$$

Equation 15 describes the current and, at the same time, the radiant intensity as a function of time.

To find the time at which the current, or radiant intensity, reaches its maximum value, Equation 15 can be differentiated with

respect to time and set equal to zero. If this is done, the following results:

$$t_m = \frac{1}{\beta} \arctan \left(\frac{2L\beta}{R_G}\right), \tag{16}$$

where t_m represents the time at which the discharge current reaches its maximum value. The arctan term can be expressed as a series as follows:

$$t_m = \frac{1}{\beta} \sum_{n=1}^{\infty} \frac{(-1)^{n+1}\left(\frac{2L\beta}{R_G}\right)^{2n-1}}{2n-1} \quad . \tag{16}$$

Equation 17 results from simplification of Equation 16.

$$t_m = \frac{2L}{R_G} \sum_{n=1}^{\infty} \frac{(-1)^{n+1}\ (2L\beta)^{2n-2}}{(2n-1)\ R_G{}^{2n-2}} \quad . \tag{17}$$

Equation 17 gives the time at which the radiant intensity reaches its maximum value and hence describes the "rise-time" of the radiant pulse. Note, that when n=1 in Equation 17, t_m is simply given by $2L/R_G$. The series in Equation 17 converges only if $R_G^2 > 2L/C_L$. When $R_G^2 > 2L/C_L$, Equation 17 reduces to:

$$t_m = 0.95 \left(\frac{2L}{R_G}\right) \quad . \tag{18}$$

If the series is nonconvergent, it would represent a physically unreal condition wherein the discharge current never reached a maximum value. Therefore, conditions must be arranged such that

$R_G^2 > 2L/C_L$. Since $4L/C_L > R_G^2$, which arose from the assumption of unreal roots, the operating conditions of the lamp are given by:

$$\frac{4L}{C_L} > R_G^2 > \frac{2L}{C_L} . \tag{19}$$

Operation within the limits given by Equation 19 corresponds experimentally to gap spacings of between 1.0 and 5.0 mm which yield pulse decay times varying from 7 to 15 nsec.

IV. EXPERIMENTAL

A. Instrumentation

To pulse the spark source repetitively, a square wave (0-100 Hz) from a Heath Company model EU-81A or a Wavetek model 116 function generator was used as the trigger for a Xenon Corporation model 437 Nanopulser power supply. This supply produces pulses of approximately 8 kV which were used to fire the lamp. Upon receipt of a trigger command from the function generator, the power supply discharges a 15 μF capacitor bank that is initially charged to about 100 V. The discharge current path is through an induction coil which produces a back e.m.f. equal to its inductance times the rate of change of the current. The back e.m.f. is a high voltage spike which charges the parallel coaxial and spark gap capacitors, until the voltage across the spark gap reaches V_B. Thereupon, the spark acts in the manner described in the previous section.

To detect the radiation emitted from the spark gap, the observation system consisted of a Heath model EU-700 scanning monochromator and a Heath model EU-701-30 photomultiplier module which contained an RCA 1P28A photomultiplier tube (S5 response). The dynode chain of the photomultiplier tube was modified by connecting capacitors, in a series mode (54), of 0.005 μF, 0.005 μF, and 0.001 μF on the last three dynodes of the photomultiplier tube, respectively. Capacitors of 1 kV rating were used and these were

connected directly on the resistor string located at the socket of the tube to minimize inductive effects. The capacitors were required to supply the high peak current in the photomultiplier during the radiant pulse. Hence, the modified dynode chain allows a large peak current output while at the same time it stabilizes the interelectrode voltage on the dynode chain.

The anode of the photomultiplier tube was connected with 50 Ω cable to a Tektronix 564 storage oscilloscope with 3S1 and 3T2 sampling plug-ins. The 3T2 time base of the oscilloscope was triggered either internally by the radiant pulse itself or externally by the sync. pulse supplied by the function generator. It was found that better triggering could be obtained when operated in the internal mode. Data were obtained either from photographs taken of the oscilloscope screen or by connecting the output of the 3S1 sampling amplifier to a minicomputer. The interface between the system and the computer is discussed in Section C.

B. Light Source Holder

Since the control over the electrical characteristics offered by the "vernier" assembly shown in Figure 1 was minimal, it was decided to reduce the length of the brass grounding bar to 6 cm so that the spark source would be easier to handle. To collimate the emitted radiation from the spark, a fused silica, bi-convex lens of 2.54 cm focal length and 2.54 cm diameter (Esco Optics) was mounted in a lens holder which was located so that the spark was at the focal plane of the lens.

For precise positioning of the source it was mounted in a holder, whose construction details are shown in Figure 3. The holder was mounted directly on the Heath spectrophotometer base and thus offers the experimenter a three dimensional control of the radiation output relative to the monochromator entrance slit, as well as radial control of the emission beam.

C. Computer Interface

In order to obtain information that was needed to characterize the light source, it was decided to interface the instrument described above to a PDP-Lab 8/e minicomputer. Two different interfaces, coupled with two different programs, were designed. One was used for current integration, while the other was used to obtain time-resolved spectra.

1. Interface for Time Intergration and Reproducibility Measurements

In the characterization stage, a need arose to check the reproducibility of the radiant pulses from the source. It was, therefore, decided to integrate the current obtained from the photomultiplier tube (PMT) over the effective on-time (100 nsec) of the lamp. A conventional amplifier cannot be used for this purpose due to the short times involved. Therefore, the sampling oscilloscope was used. It would have been possible to perform the reproducibility check by comparing photographs of the oscilloscope screen. To avoid the tedium associated with photographic methods and to increase the

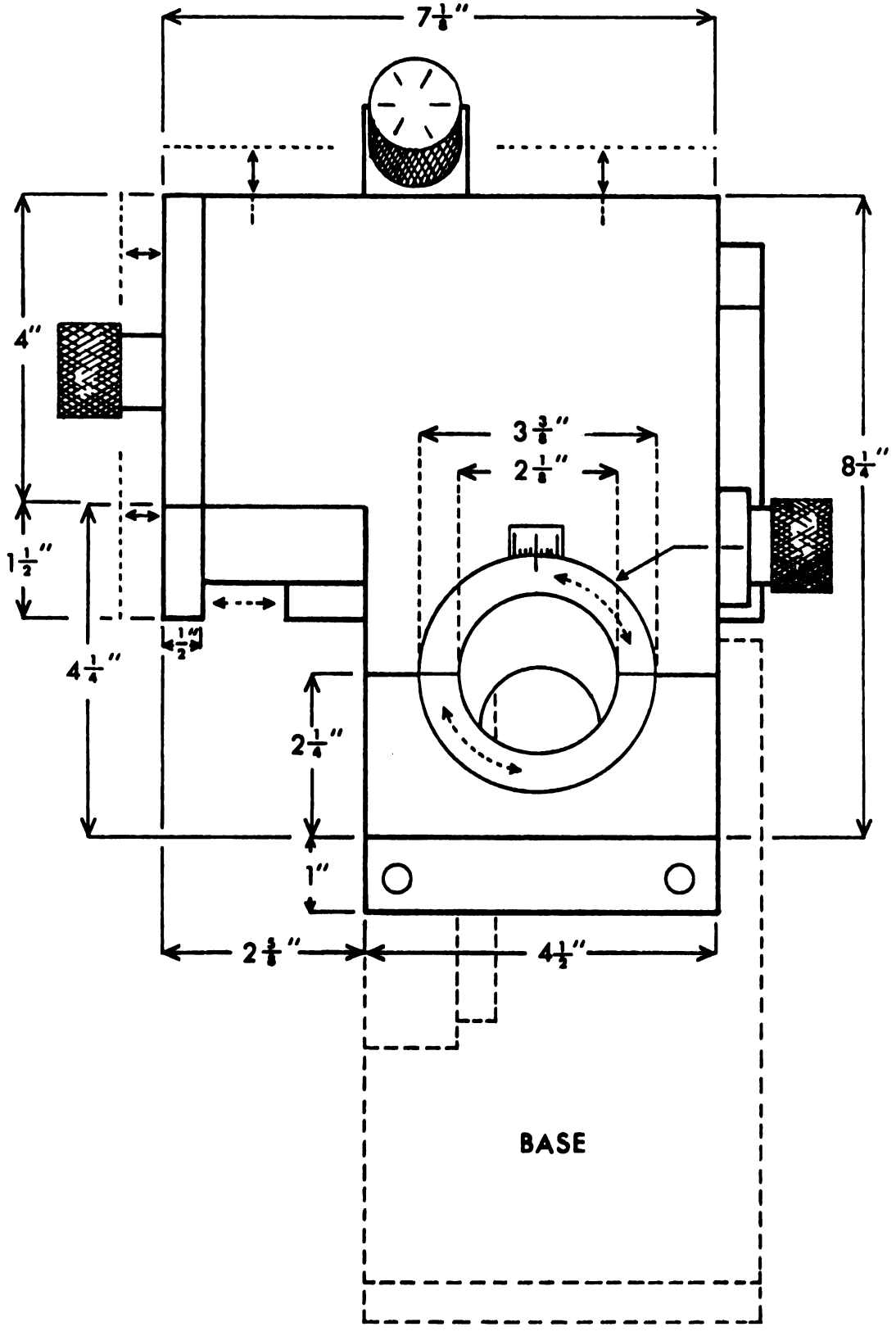

Figure 3. Construction details of light source holder.

precision of the measurements, digital integration of the radiant pulses was performed by the computer.

The interface and the flow chart of the program for digital integration of the radiant pulse over some preselected time interval is shown in Figure 4. To initiate the program, the number of time-windows (the number of sweeps across the oscilloscope screen) to be integrated, and the number of points to be taken over that time window are selected. Generally, ten time-windows (runs) of 1000 points per run were chosen. The number of points per scope-screen was set internally on the oscilloscope (55) at 100 points per division.

Schmitt Trigger 4 (ST4) fires when the voltage on the sweep output line has returned to zero. When it fires, it implies that the oscilloscope's time base has returned to the starting point in time which is the beginning of the sweep across the face of the scope.

Data are then collected at a rate determined by the firing frequency of the lamp, until the preset number of points is collected. Once ST4 has fired, the computer then waits for ST1. Once ST1 fires, it signifies that the lamp has fired and that a voltage corresponding to the radiant intensity at that instant in time is available at the output of the 3S1 sampling amplifier. The computer then delays for 100 μsec, to allow the amplifier to settle to its final value, and then the voltage from the amplifier is converted by the analog-to-digital converter (A/D) and stored in the computer. The value of the point stored in the computer, then represents the

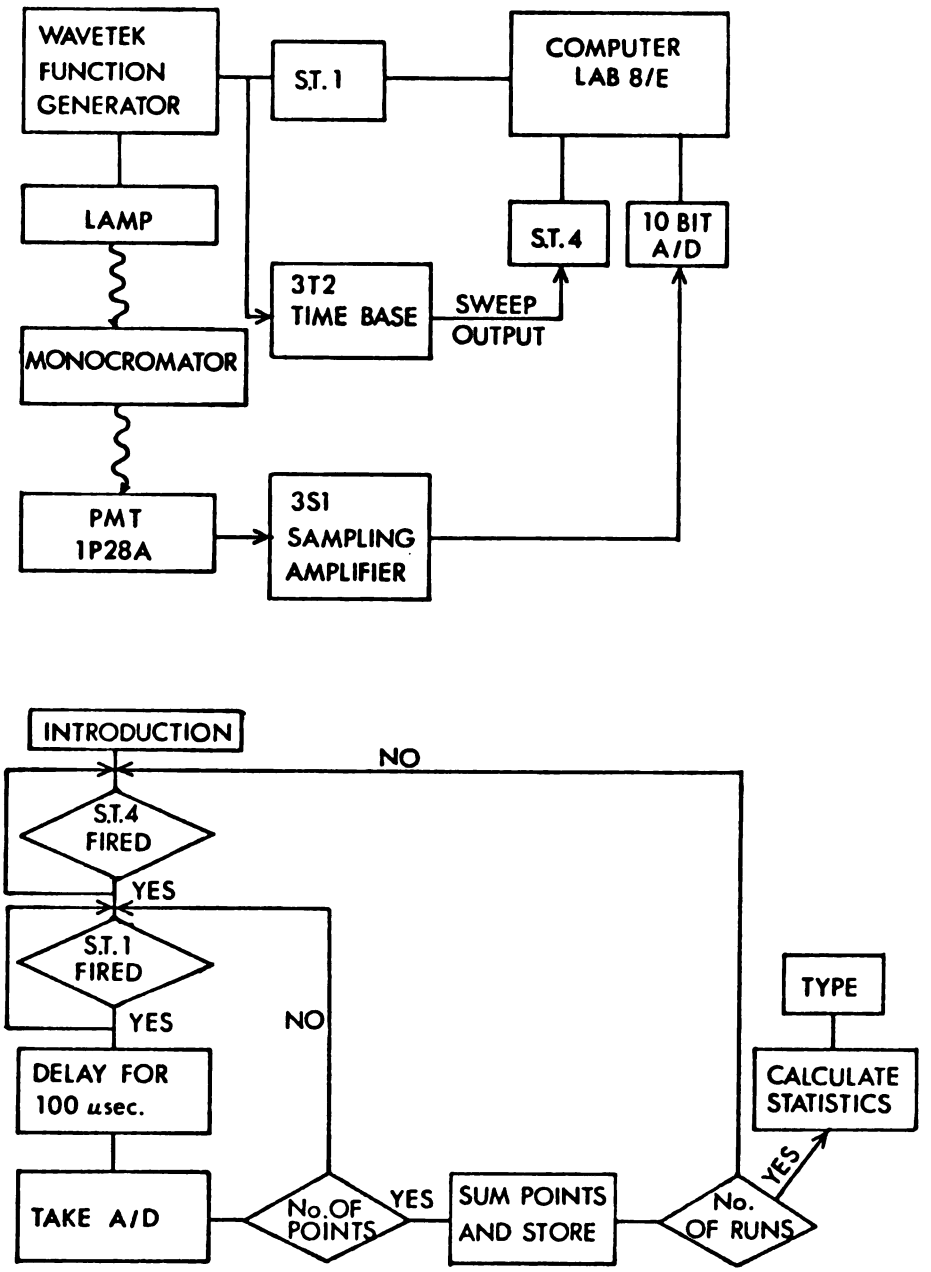

Figure 4. Block diagram of the hardware and program flow chart for time integrating.

intensity of the radiant pulse, over the bandpass of the monochromator, at the instant of time bounded by the 350 psec integration time of the 3S1 sampling amplifier (56). The time base is then stepped to its next position in time, and the process is repeated until the correct number of points is obtained. The data points are then summed and stored. This value then represents a single run. The integrated, sampled points thus obtained represent the intensity of the radiant pulse. Since the integration time of the amplifier is 350 psec, 1000 points obtained over a 100 nsec time-window correspond to a complete integration of the signal because data points are taken which are spaced by 0.1 nsec which is smaller than the integration time of the amplifier. The process then continues until the correct number of runs has been obtained. The runs are then averaged and the standard deviation (S.D.) and the relative standard deviation in percent (R.S.D.) are calculated and reported.

The system described was used to check the reproducibility of the light pulse over a 100 nsec time interval at various wavelengths. The R.S.D. was found to be independent of wavelength, and with 10 time-integrated runs was found to be 0.92%.

2. Interface Used to Obtain Time-Resolved Spectra

To obtain signal-averaged, time-resolved spectra, the interface and the flow chart of the program shown in Figure 5, were designed. The interface is explained in greater detail in Figure 6.

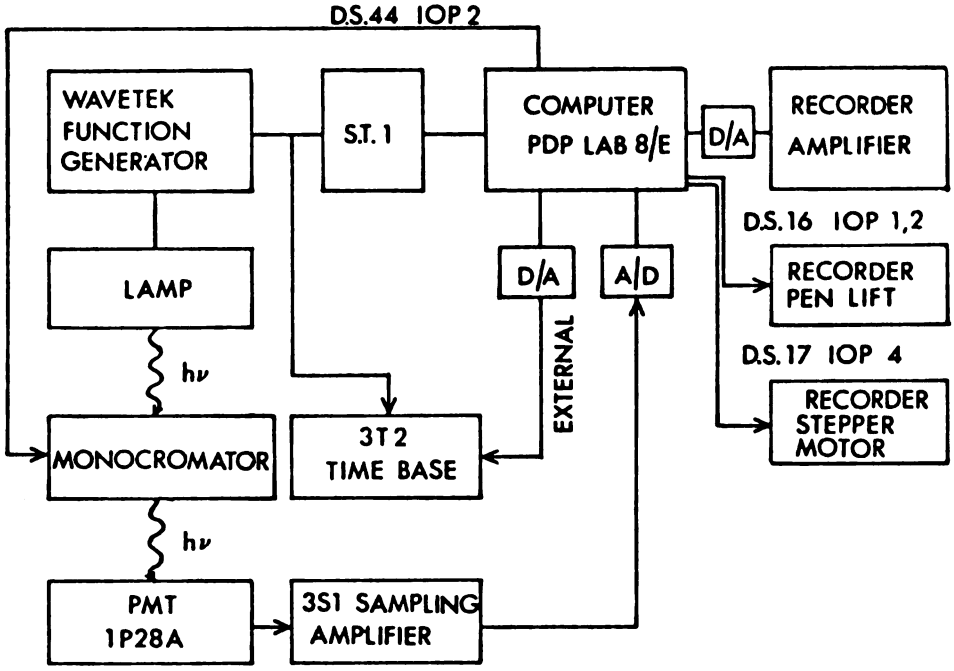

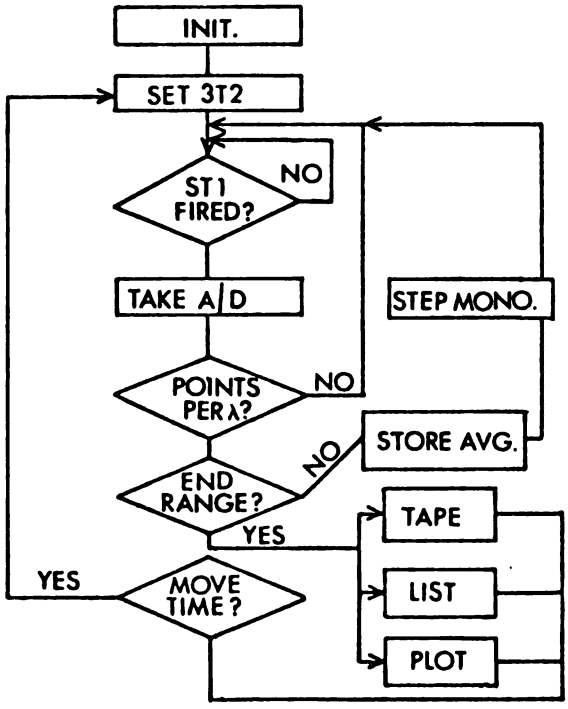

Figure 5. Block diagram of the hardware and flow chart of the program for obtaining signal averaged time-resolved spectra.

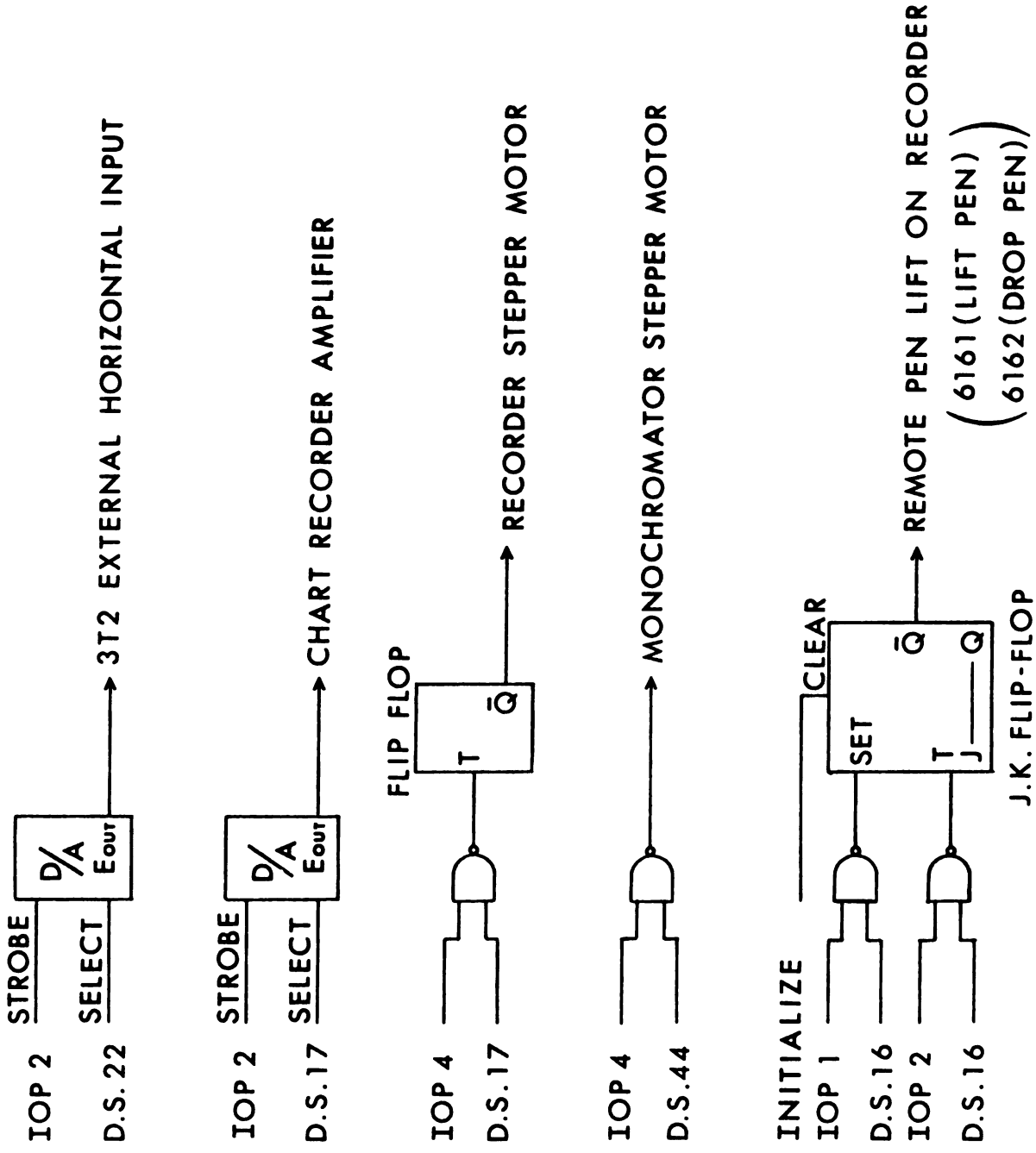

Figure 6. Details of interface used for time-resolution.

The computer is interfaced to the system through a Heath Company Computer Interface Buffer and a Heath Model EU-801 Analog Digital Designer. The computer outputs the spectra through the interface to a Heath Model EU-205-11 chart recorder with a Heath EU-200-01 Potentiometric Amplifier.

The program begins by setting the 3T2 time base of the sampling oscilloscope to some preselected instant in time. This instant in time is then held on the time base while the monochromator is scanned by the computer through some preselected wavelength interval. The operation of the program is somewhat similar to the one described earlier in that the program takes a preset number of data points over a wavelength interval. The points obtained are averaged, the average is stored, and the wavelength is then incremented by the computer. The process continues until the end of the wavelength scan is reached. Computer outputs can be in the form of a binary tape, a floating-point listing, a plot of the spectrum on the recorder, or any combination of the above. After completing the output routine, the computer moves the time base of the sampling oscilloscope to a new instant in time and the process is repeated until the correct number of time-resolved spectra has been obtained. The spectra obtained are discussed in a later chapter.

V. LIGHT SOURCE CHARACTERISTICS

In this chapter the source is characterized in terms of its electrical analog parameters, its on-time and its emission dependence upon the gap length. The performance of the light source for fluorescence lifetime determination is demonstrated by experimental measurements of the decay time of quinine sulfate. The time-integrated and time-resolved spectral characteristics of the source are presented in a subsequent chapter.

A. Calculations of Electrical Parameters

A photograph of the photomultiplier output following repetitive flashes of the lamp is shown in Figure 7 to illustrate the lamp decay itself. To obtain the photograph shown, ten traces each containing about 200 points were superimposed and the lamp was therefore fired 2,000 times. The line shown at the bottom of the photograph represents the base line of the measurements (the shutter closed condition).

From curves such as the one shown in Figure 7, the electrical parameters L and R_G can be calculated if the capacitance C_L is known. The capacitance C_L can be calculated by the following equation for the capacitance of a coaxial line (57):

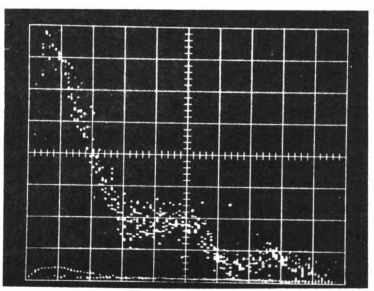

Figure 7. Oscilloscope photograph illustrating the radiant pulse from the spark source. Horizontal scale 10 nsec/div., vertical scale 100 mV/div. (scale inverted).

$$C_L = \frac{2\pi\varepsilon_0 K \ell_L}{\ln\left(\frac{a + t_H}{a}\right)} , \qquad (20)$$

where ε_0 is the permittivity, K is the dielectric constant, ℓ_L is the length of the dielectric, a is the radius of the aliminum bar, and t_H is the thickness of the polyethylene tube. The radius of the aluminum bar is 2.04 cm, ε_0 is 8.85 x 10^{-12} $coul^2/nt\text{-}m^2$, K is 2.3, and t_H is 0.54 mm. Substitution of the above values into Equation 20 yields a capacitance of 192 pF for the line. Similary, the capacitance of the transmission cable and the capacitance of the gap are 6.6 pF and 4 x 10^{-3} pF, respectively. Hence, the simplifying assumption made earlier that $C_L \approx C_L + C_C + C_G$ is now shown to be quite valid.

From the time at which the discharge current reaches its first maximum, and from the two later current maxima observed in Figure 7, L and R_G can be calculated. From Equation 18 we know that the time required for the radiant intensity to reach its maximum value is given by 0.95 ($2L/R_G$). However, before the rise time given by Figure 7 can be used, the rise time of the observation system to a delta function must be obtained. Figure 8 shows the response of the system to a single dark current pulse which can be used as a delta function for evaluation. The rise time of the photomultiplier-oscilloscope combination is about 2.8 nsec. Since the rise time of the sampling amplifier is about 0.3 nsec, the rise time of the PMT was found to be, as quoted by the manufacturer, equal to 2.7 nsec (54).

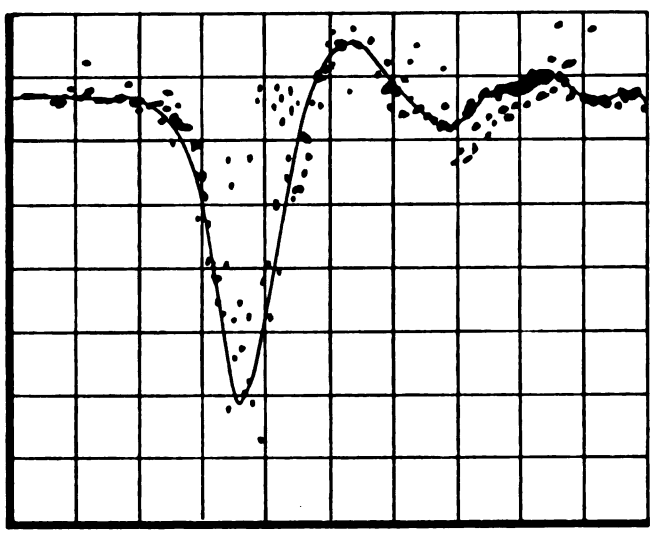

Figure 8. Response of the detection system to a dark current pulse. Horizontal scale 2 nsec/div., vertical scale 100 mV/div.

From Figure 7 the rise time of a radiant pulse is shown to be 4.8 nsec. Since the rise time of a system is the square root of the sum of the squares of the rise time of each component (58), the equation that relates the true t_m to the observed rise time (t_m') is given by,

$$t_m' = (t_m^2 + t_r^2)^{1/2} , \qquad (21)$$

where t_r is the rise time of the PMT-oscilloscope combination. If the values for t_r (2.8 nsec) and t_m' (4.8 nsec) are substituted into Equation 21, t_m is found to be 3.7 nsec. Hence $2L/R_G$ equals 3.5 nsec.

We can solve for L and R_G if we recall the equation for the discharge current, Equation 15, given earlier. Since we observe two later current maxima, it implies that $\sin(\beta t)$ is a maximum at those two times. Hence, $\sin(\beta t)$ is a maximum at 49 nsec and at 77 nsec. Therefore, Δt = 28 nsec and $\beta \Delta t = \pi$. Substitution for β yields,

$$L = \frac{\Delta t}{2\pi^2}\left(\frac{\Delta t}{C_L} - \sqrt{\frac{\Delta t^2}{C_L^2} - \pi^2 R_G^2}\right). \qquad (22)$$

Combining Equation 22 with $2L/R_G$ = 3.5 nsec, yields an equivalent inductance L of 53 nH and a gap resistance R_G of 31 Ω.

One can perform a similar calculation, to that performed for the capacitance, to obtain the inductance of the coaxial line. This was done and a value of 2 nH was obtained. Hence, essentially all the resistance, and the inductance in the circuit are contributed by the spark gap. This then explains why all attempts at varying the

discharge parameters by varying the lock-nut position discussed in the Experimental section proved fruitless.

The value of the breakdown voltage V_B can be found by applying the Toepler equation (59), which states that

$$R_G = \frac{k\ell}{CV_B} , \qquad (23)$$

where k is the Toepler constant which equals 1.5×10^{-4} Ω/cm for air, ℓ is the spark length in cm, C is the capacitance, and V_B is the breakdown voltage. Substituting the values for the spark used into Equation 23, yields a breakdown voltage of 6.5 kV for a 2.5 mm spark length. The breakdown voltage for needle point electrodes for a 2.5 mm gap is experimentally found to be 3.0 kV (53). Hence, there seems to be a contradiction between the voltage calculated by the Toepler equation and the voltage determined experimentally. Recall, however, that the power supply produces a time-varying voltage which the spark gap follows. Hence, while the voltage at which the spark should break down is 3.0 kV, the voltage that is on the capacitor at the instant that the spark breaks down is actually 6.5 kV. This difference arises from the fact that while the spark is forming, the formative spark Lag (60), the capacitor is still being charged to a larger voltage by the power supply. Hence, the breakdown voltage that is used in this work, represents the actual voltage on the capacitor at the instant that the capacitor discharges rather than the voltage at which the spark will break down under static conditions.

Using the values of L, R_G, C_L and V_B that have been obtained, we can now substitute them into Equation 15 and obtain a theoretical plot of discharge current as a function of time as is shown in Figure 9. Comparison of Figure 7 with Figure 9 shows that Equation 15 accurately predicts the light output, which should be directly related to the current (37), only for the first 20 nsec. After that time, no correlation exists between discharge current predicted by Equation 15 and the light intensity. Using the values for current and voltage obtained from Figure 9, we find that the peak current is about 130 A while the peak electrical power dissipated is on the order of 10^6 W.

B. Absolute Emission Intensity

From the dissipated electrical power, the optical power emitted can be calculated from a knowledge of the electrical-to-optical conversion efficiency. According to McMahon and co-workers (50), a value for the conversion efficienty of 5×10^{-3} can be assigned to N_2 at 1 atm pressure with an accuracy of about a factor of 2. The average electrical power dissipated over the first 20 nsec is about 4×10^5 W. Therefore, the total power dissipated over the first 20 nsec is about 8×10^6 W. If a conversion efficiency of 5×10^{-3} is assumed, the total radiated peak power is on the order of 4×10^4 W with an accuracy of about a factor of 4. Therefore, the number of photons emitted over all wavelengths is on the order of 10^{15} per flash or about 3×10^{11} photons per flash per angstrom at the Hg 253.7 nm line. Since the radiation is emitted over a

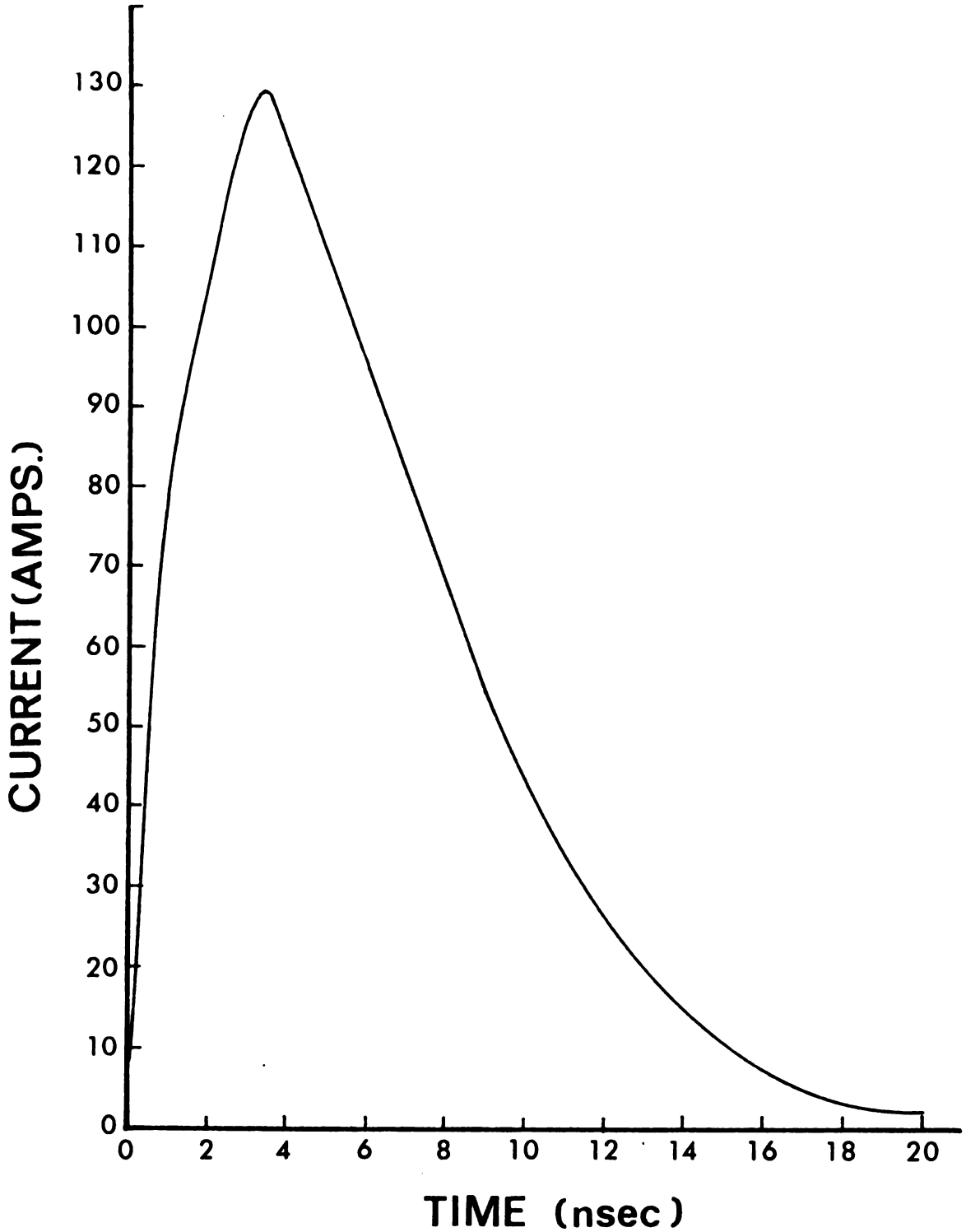

Figure 9. Theoretical plot of Equation 15 showing the discharge current as a function of time.

luminous area of about 10^{-2} cm^2, the radiant emittance observed is on the order of 4×10^6 W/cm^2.

The theoretical emission of 3×10^{11} photons per flash per angstrom at 253.7 nm was confirmed experimentally. Assuming that the lens collects 1% of the radiation emitted and assuming that the value of 3×10^{11} photons per flash per angstrom is valid, 3×10^9 photons will be collimated in a luminous area of π cm^2. Using a slit width of 50 μm (a 0.1 nm bandpass) and a slit height of 1 cm, the monochromator aperature would be 3×10^{-3} cm^2. Therefore, 3×10^6 photons would enter the monochromator and assuming a 5% transfer efficiency, 1.5×10^5 photons would impinge on the photocathode of the photomultiplier tube. Assuming a quantum efficiency of 20% for the photocathode and a gain of 10^5 (at a voltage of 0.8 kV), we would obtain 3×10^9 photoelectrons over the effective "on-time" of the radiant pulse per angstrom if we assume that 3×10^{11} photons per angstrom is valid. Converting photoelectrons to current, it is found that the average photocurrent that is experimentally observed is within a factor of five of the photocurrent predicted from the above discussion. Recalling all the assumptions made, it appears that the value of 3×10^{11} photons per angstrom per pulse at 253.7 nm is probably accurate to a factor of two.

C. Emission Intensity as a Function of Gap Length

Photographs similar to that shown in Figure 7 were taken of the photomultiplier output as a function of time for repetitive lamp flashes with gap lengths varying from 1.8 - 5.0 mm at a single

wavelength setting in the uv region. Measurements were made of the area bounded by the exponential rise and decay of the photomultiplier current, which is related to the radiant energy (number of photons emitted over the monochromator bandpass) incident on the photomultiplier. A measured quantity, P_L, related to the radiant power emitted over the spectral bandpass can be obtained by dividing the measured area by the measured "on" time of the lamp. Because the small oscillations of the lamp output after the first maximum make exact measurements difficult, approximate areas and on times were measured by constructing a triangle bounding only the first current maximum.

Several observations about the effect of gap length can be made from the approximate radiant energy and power measurements described. First, the time at which the lamp output reaches its first maximum (t_m) remains constant and independent of gap length. The observation implies that $\frac{2L}{R_G}$ is independent of gap length. Second, it was observed that the radiant energy emitted E_L increases with increasing gap length. The radiant energy E_L is related to the electrical energy dissipated in the gap E_{EL} by an electrical-to-optical conversion factor, which is a function of the type of gas present in the gap and gas pressure only. Since E_L was observed to increase with gap length, E_{EL} must also increase with increasing gap length. The electrical energy dissipated in the gap is given by

$$E_{EL} = V_B \times \int_0^\infty i\,dt = V_B^2 C_L / 2. \qquad (24)$$

Since the breakdown voltage of the gap is a linear function of gap length (59), the electrical energy dissipated or the radiant energy emitted should be a linear function of the square of gap length. A plot of E_L, made at 273 nm, vs. ℓ^2 indeed shows a linear relationship. Experimentally it was found that the radiant power P_L increases linearly with ℓ, which implies that the on-time of the lamp increases linearly with increasing gap length, and the on-time will affect the decay time.

D. Decay Time as a Function of Gap Length

Another very important parameter for the experimenter to be able to predict is the lamp decay time τ and its relationship to gap length. The decay time τ is defined here as the time difference between t_m and the time $t_{1/2}$ required for the output intensity to fall to 1/e of its value at t_m as shown in Equation 25.

$$\tau = t_{1/2} - t_m . \tag{25}$$

The time $t_{1/2}$ can be found from Equation 15. Since t_m converges to 3.5 nsec, Equation 25 can be solved if t_m is set equal to 0.95 $(2L/R_G)$. The decay time τ is given by Equation 26

$$\tau = \frac{2L}{R_G}\left[\exp\left(\frac{R_G t_{1/2} - 4L}{2L}\right) - 0.95\right] . \tag{26}$$

Equation 27 results if the natural logarithms of both sides of Equation 26 are taken.

$$\ln \tau = \ln \frac{2L}{R_G} + \ln \left[\exp \left(\frac{R_G t_{1/2} - 4L}{2L} \right) - 0.95 \right] . \qquad (27)$$

For gap lengths greater than 2 mm, 0.95 is much less than the exponential term and hence can be neglected. We have observed that the decay time increases as the gap length increases. Recall, however, that $2L/R_G$ remains constant as the gap length is changed. This states that $R_G/2L$ must also remain constant. Since τ increases with gap length, the only variable in Equation 27 which can depend on gap length and hence affect τ, is $t_{1/2}$. We can therefore transfer Equation 27 into:

$$\log \tau = \log \left(\frac{2L}{R_G} \right) + K\ell^n , \qquad (28)$$

where K is a constant, and ℓ^n is the functional dependence of $t_{1/2}$ upon ℓ. The correct value of n will be given when the extrapolated curve represented by Equation 28 intercepts the ordinate at log $(2L/R_G)$ = 0.54 nsec (when log τ = 0.54 nsec).

Experimental decay times were obtained from oscilloscope photographs for various gap length. The decay times were then plotted vs. various values of n. Figure 10 shows a plot of log τ vs. gap length for n = 1. The best straight line was drawn through the experimentally determined decay points and it was found that the intercept was at log τ equal to 0.59 nsec. Hence, within the experimental error due to the visual reaching of the decay time off the photographs, the decay time as a function of gap length is given by:

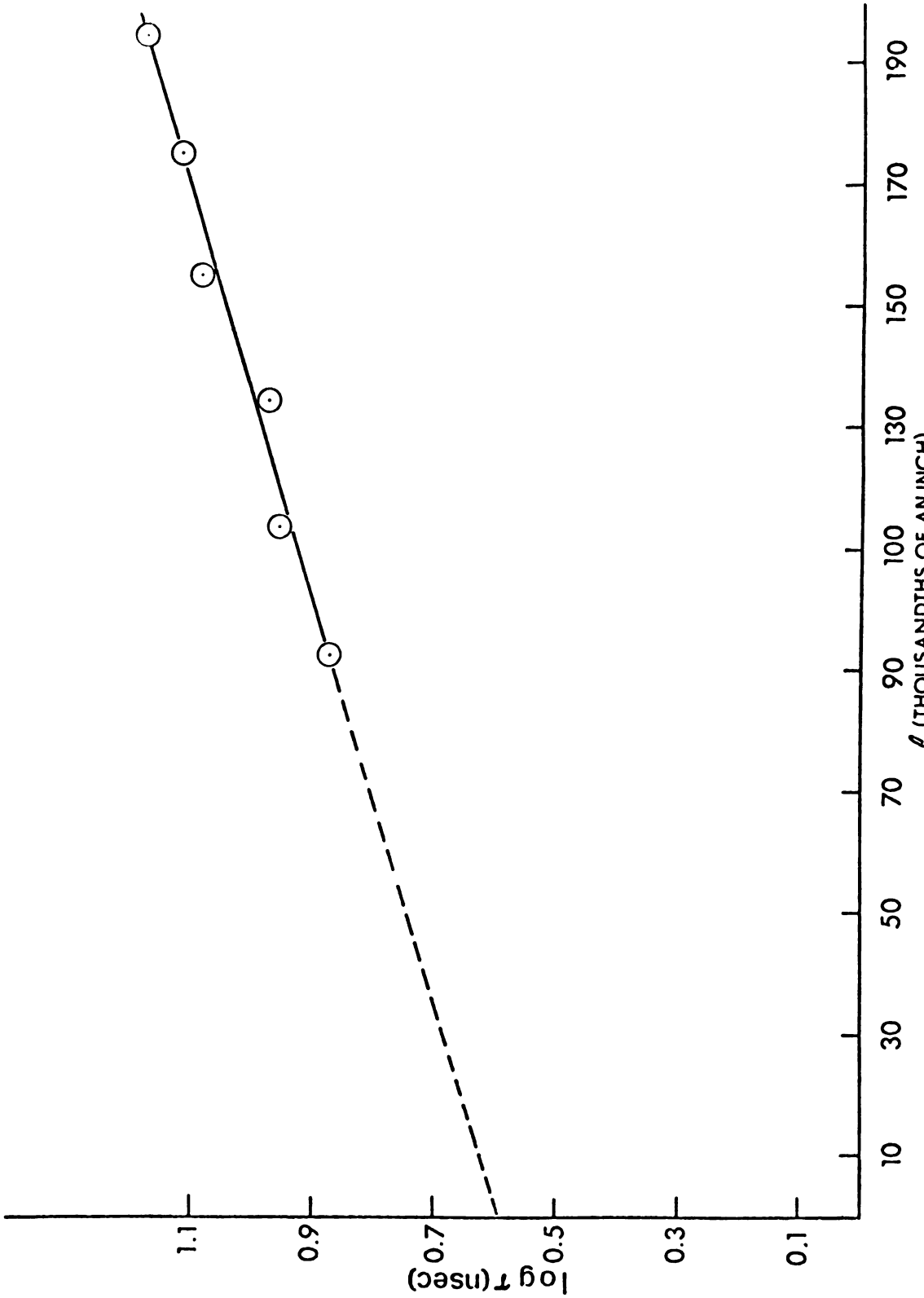

Figure 10. Graph of the logarithm of the decay time vs. gap length.

$$\tau = \frac{2L}{R_G} \exp(K\ell) \ , \qquad (29)$$

where K = 0.31 and ℓ is expressed in mm. Equation 29 is valid only when the gap length is greater than 2 mm and can be used to predict the decay time of the lamp at a given gap length. The decay time predicted by Equation 29 can be used by the experimenter to deconvolute the observed fluorescence decay time of the sample with the excitation function according to the deconvolution equation and hence, the experimenter can quickly obtain the true fluorescence lifetime of a sample.

E. An Application to Fluorescence Lifetime Measurements

To check the performance of the lamp for lifetime measurements, a 10^{-5} M solution of quinine sulfate in 1.0 N H_2SO_4 was prepared from quinine sulfate which had been recrystallized three times from distilled water and then vacuum dried. The solution was placed in a 2.0 cm quartz cuvette, and the fluorescence emission was observed at right angles relative to the excitation source. No excitation monochromator was used. However, an emission monochromator was used which was set at 420 nm with a slit width of 400 μm (a 0.8 nm bandpass).

The fluorescence decay observed on the oscilloscope screen is shown in Figure 11. The curve was obtained under conditions similar to those used to obtain Figure 7. The fluorescence decay time manually calculated from the photograph shown, unconvoluted for

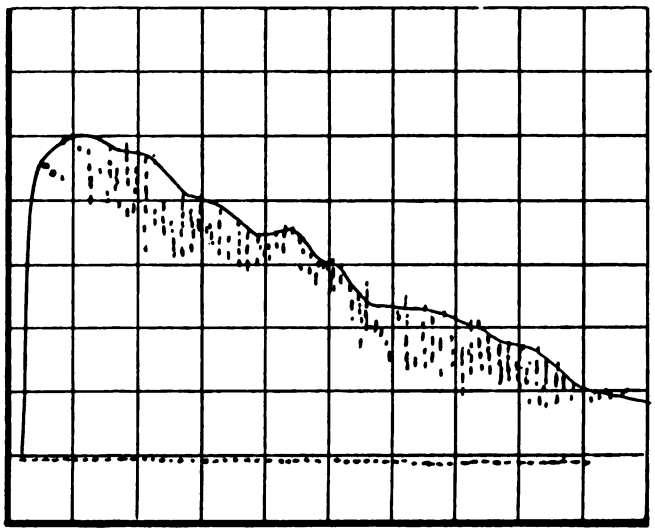

Figure 11. Fluorescence decay of 10^{-5} M quinine sulfate in 1.0 N H_2SO_4. Horizontal scale 10 nsec/div., vertical scale 100 mV/div. (scale inverted).

lamp response, gave a lifetime of 23 $\pm$ 3 nsec, which is in good agreement with other published results (14, 25). The uncertainty in the decay time can be substantially reduced by signal averaging. The accuracy can be increased by deconvolution with the lamp's decay time, Equation 29. Similar photographs were obtained for solutions of quinine sulfate down to concentrations of one part-per-trillion, and quinine sulfate could be detected according to its decay time at this concentration.

VI. SPECTRAL EMISSION CHARACTERISTICS

The experimenter needs to know the spectral distribution of the emission from the light source, and the total time-integrated emission intensity. The spectral distribution is, however, strongly dependent upon both time and gap length. Hence, a time-resolved spectral characterization of the light source is of much greater importance than the time-integrated spectra. In this chapter, both the time-integrated and the time-resolved spectra are presented and discussed.

A. Time-Integrated Spectra

It was found that the easiest method of obtaining time-integrated spectra was to bypass the sampling oscilloscope and to connect the photomultiplier output directly to a strip chart recorder. The monochromator was operated with a 0.06 nm bandpass and was continuously scanned, which synchronized the chart recorder motor, from 200 to 600 nm. The spectrum of the light source obtained under these conditions is shown in Figure 12. The spectrum shown is uncorrected for both photomultiplier and monochromator response and was obtained at a spark gap length of 2.0 mm. In Figure 12, note that the continuum has an approximately equal intensity distribution in the near uv and in the blue region of the spectrum. Note also the strong emission due to NII lines that lie on top of the continuum.

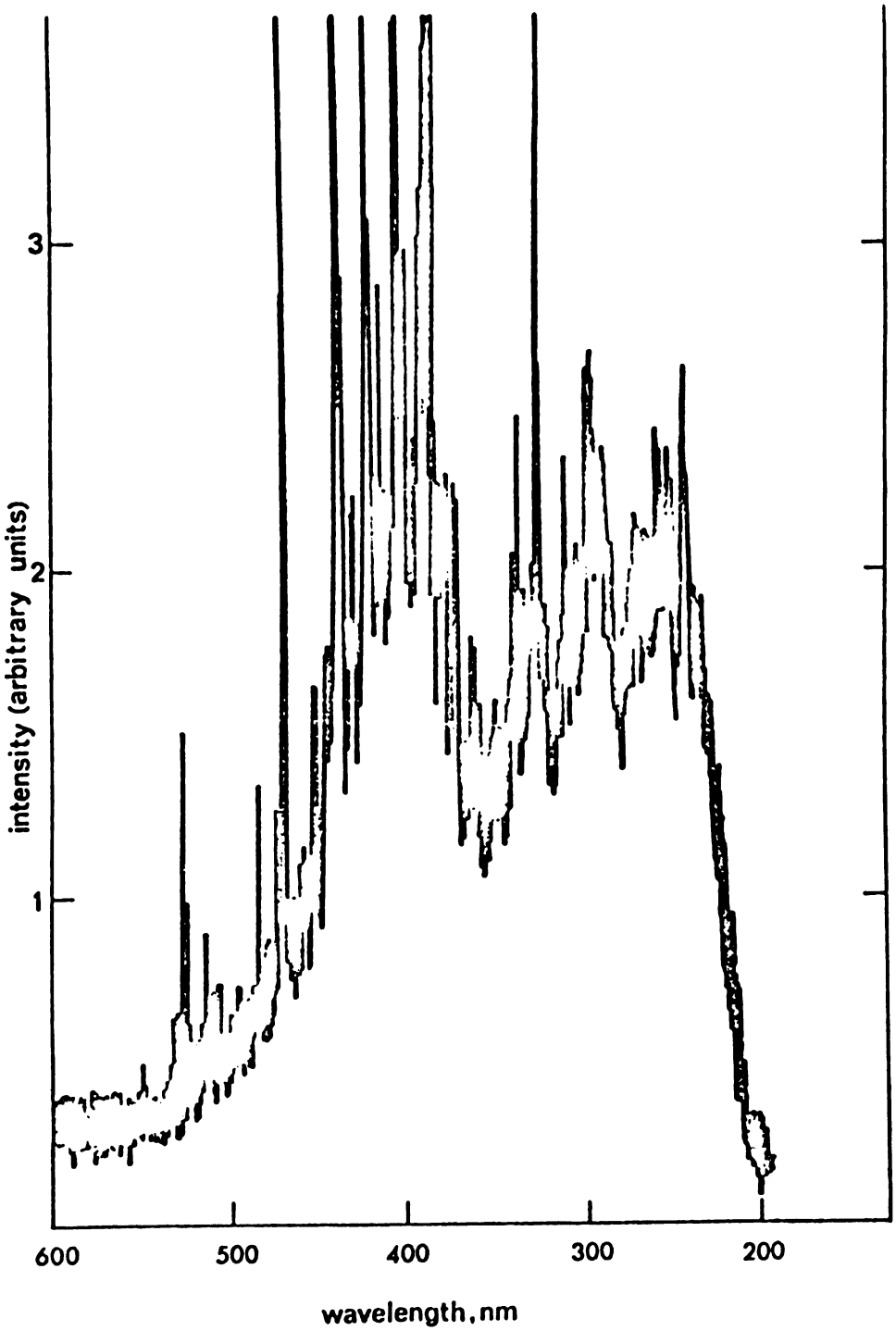

Figure 12. Time-integrated spectrum of the light source with a gap length of 2.0 mm.

As the gap length increases, the spectrum obtained shifts gradually to that shown in Figure 13, for a gap length of 4.5 mm. Note that the intensity of the continuum has become much more pronounced in the uv and that the strong NII lines observed at smaller gap lengths has diminished greatly. Hence, increasing the gap length changes the reactions that occur in the spark. One can now obtain a slight tuning of the spectral emission merely by changing the gap length. If a sample absorbs more radiation in the uv, the gap length can be increased with a corresponding large increase in the emission intensity obtained in the uv.

B. Time-Resolved Spectra

The spectra shown in Figures 12 and 13 represent the total time emission of the spark. Of greater importance is the emission of the spark at various instances in time which then add to produce Figures 12 and 13. Perhaps, through the knowledge gained from the time-resolved spectra, one could understand and hopefully manipulate the reactions that produce the observed emission.

To obtain signal-averaged, time-resolved spectra, the interface discussed in the Experimental chapter was used. The computer was instructed to take 60 points over an 0.1 nm range. These points were averaged and stored. The lamp was fired at 60 Hz and the monochromator scanned at 0.1 nm/sec. The photomultiplier tube was operated at 0.8 kV, while the 3S1 amplifier was set at 200 mV/div. For the chart recorder output, the stepper motor was run by the computer at 15 sec/in which corresponded to an output rate of

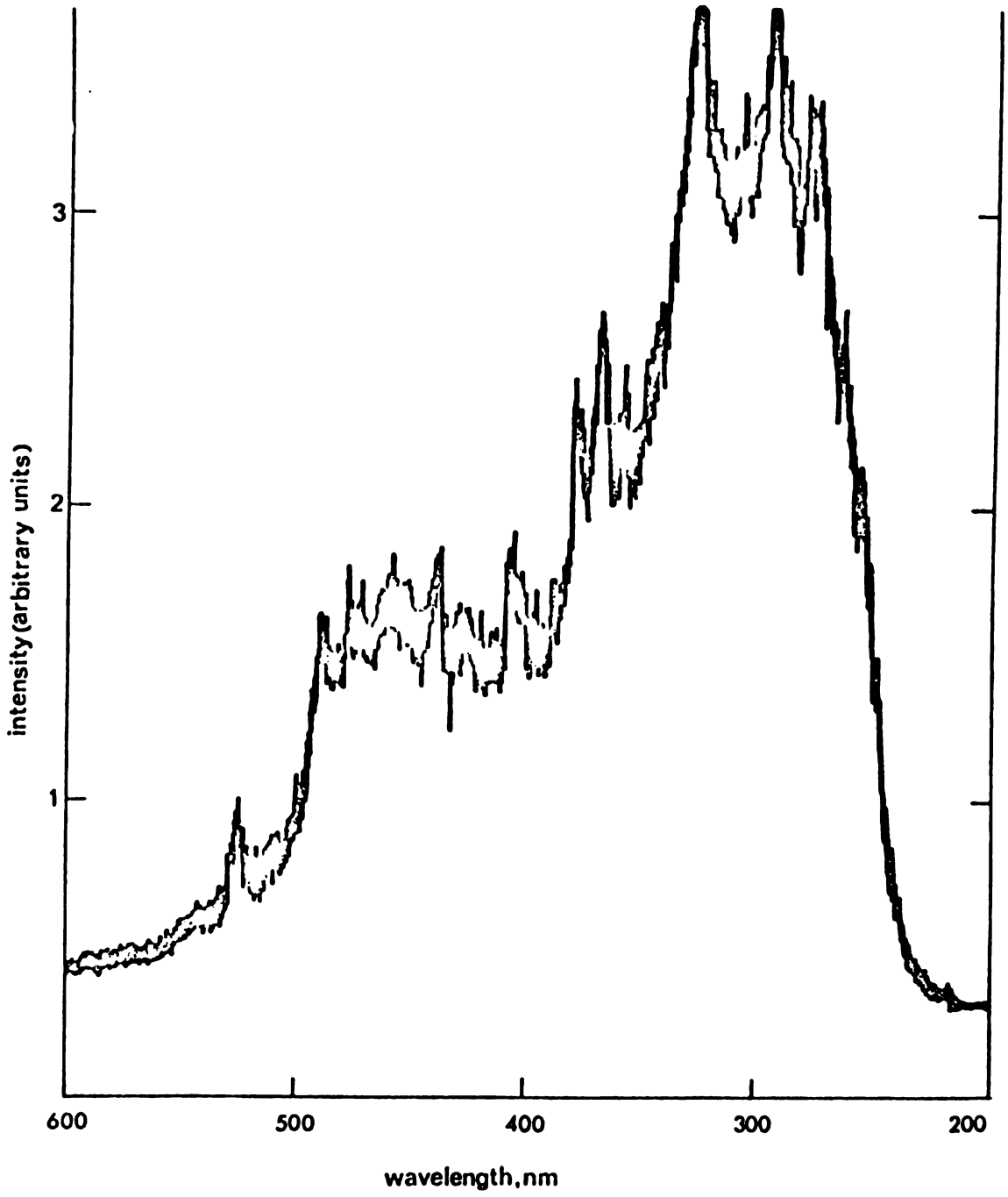

Figure 13. Time-integrated spectrum with a gap length of 4.5 mm.

1 nm/in. Spectra were obtained under these conditions from 200 to 600 nm. The times at which the spectra were obtained ranged from prebreakdown to 120 nsec after t_m. The last spectrum at 120 nsec after t_m was obtained at double the sensitivity of all the others.

1. Prebreakdown Spectra

The only emission observed in prebreakdown is shown in Figure 14. This spectrum was obtained under conditions outlined above at a time of 6 nsec before the emission intensity of the continuum reached its maximum value at t_m, and hence 2.3 nsec before the onset of the discharge current.

The spectrum shown in Figure 14 is identified as emission from the second positive band system (SPBS) of molecular nitrogen (61). Emission from the SPBS is observed from upper vibrational levels up to and including the fourth vibrational level of the $C^3\Pi_u$ state in its transition to the $B^3\Pi_g$ state.

Walters and Malmstadt (62) studied the initial breakdown characteristics of an air spark. They observed emission from the SPBS. However, they noted that no bands resulted for vibrational level greater than V' = 3. Basing a dissociation theory on this fact, Walters and Malmstadt concluded that a radiationless transition between the $C^3\Pi_u$ and the $^3\Sigma_g^+$ states occurred, and, therefore, direct dissociation by electron collisions with N_2 molecules in the $^3\Sigma_g^+$ state resulted in dissociation.

However, as was noted above, emission from the V' = 4 vibrational level of the $C^3\Pi_u$ state is shown clearly in Figure 14.

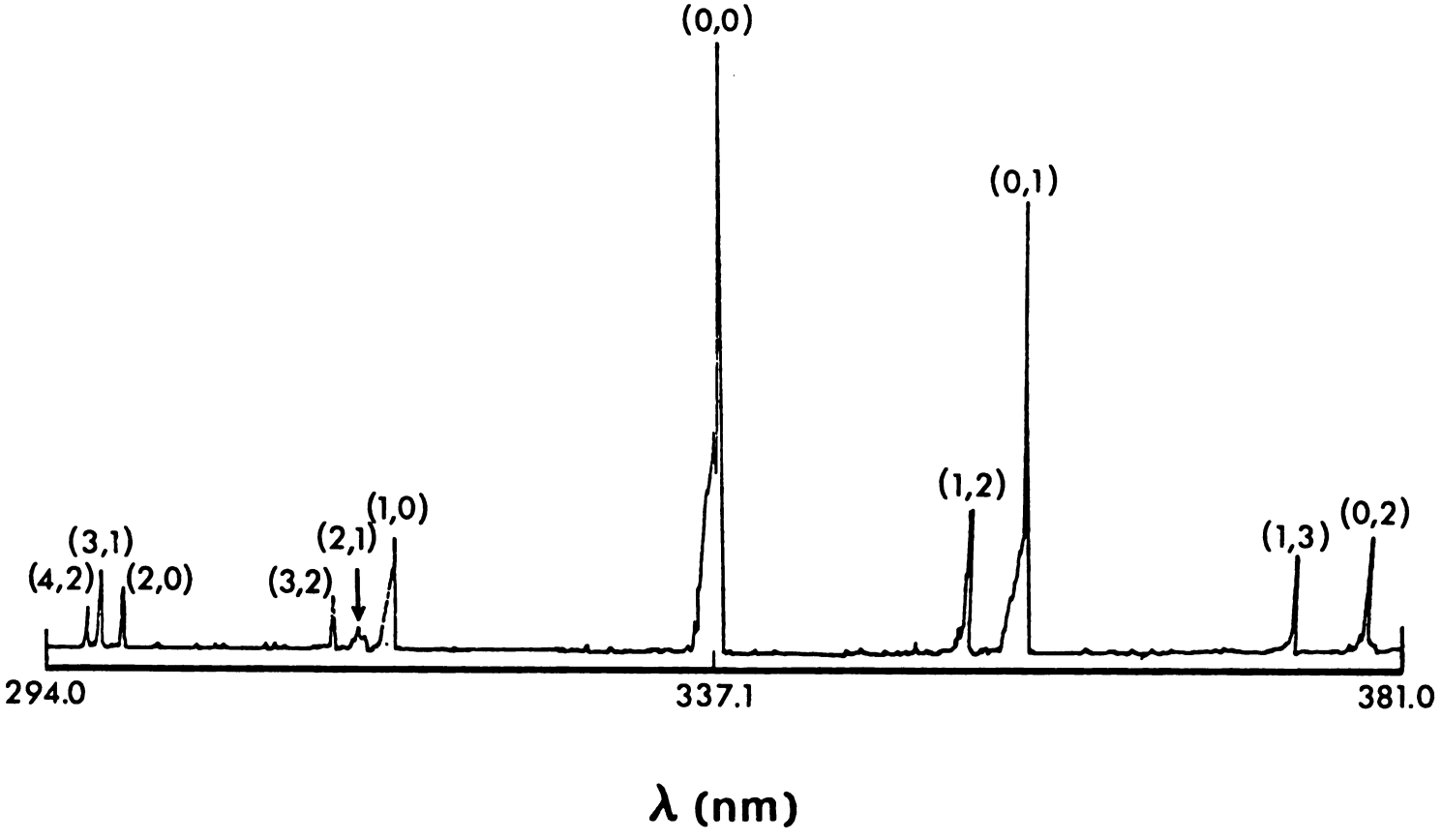

Figure 14. Prebreakdown emission spectrum of the second positive band system of nitrogen.

Both Gaydon (63) and Barnes (64) have also observed emission from this vibrational level. It, therefore, seems clear that there are alternative dissociation paths to that suggested by Walters and Malmstadt. The simplest dissociation path would appear to be direct dissociation of N_2 molecules, in the $C^3\Pi_u$ state, into $N(^4S^0) + N(^2D^0)$ states by electron collision, for molecules whose energy then exceeds the energy of the V' = 4 level of the $C^3\Pi_u$ state. Another possibility is predissociation through the $^5\Pi_u$ state. This state is predicted theoretically and Gilmore (65) believes that the $^5\Pi_u$ state provides a plausible explanation for the predissociation of the $C^3\Pi_u$ state.

The SPBS is the only emission observed in prebreakdown in this work. No other emission, either from atoms, ions or molecules, is observed in time coincidence with the SPBS before current begins in the spark.

The time course of the emission from the 337.1 nm line observed in prebreakdown and breakdown is shown by curve A of Figure 15, while the time profile of the emission of the continuum at 337.4 nm is shown by curve B in Figure 15. It is obvious from Figure 15 that the emission from the SPBS occurs much earlier than the emission of the continuum produced by the dissociation of N_2 molecules in the triplet manifold. Emission from all vibrational levels shows the identical time behiavior as that observed for the 337.1 nm line. In Figure 15 it is seen that emission from the SPBS lasts until the current begins. At the onset of the current, the N_2 triplet manifold depopulates, and the SPBS emission begins to decrease. The emission then observed is due to the continuum rather than the SPBS.

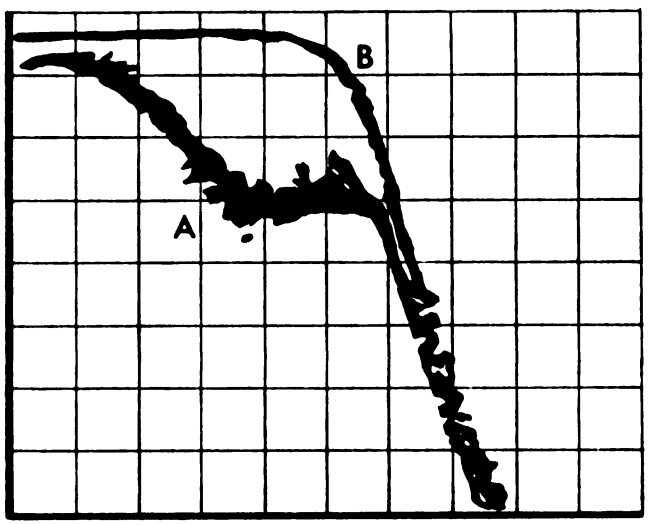

Figure 15. Time profile of the emission observed in prebreakdown (curve A) relative to post breakdown (curve B). Horizontal scale 2 nsec/div., vertical scale 100 mV/div.

The emission from the 337.1 nm line was traced back in time by using various lengths of coaxial cable to delay the signal relative to the triggering command from the spark. Emission was observed up to at least 45 nsec before current began in the spark, which indicates that the transition of the spark gap from a nonconductor to a current conducting plasma requires at least 45 nsec. If the streamer theory for spark formation is accepted (60), the data would indicate that the velocity of the streamer would be less than or equal to 2×10^7 cm/sec for the spark used.

Another observation that can be made from Figure 15, is the intensity of the emission from the 337.1 nm line relative to the continuum. The peak emission from the 337.1 nm line is approximately 1/3 of the peak emission observed for the continuum. By assuming that the width of the 337.1 nm line is as large as the monochromator bandpass, we can conclude that about 10^{10} photons are emitted, over a one nsec time period, when the emission reaches its maximum. Assuming that the ideal gas law is valid here, we find that there are about 9×10^{16} molecules of N_2, that exist in all electronic states, are to be found within the luminous area occupied by the spark. Since the natural radiative lifetime of the SPBS has been found (30, 66) to be about 40 nsec, and we observe about 10^{10} photons in a one nsec time interval, the data suggest (assuming only spontaneous emission) that there are about 2×10^{12} N_2 molecules in the V' = 0 vibrational level of the $C^3\Pi_u$ state which should emit the 337.1 nm line and return to the V' = 0 level of the $B^3\Pi_g$ state. If we were now to sum over all the observed emissions from the $C^3\Pi_u$

state, it would suggest that at least 10^{13} molecules of N_2 would have been observed to emit in their transition from $C^3\Pi_u$ state to the $B^3\Pi_g$ state if the discharge current would not have been allowed to depopulate the $C^3\Pi_u$state (as shown in Figure 15). Hence, it appears that an appreciable portion of at least 0.01% (recall that radiationless transitions are not considered) of the total available N_2 molecules which are easily capable of being ionized by direct electron impact, exist in the highly excited $C^3\Pi_u$ state. The author feels, as do others (67), that the emission observed from the SPBS is not spontaneous but rather stimulated emission, although no conclusive experimental justification can be presented at present for this belief. In any event, it appears, from the data, that the current conducting plasma is formed very near to the time at which the spark accepts the discharge current, and that the plasma is probably formed by direct dissociation of N_2 from the $C^3\Pi_u$ state. No emission from the first positive band system ($B^3\Pi_g \rightarrow A^3\Sigma_g$) is observed in prebreakdown due to its long radiative lifetime of 10 μsec.

2. Post Breakdown Spectra

Time-resolved spectra were obtained for times of 0, 10, 20, 40, 80 and 120 nsec after t_m. Figure 16 shows the emission of the spark at t_m. Note that the strong continuum, which resembles blackbody emission, extends from 200 nm, the beginning of the rise of the PMT, to 400 nm. Note also the three sets of absorption doublets between 200 to 230 nm. These are due to absorption of the continuum

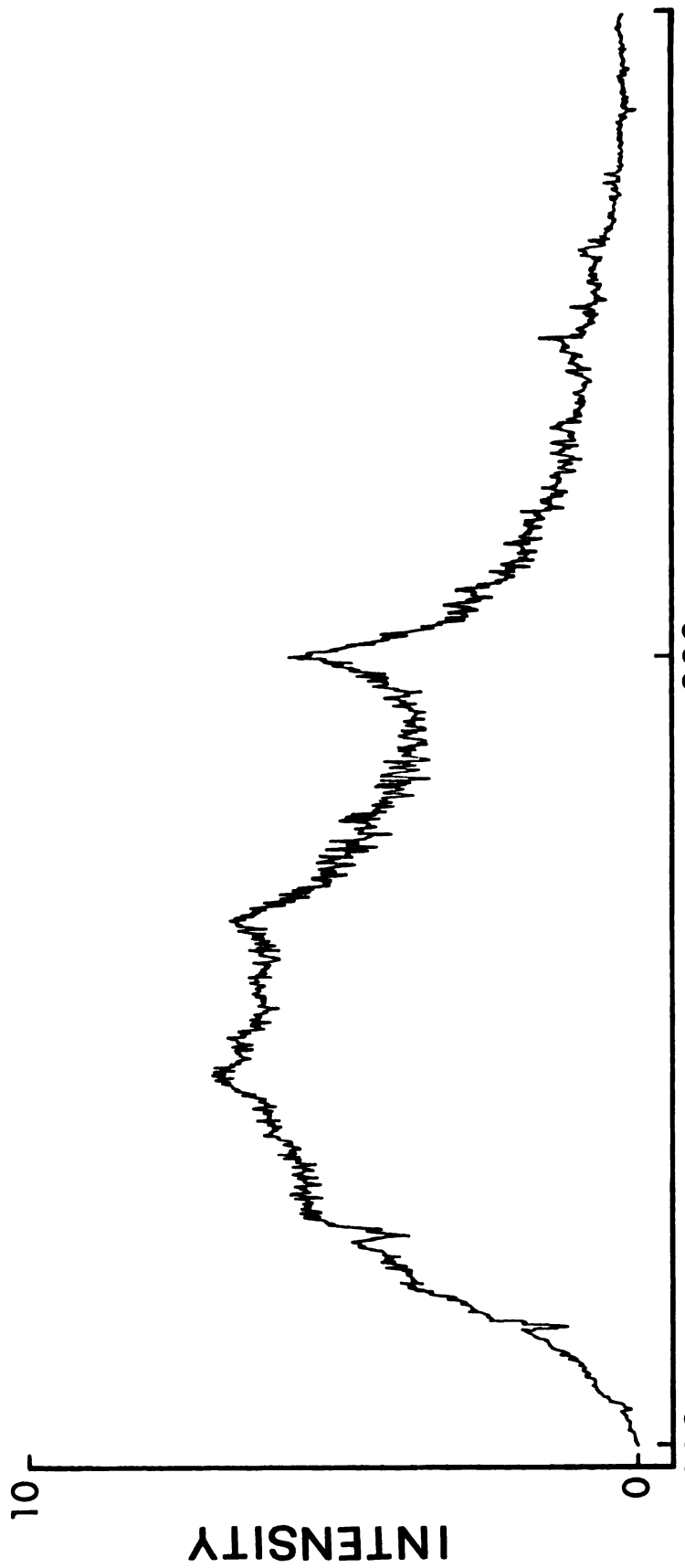

Figure 16. Time-resolved spectrum of the emission from the spark source at the time the discharge current reaches its maximum value.

by the γ system of NO (61). Hence, both N_2 and O_2 dissociate and combine to form NO in a time less than 3.5 nsec.

Due to their complexity, the remaining spectra have not been completely analyzed as to the species responsible for the emission, and, therefore, to the reactions that occur at various instances in time. The spectra are, however, presented for completeness and are shown in the Appendix for various times after spark breakdown.

VII. COMMENTARY

The spark source developed in this work has been shown to be an excellent excitation source for obtaining fluorescence decay times. The emission from the source has been shown to be on the order of 10^4 W per spark with a variable decay time of between 7-15 nsec.

It should be realized, however, that there are samples whose short decay times of 2-10 nsec do not warrant the use of the source that was described. For obtaining these decay times, the author would recommend a system based on the single-photon approach where one uses a light source of very short duration and very low intensity. The author does not recommend one source over the other because each has its own merits which depend upon the absorption coefficient and the decay time of the sample of interest.

It should be obvious, from the spectral characterization, that plasmas, in particular sparks, are not well understood. The various interrelated parameters such as current, voltage and spectral emission need to be studied on a time-resolved basis for an understanding of the mechanisms involved in spark formation through the production of the current-carrying plasma. The need for a more detailed understanding of the kinetics of atomic and molecular spark reactions is needed not just to be able to manipulate the emission

of the filler gas when it is used as a light source. Mechanistic information is also needed by the spectroscopist who uses the spark as a tool for elemental determinations by emission spectroscopy. The use of the spark as a source for quantitative and qualitative elemental determinations, will be discussed in Part II of this work.

PART II

A MINIATURE SPARK SOURCE FOR EMISSION SPECTROCHEMICAL ANALYSIS OF SOLUTIONS

I. INTRODUCTION

The direct spectrochemical analysis of metals is often performed by means of electrical discharges, such as the arc and the spark. The discharge vaporizes a portion of the sample and simultaneously excites a fraction of the vaporized material.

Historically, the general analytical characteristics of the arc have been described as high sampling rates, high detectability and poor reproducibility. The poor reproducibility arises from the fact that sampling from the metal electrodes in the continuous arc tends to be erratic. Since the sampling process is basically thermal, the excessive heat generated by the arc causes most electrodes to melt. Also, the tendency of the arc to burn for some time at one spot gives rise to erratic volatilization and fractional distillation. Since the concentration and the nature of the volatilized species in the arc influence the physical characteristics of the arc, workers have been forced to dilute the sample in a spectroscopic buffer, which results in an inherent disadvantage since dilution reduces sensitivity. However, even when using the buffer, fractional distillation still remains a problem and, therefore, the sample is burned to completion. The resulting emission is then time-integrated photographically for concentration determination.

In contrast to the arc, historically the spark's characteristics were described as low sampling rates and hence low detectability, and high reproducibility. Sampling in the spark is more favorable than in the arc because each spark strikes a different spot on the electrode surface. However, each spark changes the electrode surface and this causes the emission observed to change with sparking time.

The reason for the low sampling rate is the fact that the spark conducts current only for a very short time relative to the repetition rate. Since the total mass of sample eroded from the electrodes is directly proportional to the number of coulombs passed through the spark, efforts at increasing the detectability have necessitated that more energy be dissipated by the spark. This entails the use of massive power supplies that present some serious disadvantages. Some of these are the difficulty of operation, the high cost, the large RF interference, and the large amount of audible noise associated with their operation.

One of the major attractive features of the spark relative to the arc is that the emission from the spark need not be time-integrated. It is preferable to observe the emission in a time-resolved mode which allows the experimenter the opportunity to preselect the optimum observation time, corresponding to the time at which the signal to background ratio (S/B) is a maximum. Hence, the spark should prove to be more advantageous as an excitation source if the sampling rates, and hence its detectability, can be

improved without the need for a large power supply with all its inherent disadvantages.

Therefore, if one were able to separate the vaporization steps from the excitation step, one could easily optimize the sampling step external to the spark, and a relatively low energy spark could be used for excitation. Since the excitation energy must still come from the spark, it was decided that the low energy, high power (short on-time) spark discharge described in Part I of this work could prove to be a valuable excitation tool for emission spectrochemical analysis if the vaporization procedure were under external control.

The low energy spark could increase the spark-to-spark reproducibility since there would be little change in the geometry of the electrode or the amount of sample within the spark gap, which would have to be under external control. The high reproducibility produced would allay the use of internal standards, now commonly used in spark emission spectroscopy, to compensate for spark-to-spark variations.

A regular, controlled supply of material to the excitation zone is imperative in order to obtain a representative and reproducible amount of sample in the spark gap. To ensure that problems associated with sample inhomogeneity were overcome, a solution technique was chosen as the sampling procedure. Another attractive feature of solution techniques is the ease with which synthetic standards can be prepared.

A solution technique was designed as the introduction system for the miniature spark described in Part I. Samples, which are dissolved in water, are pneumatically aspirated by a stream of argon into a desolvation chamber in which the water is removed from the droplets formed. The dry salt crystals that remain are carried with the argon into the spark. The emission from the elements in the sample is then observed photoelectrically with a time-sliced or a time-resolved mode of detection.

In an effort to characterize the spark plasma as a function of time, data were obtained by time-resolved spectroscopy. The spectral emission, the excitation temperature, the degree of ionization and the electron concentration were measured as a function of time.

Calibration curves and detection limits, obtained by time-slicing and time-resolution, are reported for a variety of elements. The analytical curves are linear and generally have unity slope. The detection limits obtained for all elements studied are in the sub-PPM range. Interelement effects of aluminum on calcium and of cesium on calcium are reported as a function of time.

II. HISTORICAL

A. Introduction

The following statement was taken from an article published by Hultgren (68) in 1932.

> The three principle means of exciting emission spectra which have been used in quantitative analysis are the electric arc, the spark, and the flame. The arc and spark methods combine the advantages of a high and to some extent controllable excitation with certain drawbacks. While the high excitation makes these methods applicable to a large number of elements, and gives a great sensitivity, the difficulty of uniformly introducing representative samples of the material to be analyzed into the spark or arc gases, and the fact that the emission of one element is not independent of the other elements present, lead to some difficulties. The flame method while very reproducible and nearly free from the objective just cited, is limited in applicability to those few elements which have relatively low excitation potentials.

It has been the object of workers, including the author, in the area of spectrochemical analysis to make Hultgren's statement obsolete.

Perhaps the greatest change which has occurred since 1932 was the introduction of atomic absorption spectroscopy as a method of analysis by Walsh (69). Later, Winefordner and Vickers (70) showed that atomic fluorescence spectroscopy could also be used for spectrochemical analysis. In both techniques, atomic excitation is accomplished through the use of an external radiation source. Hence, excitation levels which cannot be reached through collisional means in the flame, can be attained through absorption of radiation.

However, before the excited states of an atom can be populated, either through thermal or radiational excitation, there must exist a concentration of neutral atoms in the vapor state. The flame is required to vaporize and to atomize the sample. Therefore, Hultgren's argument of the limited energy in the flame is still somewhat valid.

Attempts have been made to increase the energy (the temperature) or change the chemical characteristics of the flame. Workers have attempted to increase the flame temperature through the use of more energetic fuels such as cyanogen (71) or even perchlorofluoride (72). Because of the difficulties in obtaining and handling these fuels, it is understandable that they have not become popular under practical conditions.

The use of pre-mixed high temperature flames has been reviewed by Willis (73, 74). By the N_2O/C_2H_2 flame one can obtain an increase in sensitivity over conventional low temperature flames. However, elements such as Mo, B, P to name but a few, that form refractory oxides are quite difficult to determine in trace quantities (PPM level) even when fuel-rich high temperature flames, in which reducing conditions prevail, are used (75, 76).

Because of the physical limitations of excitational energy associated with the flame, experimenters have been forced to look elsewhere for excitation sources which possess the requisite energy required for the analysis of refractory materials and elements which form refractory oxides. Present trends have been in the design of various forms of plasma excitation sources. The spark, even though

it is a plasma of transitory nature and hence possesses the necessary energy for the analysis of refractory substances, has been overlooked as an excitation source by the majority of workers.

The spark, for spectrochemical analysis, offers the experimenter a source of very high excitation energy. For maximum application of spark spectrochemical analysis, the author believes that the sample should be introduced to the spark as an aerosol of a solution of the sample and that the emission from the spark should be observed with some form of emission time-resolution. In the sections to follow, the various forms of spark solution analysis and the various methods used for obtaining time-resolution are described.

B. Spark and Arc Solution Analysis

The use of solutions for spectrochemical analysis has rapidly increased in popularity over the past several years. The reasons for this trend can be attributed to: (1) the elimination of effects due to the sample history, (2) the reduction of problems associated with nonhomogeneity, (3) the reduction of effects due to volatilization differences among the elements, (4) the controlled rates of introduction, and (5) the ease of preparation of a series of standards. Although interelement effects can not be eliminated, it is easier to compensate for them in solutions than in solids, through the preparation of the standards.

1. Indirect Solution Analysis-- The Residue Methods

Rivas (77) first proposed sparking to a direct residue from a solution sample which remained on a graphite electrode after evaporation. However, the most successful application of the residue method was the copper spark technique described by Fred and co-workers (78). Another residue technique, involves heating a graphite electrode while dipping it into a solution (79). The residue methods are particularly applicable to analysis of samples that are available in very limited quantity, on the order of 50 µl.

Spark residue methods have not become widely used because the composition of the radiating vapor changes as the sample is consumed. Residue methods are inherently time consuming and possess only fair sensitivity and reproducibility (80). Many workers have considered it advisable to avoid these and other difficulties by feeding the solution into the spark in some continuous manner, which would tend to limit selective volatilization.

2. Direct Methods for Solution Analysis

Various methods for direct solution analysis have been proposed by a variety of authors. Most of these methods employ spark excitation as a means for elemental analysis.

The methods that have been proposed, consist of introducing the solution into the spark in some continuous manner, and they can be divided into the following classifications: (1) spark-to-bulk liquid, (2) spark-to-liquid film, and (3) spark-to-liquid mist. The

last classification, also known as the spark-in-spray technique, is discussed in a subsequent section.

One of the earliest methods for spark solution analysis consisted of passing a spark between a solid electrode and the free surface of a liquid. Using a constant-level liquid chamber, Jolibois and Bossuet (81) were able to perform analysis with direct current excitation. Walti (82) introduced the solution to be analyzed into the lower electrode through a hole punctured in its side. Twyman and co-workers (83), by using a constant-level control, also introduced the solution through a hole bored in the lower electrode. Attempts have also been made to strike a spark between two liquid surfaces. Duffendack and Thomson (84) discharged the spark between facing capillaries through which the liquid was flowing.

In all the spark-to-bulk solution techniques mentioned above, the spark strikes a body or column of liquid, and hence a great deal of spattering occurs. If one were using corrosive liquids, as are commonly used for dissolution, spattering presents a major problem. To minimize the spattering, several techniques have been developed which introduce the liquid into the spark as a thin film which is supported on a solid electrode.

Perhaps the most common of the spark-to-thin film techniques is the rotating disc (80). The technique basically consists of a motor driven disc, which dips into the solution and carries a thin film of the liquid into the spark gap. A small volume of the solution is then evaporated by the spark discharge. Using this technique, Baer and Hoag (85) were able to obtain sensitivities

in the PPM range. Kopp and Kroner (86) used the rotating disc for the simultaneous determination of 19 elements in natural waters with a direct reading spectrograph, and obtained very good sensitivities when a preconcentration procedure was used.

As would be expected with the rotating disc technique, the thickness of the film formed is controlled not only by the speed of rotation, but also by the viscosity of the solution. Another serious problem associated with this technique is that while a fresh solution is continuously brought to the surface, the intensity of emission does not remain constant over a series of sparks because the surface to which the solution adheres is continuously being modified by the spark.

To overcome problems associated with mechanical assemblies, an introduction system based on capillary action was designed by Feldman (87). In the pourous-cup technique developed by Feldman, the solution seeps through the electrode and forms a thin film which is evaporated by the spark discharge. The pourous-cup technique, although easier to operate, still suffers from the same viscosity and electrode problems associated with the rotating disc technique.

An even simpler method of introduction, also based on capillary action, is the vacuum-cup technique developed by Zinc (88) in which a solution is brought through a fine capillary in the electrode, to the tip of the electrode continuously because some of the solution is being vaporized by the spark. Again, problems associated with spattering, viscosity, and effects due to change in the electrode shape with time, could not be overcome.

It, therefore, appears that methods involving either spark-to-bulk solution or spark-to-film techniques are not necessarily the methods of choice for the analysis of complex, solution samples. In the next section, it is shown that a method based on an aerosol technique is preferable for solution analysis.

C. Spark Through Aerosol Techniques

Workers in the area of flame spectroscopy have traditionally used an aerosol technique for analysis. Generally, a solution of the sample is prepared and the solution is pneumatically aspirated into the flame by the Venturi effect. The resultant spray is then composed of a series of liquid droplets whose size is determined by various physical parameters (89, 90).

Unfortunately, aerosol techniques have been of limited utility in spark emission spectroscopy. In this section, some of the early methods based on the spark-in-spray techniques are presented. It is also shown that an introduction system utilizing desolvation of the aerosol produced from a pneumatic nebulizer, should prove to be a valuable tool for the introduction of samples into a low energy spark discharge.

1. Spark-in-Flame Technique

Hultgren (68) overcame the difficulties inherent in ordinary spark vaporization by dissolving the sample and aspirating the solution into a flame through which a spark was passed. He concluded that the technique was rapid and could be used to give moderate

precision for the simultaneous analysis of solutions containing several elements in even widely varying concentrations.

Ludegärdh and Philipson (91) compared the spark-in-flame method to direct analysis by flame emission. They found that, of the 32 elements studied, only a few showed improved results in the spark-in-flame method. The elements that showed improved results possessed either high boiling points or formed very stable monoxide compounds in the flame. The authors concluded that the spark-in-flame method was a useful complement to flame emission spectroscopy.

2. Spark-in-Spray

Since the flame contributes little in the way of excitation energy relative to the spark, other workers have used the spark-in-spray technique directly. Uzumasa and Okuno (92, 93) sprayed the analyte solution, using air as the aspirating gas, into a 10 kV spark gap and obtained detection limits between 10^{-4} - 10^{-6} M for a variety of elements. Lamb (94) used the spark-in-spray technique for the direct analysis of Mg in blood. Using KNH_4SO_4 as a spectroscopic buffer and as an internal standard, Lamb was able to determine Mg in the 10 PPM range with a relative precision of about 2%. The technique was also applied by Malmstadt and Scholz (95) to the determination of vanadium and iron impurities in $TiCl_4$ solutions, using Ti as the internal standard. Employing a commercial Beckman atomizer with O_2 as the aspirating gas and spraying the solution between graphite electrodes, the authors were able to obtain precisions of 1.2% for V and 4.8% for Fe. They, therefore,

suggested that the technique should have general application for the accurate emission spectrochemical analysis of solution samples.

More recently, Kobayashi (96) used the technique for the direct determination of Ti in steel and Hf in zircon. The authors used a Beckman atomizer and La as the internal standard, and sprayed the solution into the spark between carbon electrodes. Kobayashi obtained superior detection limits of 30 PPB for Ti and 6 PPM for Hf with precisions of about 4%, at concentrations one order of magnitude greater than the detection limit. Russian workers (97) performed spectrographic analysis of Ti alloys by aspirating solutions of the sample into the spark through hollow graphite electrodes. The design used by the Russian workers was based on the idea proposed by Owen (98) for introducing aerosols of solution into a spark excitation gap through gas transport electrodes.

There are some serious drawbacks to the spark-in-spray method. These drawbacks arise because the mist does not leave the area of the spark completely. Rather, the droplets within the mist can combine to form larger drops, which can contaminate the electrodes and the whole assembly. Barnes (64) points out that if the technique is used for continuous sample introduction, great care should be taken to ensure that the solution mist does not strike the electrodes. Scribner and Margoshes (80) stress that extreme care should be taken to avoid memory problems, while Malmstadt and Scholz (95) point out that an exhaust hood should be placed directly over the spark to collect as much of the waste solution as possible. Feldman (87) states that there will always be a

certain amount of spattering and dripping when the mist comes in contact with the solid electrodes.

Schalge (99) studied the interaction between the spark and the spray. He concluded that the sample does not appear to be atomized directly in the spray, but rather that the spray particles deposit onto the electrodes and are then vaporized by the spark. This appears to be the case if one considers that the average particle formed by a conventional pneumatic aspirator has a diameter on the order of 20 μm (100). It appears impossible that the spark could completely desolvate the 20 μm particle before it could atomize the resultant salt particle. Even if direct atomization of the spray did occur, one would be relying on the inefficient spark vaporization process discussed earlier. Coupling then all the ciriticisms presented, it would appear that for the spark-in-spray technique to show any improvement over conventional spark-solution techniques, the particle size should be decreased drastically and great care should be exercised to avoid electrode contamination. A much simpler alternative, however, would involve desolvation of the aerosol particles before the particles entered the spark gap.

3. Desolvation of the Aerosol

Desolvation systems for the removal of solvent from pneumatically generated aerosols, have been described by a variety of authors. Hell (101) was the first to describe such a system for atomic flame spectroscopy. In his system, the solution is sprayed into an infrared heated spray chamber to which is attached a condenser

for the removal of the solvent. Venghiattis (102), employing a system similar in essence to Hell's design, found that an improvement of almost an order of magnitude in sensitivity could be obtained in atomic absorption spectroscopy.

Veillon and Margoshes (103) greatly simplified the heated spray chamber and condenser design. Their design consists of a glass desolvation chamber which is heated with heating tape. The desolvation chamber is connected directly to a slightly modified Freidrichs condenser through which water maintained at 10°C is passed. The total system is simple to operate and convenient. The authors measured an overall efficiency, defined as the ratio of solute-out to solute-in, of 35% for the entire sample introduction system. This is an extremely high efficiency when compared with other spray chamber designs (104). Veillon and Margoshes (105) used the system that they had designed as the sample introduction system for a radio frequency plasma. Since their work, others (106-108) have also used similar designs to introduce material into various forms of plasmas.

Prior desolvation would seem to overcome many of the disadvantages of the spark-in-spray technique. Therefore, the desolvation system designed by Veillon and Margoshes (103) in conjunction with spark excitation should prove to be an attractive alternative.

The salt particles formed by pneumatic aspiration followed by desolvation would be quite small. For example, consider a solution of 1 PPM of Mo. An average particle diameter of 20 μm (100) before desolvation, would result in (assuming complete solvent

removal), a dry salt crystal with a roughly spherical shape (101) and a diameter of about 0.1 μm. The dry salt crystal would weigh only 4×10^{-15} g and would contain only 2.4×10^{7} atoms of Mo. Hence, rather than appearing as a droplet which weighs some six orders of magnitude more and is an appreciable fraction of the carrier gas by weight, the dry particle would appear as a microscopic impurity in the carrier gas. Therefore, the possibility of the particle changing the excitation characteristics in the spark gap would be eliminated.

With an introduction system based on the design of Veillon and Margoshes, it has been found that there exists no need for internal standardization. Also, as is shown later in this work, the emission from the spark, disregarding the emission of the sample, is completely unchanged even if samples containing large concentrations (up to 200 PPM) of salts are aspirated.

Marinkovic and Vickers (109) were the first to apply the introduction system of Veillon and Margoshes (103) to an electric discharge. In their system, solutions are pneumatically nebulized into a nebulization chamber. Attached to the nebulization chamber is a desolvation system similar to that used by Veillon and Margoshes. The dry salt particles that leave the condenser are swept by the argon nebulizing gas into a long-path DC arc. Calibration curves for the elements in the solution sample are then obtained by atomic absorption spectroscopy. In their application, the arc was merely used to atomize the dry salt particles, while a hollow cathode lamp was used as a radiational excitation source. It would have been

equally feasible to obtain analytical data directly by arc emission. However, in that case the irreproducibility of the arc would have limited the sensitivity.

Aside from the work previously cited (109), there have been other uses of spark-solution techniques in atomic absorption spectroscopy (AAS). Since the principal limitation of the flame is its difficulty in atomizing refractory oxides, Robinson (110) replaced the flame with the spark and used the spark-in-spray technique as the atomization source in AAS for the analysis of Al. Using a hollow cathode lamp as a primary radiation source, Robinson was able to detect 3 PPM of Al.

On the other hand, Strasheim and Human (111) devised a unique system in which a time-resolved spark was used as a primary radiation source for multielement atomic absorption analysis. In their system, the elements of interest were introduced into the spark by the rotating disc solution technique, while the sample under investigation was atomized into a long path length flame. Through the use of time-resolution, the authors found that even though the absolute emission from the spark decreased as a function of time, the absorption by the sample in the flame increased with time. They attributed this behavior to the well-known effect (112) of the increase in the singal-to-background ratio emission observed during the later stages in the spark period.

Regardless of whether the spark is used as a primary radiation source for AAS or as the emission source in conventional emission

spectroscopy, to obtain maximum sensitivity, the emission should be isolated in time by time-resolved techniques.

D. Time-Resolved Spectroscopy

Workers in the area of plasma physics have used time-resolved techniques to characterize plasmas by means of radiation-time profiles. Time-resolved plasma emission data can be used for ion and electron concentration measurements, partition function calculations, temperature measurements, and Stark effect line shifts and/or line broadening measurements. Since the conditions in a spark plasma vary continuously with time, it would be of great advantage to be able to examine the spectra emitted at different stages of the "on-time" of the spark.

Various forms of "time-resolution" have been used by analytical chemists to improve sensitivity in spark spectrochemical analysis. Two different approaches to time-resolution have been proposed in an effort to increase signal-to-background ratios (S/B). In one approach, which we shall call time-slicing, the emission from the spark is continuously integrated from a preselected time after spark initiation. Hence, in this approach the emission from the early portion of the spark is suppressed while the remainder of the emission is detected. In the second approach, which shall be termed time-resolved, the emission is integrated over some preselected time interval. Hence, integration of the emission begins at one preselected instant in time and is stopped at a second instant in time.

The two approaches for emission monitoring as a function of time have been used with two types of detection systems. Both multichannel and single channel detection systems have been employed with a variety of time-resolving elements and these are described in the section to follow.

1. Multichannel Detection System

Multichannel detection, consisting of either a prism of grating spectrograph for wavelength dispersion and standard photographic recording, offers the experimenter the advantages of simultaneous wavelength recording. The time-resolving methods commonly used with multichannel detection include the rotating disc, the rotating drum or moving film, the electro-mechanical and electro-optical shutters, and the rotating mirror.

In an air spark discharge, it has been known for a considerable time, that atmospheric lines and continuous background disappear before the arc lines of the metal are fully developed. The earliest reported observation of this was obtained through the use of time-resolution studies with a moving film (113). The moving film technique was first applied to qualitative analysis by Dutton (114).

In moving-film spectrographs, the spectral time history of an event can be obtained in several ways. In one, a framing process produces a large number of discretly exposed, individual, sequential spectra on the same film strip. In another, spectral images produced by a pinhole entrance aperture are recorded with

the moving film technique to give a streak spectrogram with a continuous time-axis. Similar results can be obtained through the use of the rotating-film technique (115) for which a maximum time resolution of 10^{-7} μsec has been reported.

As opposed to continuous time recording, electro-optical and mechanical shutters can be used to obtain a "snapshot" of the emission at a particular instant in time. Electro-optical shutters (116) have been used for the study of spark discharges since 1926. The shortcomings of electro-optical shutters were discussed in Part I of this work and will not be repeated here. Mechanical shutters are of limited utility because their switching times give opening times on the order of 40 μ sec (117).

The most common method of time resolution involves the use of a rotating mirror as the time-resolving element, which has been completely described by Bardócz (118). Using the rotating mirror as the time-resolving element, Bardócz and co-workers (119, 120) have conclusively shown that lower detection limits can be obtained than by conventional time-integrated spectroscopy. Coupling time and spacial resolution, Walters and co-workers (62, 121, 122) have attempted to elucidate the various processes responsible for spark formation, energy transfer, and cathode sampling.

Another method commonly used for obtaining time-sliced continuous spectra, is the rotating-disc technique whose principles of operation were described by Bardócz (118). Using the rotating-disc, wherein an arbitrary time interval is screened out, workers

(122-125) have again reported that they have observed improvements in sensitivity by not integrating the initial radiation produced by the spark discharge. The reported works have demonstrated that both time-resolution and time-slicing improve the S/B and thereby the sensitivity.

In all the work discussed above, photographic detection was used so that the entire spectrum could be recorded simultaneously. The error inherent in photographic photometry is at least 2% and may be more with emulsions having much grain. Photographic detection also requires considerable amounts of time and effort for emulsion calibration.

Photoelectric detection, under favorable conditions, is capable of 0.2% precision in the measurement of line intensities, and this will be reflected in improved precision in analysis, when the precision of the intensity measurement is the limiting factor. When necessary, provision can be made for integration of the emission signal over some preselected period of time. With photoelectric detection, it is relatively simple to achieve time resolution since electronic methods of resolution can be applied directly. One limitation of the photoelectric spectrometer is that it can only make measurements at one instant in time at selected wavelengths, where slits and detectors are located. This limitation appears to be a thing of the past with the recent introduction of solid-state photodiode arrays and vidicon phototubes as detectors for spectrochemical analysis.

2. Single Channel Photoelectric Detection

Methods of time resolution obtained with photoelectric detection are described extensively in the literature. Perhaps the easiest method for time resolution is direct oscilloscopic observation. Olsen and Huxford (124) directly studied the variation of ionic concentrations in a plasma produced by a flash discharge through neon and argon at low pressure. Tsui-Fang, et al. (125) used the oscilloscopic method to study transient effects in short spark discharges. Walters (126), with state-of-the-art instrumentation in the form of a sampling oscilloscope, studied the production and properties of a spatially stabilized atmospheric pressure spark discharge with time resolution in the sub-nsec range.

The technique of photomultiplier gating was used by Crosswhite and co-workers (127) as a time-slicing technique for the analysis of silicon in iron samples. Spark excitation and single channel detection were employed. Linear working curves were obtained when the initial portion of the spark was suppressed. The authors claimed that "for spectrochemical analysis purposes, the spectrum recorded photoelectrically combines the stability and reproducibility of the condensed spark with the sensitivity of the DC arc."

Time-resolving techniques based on photomultiplier gating have also been recently applied to spectrochemical analysis by Schroeder (128) who showed that great improvements in the S/B could be obtained with time resolution, using an integrating direct-reading spectrometer. In his system, a series of photomultipliers was

sensitized simultaneously for certain specific periods of time after the onset of individual sparks. Schroeder showed, for the analysis of one percent copper in aluminum, that improvements in signal-to-background ratios on the order of 100 times could be obtained for the Cu resonance line at 324.7 nm, at 2 μsec after spark initiation.

The stroboscopic principle used by Schroeder (128) was originally used by Steinhaus and co-workers (129). Their design philosophically preceded the modern sampling oscilloscopic technique by defining the principle of time-gated repetitive signal integration. In their design, the amplifier which followed the photomultiplier tube was "sensitized" for a desired time interval and outside this time interval amplification of the photocurrent did not occur. Both the length of the time-window where amplification occurred, and the delay in time from some fixed zero position (chosen as the spark breakdown), were under the control of the experimenter.

The instrument that they described could be used in two ways. First, the time-window is held fixed at some instant in time and the wavelength changed so that a scan is made across the spectrum. This, then, will produce a time-resolved spectrum of the emission at a point in time integrated over that time-window. Hence, spectra similar to those obtained in Figure 16 and Appendix A will result, but with a longer integration time of about 0.5 μsec. The other approach is to move the time-window with respect to time zero, and to record the emission at a fixed wavelength as a function of time.

If the photocurrent from a single spark was directly transmitted to the readout system, the system of Steinhaus and co-workers (129) would have no advantage over oscilloscopic detection. What Steinhaus and co-workers did was to average over a number of sparks at identical points in time. To accomplish this, the authors set the spark repetition rate at 240 sparks/sec and used a recorder with a time constant of one second. Hence, the time constant of the recorder averaged 240 sparks taken under identical time and wavelength conditions. Since the system amplifies the output current from the photomultiplier tube only during its aperture time while the spark is on, there is little effect from dark current. The critical factor to the successful utilization of this approach for investigating time-dependent radiation emitted from the spark is that the radiation intensity, and consequently, the general physical conditions in the spark gap, must remain identical over the entire time required to obtain the spectra.

Using a short duration spark in air to a copper containing matrix, the authors (129) obtained the total spark emission at various points in time. The data obtained led them to the following conclusions:

1. "At early times (less than 2 μsec) air lines predominate and some of them are very broad."

2. "In addition (to the air lines) there are a few Cu II lines and a strong continuous background while the Cu I lines are virtually absent."

3. "After 5 μsec, the air lines and the continuous spectrum are greatly reduced in intensity, while Cu I lines appear as the strongest lines."

4. "In the later stages, the Cu I lines are the only ones remaining and the spectrum cannot be distinguished from that of a DC arc."

5. "The spectrum of the total spark light is a superposition of all stages with strong emphasis on the early ones because the light is then the strongest."

The full impact of this has largely been ignored since 1953. Walters (130) argues that the conclusions drawn by Steinhaus and coworkers definitely do not reflect the mechanism active in a high peak current, long duration spark. Walters' argument is correct. However, the major reason for using a high current, long duration spark is so that more material is eroded from the cathode in a single spark, since the amount of vaporized material is directly dependent on the number of coulombs delivered during the spark (130). Therefore, to improve sensitivity, the experimenter is required to use large power supplies with all their inherent disadvantages, as was stated before.

It is shown in a later section that when an external system is used for vaporization, a low energy spark can be used for excitation. The conclusions drawn by Steinhaus, et al. (129) are then quite valid. In fact, it is shown that when an external vaporization system is used the low energy, high power spark gives much better sensitivity with much better precision than the arc.

Applying state-of-the-art technology, Walters (131) and Piepen and Schroeder (132) modified the system designed by Steinhaus, et al. (129) and constructed an electronic time-resolving element based on a gated-integrator. The operation of the system is similar to the one proposed by Steinhaus, et al. except that field-effect transistors and integrated-circuit monostables replaced the vacuum tubes used by Steinhaus and co-workers (129). Piepen and Schroeder (132) applied the system that they had developed, to the study of emission analysis using a Q-switched laser (133, 134) as a vaporization and excitation source.

Working in the same laboratory as Piepen and Schroeder (131), Strasheim and Blum (135) used the time-resolving system for the study of a medium voltage spark with a six channel direct reading spectrograph. The six photomultipliers were under the control of six identical time-resolving systems. Using a test material consisting of 5% copper in aluminum discs, the authors concluded that for good reproducibility and sensitivity, the spark parameters must be chosen so that a uniform evaporation of the sample material takes place. From their observations the authors concluded that it is most important to select conditions for a spark to give "constant sampling effects." Since the characteristics of solid sampling by the spark change as a function of sparking time, the criteria stressed by Strasherm and Blum are quite difficult to meet.

In fact, work done by Morrison and co-workers (136, 137) in spark source mass spectrometry have shown that for the analysis of nonconducting samples, very extensive homogenation procedures,

requiring many hours, must be used. Also, Colby and Morrison (138) have found that, since the electrode distance changes as a function of sparking time and therefore the energy of the spark changes, in order to obtain increased precision, an automatic spark gap controller is essential.

Hence, to avoid the extensive extra circuitry required for an automatic spark gap controller, which is needed when the spark is the vaporization tool, the sampling process (vaporization step) must be done external to the spark. The spark would then only be required to atomize and excite the sample. The energy requirement would then be reduced substantially and hence relatively small power supplies would be adequate. Since very low energy would be dissipated, the shape of the electrodes (if a material of sufficient hardness such as tungsten is chosen) would remain unchanged for a considerable sparking time. Also, the need for a control on spark gap distance would be allayed since the distance would remain constant if no electrode material were sputtered off.

From the information presented it is obvious that the emission must be observed with some form of "time-resolution" which entails either time-slicing the initial portion of the spark, or time-resolving the emission so that only a selected fraction of the spark's "on-time" is observed. Also, solution techniques, because they offer relief from inhomogeneity problems and because they are easy to work with, should be the method of choice whenever possible. The solution approach should be coupled with an aerosol generator

and a desolvation system so that the spark is presented with dry, salt particles of the sample for analysis.

If a solution approach is not feasible, the author believes that the use of an aerosol generated from a solid would also be feasible as an introduction scheme for the spark source that is described. An instrument capable of forming fine particles (~ 2 μm diameter) directly from a solid sample has recently been described (139) and was used as a sampling technique for flame atomic emission and atomic absorption spectroscopy (140). The direct application of the aerosol generator to the miniature, high power, low energy spark source seems to be a logical extension of the work presented here.

III. EXPERIMENTAL

A. Sample Introduction System

The introduction system chosen for the miniature spark source, for the spectrochemical analysis of solutions, is shown in Figure 17. The system is similar to that described by Veillon and Margoshes (103) in that a dry aerosol generating system, employing a pneumatic aspirator, a heated spray chamber and a condenser, is used.

The solution sample is aspirated by an argon stream into the heated spray chamber. There the droplets of solution are desolvated, and the remaining dry salt particles and the solvent vapor are carried by the argon stream into the condenser, where the solvent vapor is condensed and removed while the dry salt particles remain in the argon stream. From the condenser, the dry salt particles and the argon carrier are sent into the spark through an introduction tube.

Argon was chosen as the aspirating gas to minimize oxidation, quenching problems, and spectral interferences. To perform spectrochemical analysis of carbon and phosphorous, it is necessary to eliminate both oxygen and nitrogen (141) in order to observe the ultraviolet lines of these elements. Also, Scribner (142) has found that there appears to be a reduction in matrix effects when sparking

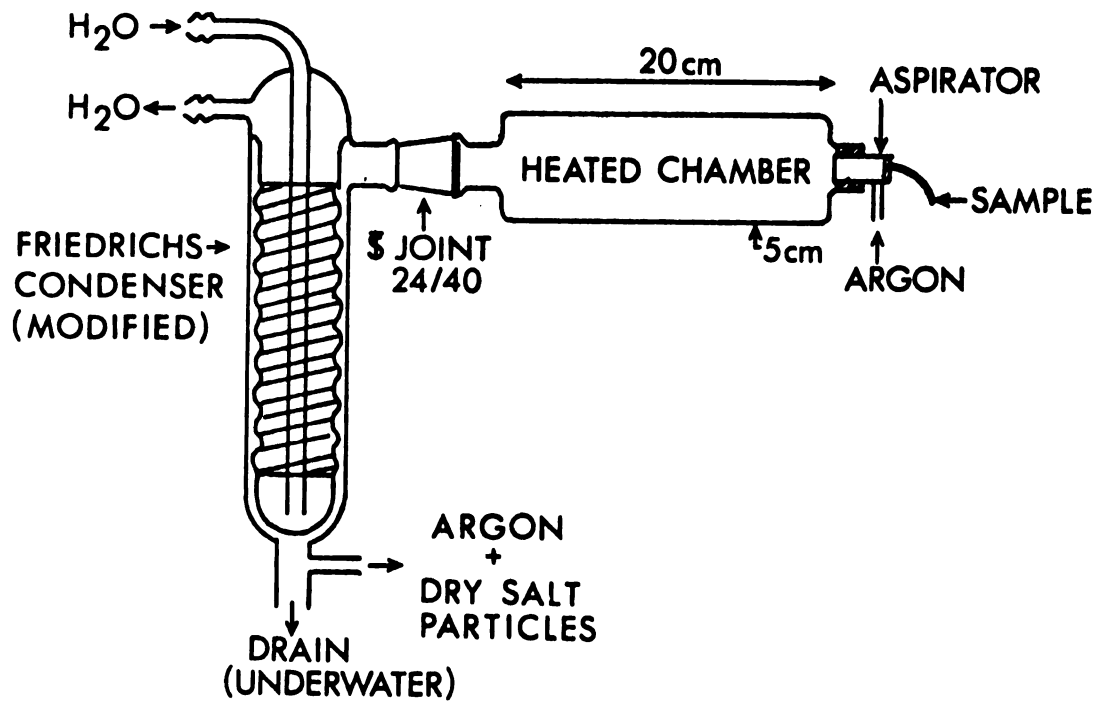

Figure 17. The introduction system chosen for the miniature spark source.

in an inert atmosphere. Both the breakdown voltage and the electrical-to-optical conversion efficiency are lower for argon than for air (50), and, therefore, the spark's background emission should be reduced in argon. Since argon is an atomic gas, the background spectrum is free from band emission. Argon also possesses a very low quenching cross-section (2) which lowers the probability of collisional deactivation. The argon used in this work was 99.995%, High Purity Grade, argon from Airco.

1. The Solution Nebulizer

The nebulizer used in preliminary studies was constructed by removing the fuel jacket from a Beckman #4020 total consumption burner and attaching the remaining portion to the heating chamber. The efficiency of the introduction system, defined as the percentage of the metal in the aspirated sample solution which emerges from the condenser as dry salt particles (i.e., metal out/metal in), was determined. The efficiency was measured indirectly (103) after nebulization of a 50 ml sample of 100 PPM Cd. The condensate was collected and washings of the condenser, heated chamber and nebulizer were added to the condensate. The resultant washings were then analyzed by atomic fluorescence.

When the Beckman atomizer was used, the efficiency was only 10%, because the Beckman atomizer operates at very low pressure, (20 PSI), which results in the formation of relatively large diameter solution droplets. If a particle is not desolvated before it strikes the walls of the glass heating chamber, it will stick to the glass

chamber walls and be lost. To increase the desolvation rate and, hence increase the introduction efficiency, the particle diameter must be small.

Nakiyama and Tanasawa (143) have shown that the Sauter (volume/surface) mean diameter of particles formed in a spray nozzle is inversely related to the velocity of the gas flow. Also, the Poisiuille equation (90) states that in order to increase solution flow rates, through the Venturi effect, the pressure differential between the entrance and exit gas ports must be increased. On the basis of these two facts, an atomizer was constructed similar to that of Veillon and Margoshes (103). With this atomizer, a large pressure differential exists across the nozzel, which produces a high velocity gas flow and small analyte droplets.

The pneumatic nebulizer constructed is shown in Figure 18. The inner capillary tube is positioned 0.15 mm above the annular opening so that maximum suction pressure can be attained (104). The nebulizer is operated at a high pressure of 3.5 kg/cm^2 (50 PSI) which causes the high gas velocity through the small diameter annular opening that is required to produce the small size droplets. The annular opening is shown by the shaded outer area in the enlargement shown in Figure 18, while the inner diameter of the capillary tube is shown by the shaded inner area. The capillary and the disc at the orifice are made of stainless steel to resist corrosion. The very thin capillary tube is tapered at the bottom of the aspirator for increased mechanical strength. To couple the aspirator to the heating chamber, a tapped steel ball-joint is screwed on the threads

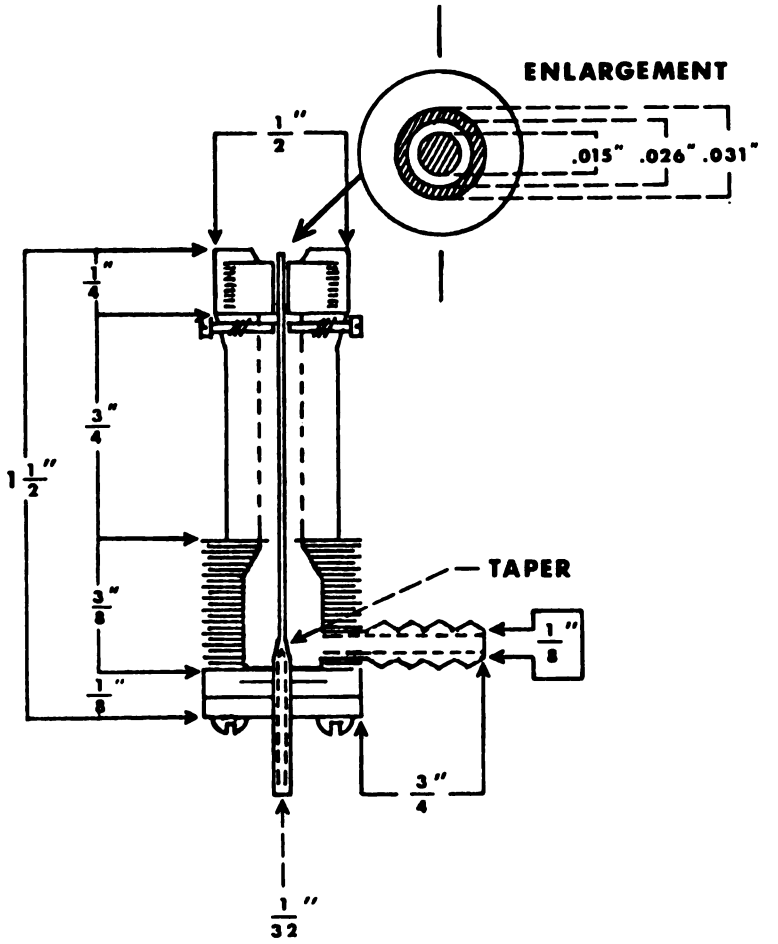

Figure 18. Construction details of the pneumatic nebulizer.

provided on the aspirator, which is fastened to a ground glass socket attached on the heating chamber.

It was found that on operating the nebulizer at a pressure of 3.5 kg/cm^2, gas leaks, particularly around the three capillary centering screws (see Figure 18), resulted. After the capillary tube position was optimized inside of the stainless steel disc, the area around the three screws was sealed with epoxy resin. When operated at a pressure of 3.5 kg/cm^2, the flow rate of argon is 3.8 l/min while the solution uptake rate is 2.5 ml/min. Under these operating conditions, the efficiency of the introduction system was found to be 22%.

2. The Desolvation Chamber

For constant heating of the desolvation chamber, shown in Figure 17, it is wrapped with heating tape (8' x 3/4", 576 W). Since water is continuously aspirated between samples, thermal equilibrium is established inside the heated chamber. Desolvation occurs in the spray chamber, while solvent removal occurs in the condenser. The efficiency of solvent removal was studied (144) by aspirating a known volume of water and collecting the uncondensed water on anhydrone. When ambient temperature cooling water was passed through the condenser, 98% of the sample water was removed by the condenser. The remaining water vapor gave rise to a very strong OH band spectrum. According to Veillon and Margoshes (103), no OH band spectrum was observed when the cooling water to the condenser was chilled to 10°C. Hence, if the emission from hydroxyl bands interfere in the

analysis, the water can be simply and effectively removed from the sample by chilling the condenser cooling water.

3. Spark Introduction Tube

Once the dry salt particles are formed, they are carried out of the condenser by the argon carrier gas. This is then coupled with tygon tubing to the spark, through an introduction tube whose dimensions are shown in Figure 19. The area of the output port (1/8" x 1/16") was chosen so that it could completely fill the spark gap length with salt particles. Introduction tubes with smaller output areas, which could concentrate the salt particles in space, were tried. Exit port areas of 1 mm^2 or less resulted in clogging when concentrated solutions (> 50 PPM) were continuously nebulized. The introduction tube area shown in Figure 19 resulted in little or no clogging and was chosen as a compromise between ease of operation and concentration sensitivity. The introduction tube is screwed directly on the spark source in such a manner that the vertical distance between the exit port and the spark gap can be easily varied. Once the vertical position has been optimized, the position is fixed by a lock-ring.

B. Spark Source

Two photographs of the spark source and positioning control are shown in Figure 20. A complete discussion of the spark source and the holder is presented in Part I of this work. Glass plates are mounted on two sides of the outer copper tube, so that the spark

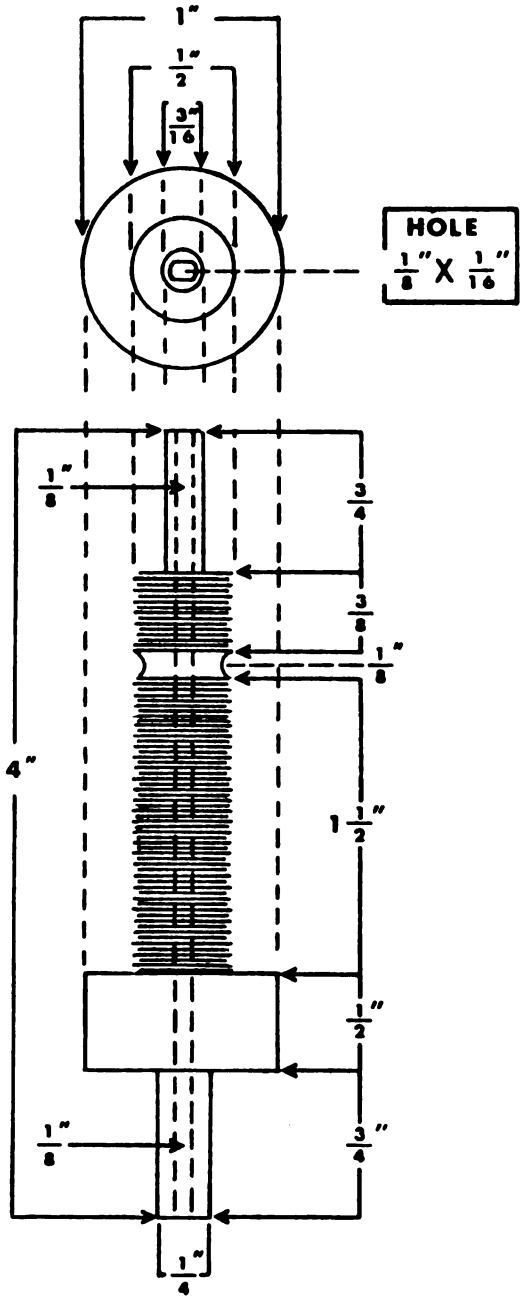

Figure 19. Construction details of the introduction tube.

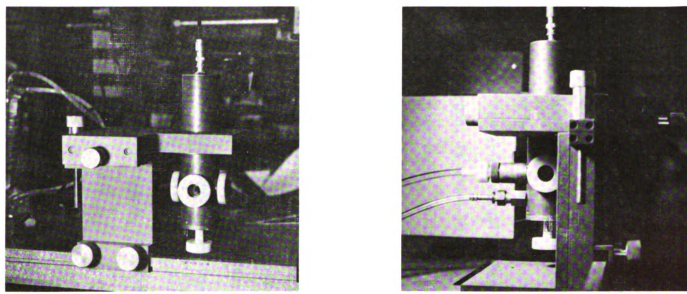

Figure 20. Photographs of the spark source and its positioner.

gap can be visually observed during discharge. On the third side, a lens is mounted to collimate the emitted radiation onto the monochromator entrance slit. The lens is positioned at a perpendicular to the introduction tube to avoid salt deposition.

The sparking lifetime of the tungsten electrodes is about 60 hours of continuous operation with an 80 Hz sparking rate. The spark source requires no physical maintenance other than the electrode replacement, after the holder position is optimized.

A diagram of the radiation visually observed while the spark discharges in pure argon, is shown in Figure 21 A. The two-pointed rods represent the electrodes, while the hash-marked area represents the introduction tube. The radiant emission of the spark is represented by the white area between the two electrodes. A constriction in the central region of the spark can be observed.

When a 20 PPM Na solution is aspirated into the heated chamber, the emission shown in Figure 21 B is observed. The entire region around the electrodes is filled with light (589 nm) due to sodium emission. The emission from the sodium extends out past the spark region, and follows the argon flow. This is also visually observed, on a much larger physical scale, in a spectroscopic plasma excitation source.

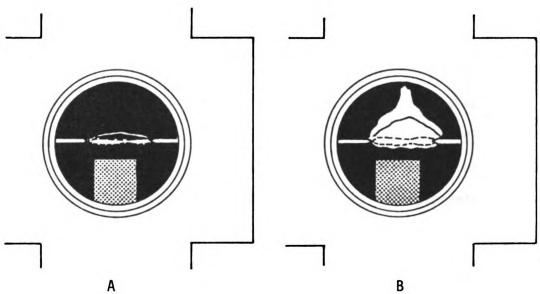

Figure 21. Diagrams of the radiation observed visually with water (diagram A) and with 20 PPM Na (diagram B).

C. Detection System

1. Oscilloscopic Detection

The detection system described in Part I of this work, consisting of a monochromator, a photomultiplier tube (PMT) and a sampling oscilloscope, was originally used to detect the emitted radiance. With the aerosol technique described above as the introduction system, the emission of the water blank and the emission from a 50 PPM Ca solution (as $Ca(C_2H_3O_2)_2$) were both monitored in time at the 393.3 nm calcium ion line. Oscilloscope photographs are shown in Figure 22 to illustrate the time course of the emission from the background (curve A), and from the sample plus the background (curve B). The solid line at the top of each curve represents the baseline for the measurements. The peak emission, shown at about 10 nsec, occurs at the time when the discharge current peaks (see Part I). Also in Figure 22, note that the time scales are 10 nsec/div in the first photograph and 1 sec/div in the second photograph, and that an 0.8 μsec time interval, between 0.2-1.0 μsec, is not shown.

In Figure 22, a comparison of curve B with curve A shows that no CaII emission is observed for the first 50 nsec. This probably occurs because in the first 50 nsec, the salt particles that enter the spark are being broken up into their elemental constituents. Also, during this period the probability of resonance emission is small because a large concentration of highly excited ions must be present to sustain the high discharge current. When the current decays, after about 50 nsec, emission

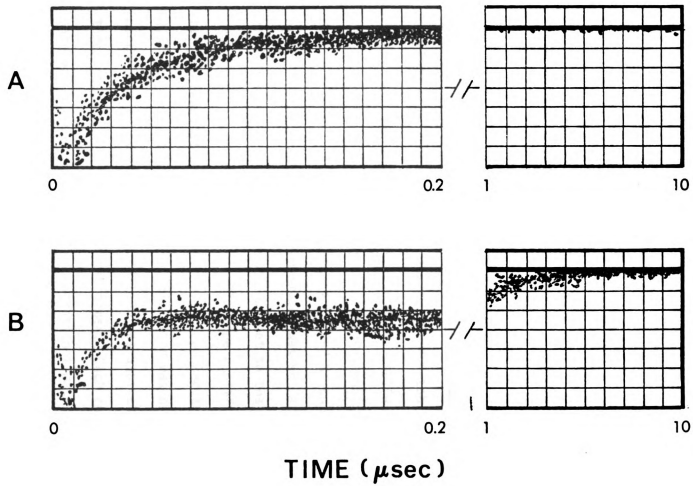

Figure 22. Oscilloscope photographs to illustrate the time course of the emission of the background (curve A) and the emission of a 50 PPM Ca sample (curve B), both observed at the 393.3 nm CaII line. Horizontal scale as noted, vertical scale 200 mV/div.

from the CaII 393.3 nm resonance line begins, after recombination of multiply ionized atoms and electrons. This is shown in the next 150 nsec when the total emission (no background correction has been made) increases sharply. Also, note from Figure 22 A that the decrease in the background level is pronounced over the first 0.2 μsec, while the decrease in signal level (A minus B) is quite small. In the later portion in time (1-10 μsec) we continue to observe an appreciable fraction of the emission from the CaII line, while almost no emission from the background.

Since photographic observations from the screen of the oscilloscope leads to large inaccuracies, it was decided that the sampling oscilloscope be interfaced to a PDP-Lab 8/e minicomputer wherein digital integration and signal averaging could be performed. The interface designed for digital integration is the one shown in Figure 4 in Part I of this work. A 20 PPM Mo solution was prepared as the test element, the monochromator was set at the 379.8 nm Mo resonance line and the slit width was set so that a 0.1 nm bandpass resulted. The output of the oscilloscope amplifier was then digitally integrated by the computer over one μsec time-windows. A 0.3 μsec delay time after spark initiation was used. To measure the background emission, a water solution was aspirated while five time integrations (runs) were performed. Each run consisted of 1000 data points, each of 350 psec integration time, spaced equally along the one μsec time-window. The computer calculated the average of the five water-blank runs and stored the result.

The same procedure was used for integrating the Mo emission. The computer then subtracted the background average from the Mo emission average. The difference then corresponded to the emission from the 20 PPM Mo solution only, and this value was stored by the computer. The average emission was printed out on a teletype along with the standard deviation (SD) and the percent relative standard deviation (RSD). In Figure 23, a typical time calibration curve is shown. The average of the emission obtained for five runs is shown by the points, while $\pm$ 1 SD unit from the average is shown by the "bars." The emission is shown at the midpoint of the integration interval of one μsec (i.e., the data point plotted at 7 μsec is the average emission observed from 6.5 to 7.5 μsec after the 0.3 μsec delay time).

Some very interesting conclusions can be drawn from the figure shown. It is clear that the emission from Mo lasts at least 10 μsec even though the current on-time is on the order of 100 nsec. Also, the RSD of all the points from two to ten μsec is between 2-5%, while the RSD of the first point (integrated from 0.3 μsec to 1.3 μsec) is 17%. This high RSD arises from the fact that the Mo emission is only a small fraction of the total emission observed. To obtain the emission signal of the sample, the emission from the blank must be subtracted. Hence, the high RSD observed is not due to the Mo emission but rather is due to the fluctuation in the spark background emission. The data shown in Figure 23 suggests that for maximum sensitivity and for precisions of 2-5%, the emission, observed from the spark during the first two μsec, must be ignored and then

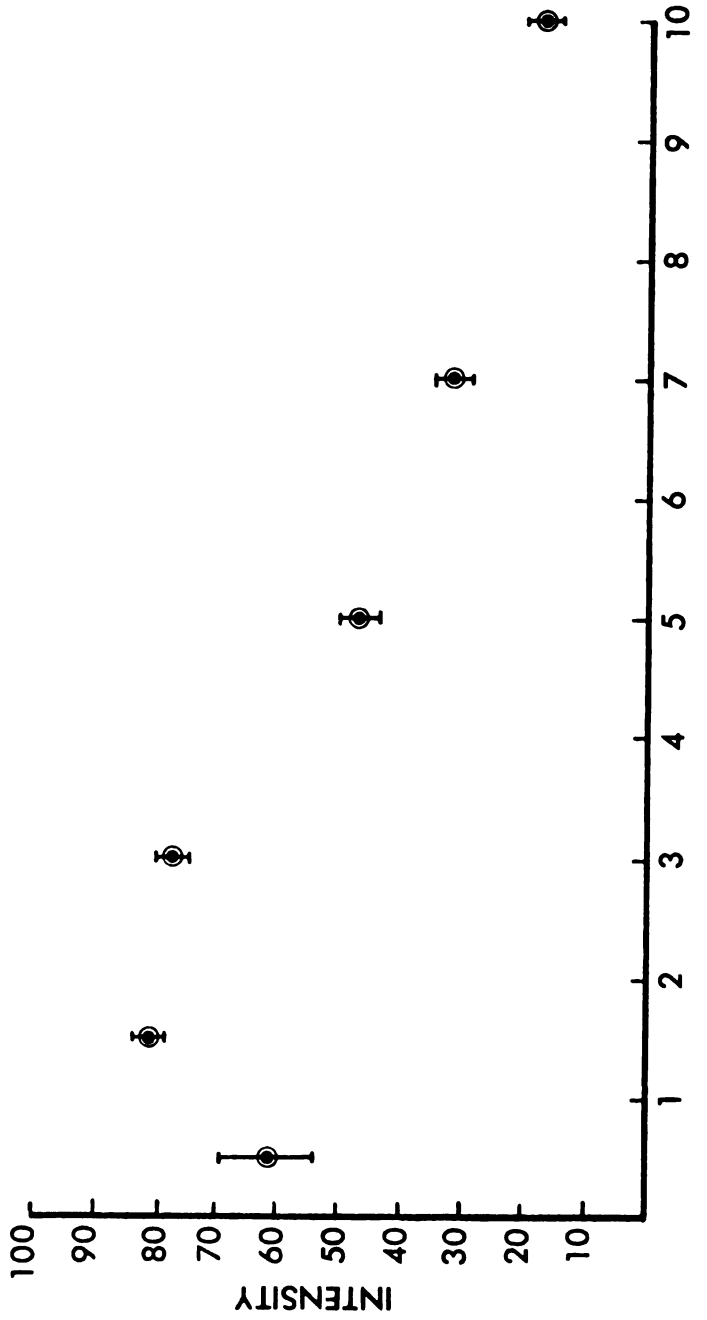

Figure 23. Time profile of the emission of a 20 PPM Mo sample in the microsecond time scale.

the emission signal from 2 μsec to at least 10 μsec (since the emission from the sample lasts at least that long) should be integrated.

Since the analytically useful emission signal is observed on the μsec time scale, there is no need to use the sampling oscilloscope for data aquisition and the computer for digital signal integration. The sampling oscilloscope suffers from the disadvantages of drift, difficulty in handling, and high cost. Also, most importantly is the fact that to obtain a total time integration of a 10 μsec signal, the time base must be set so as to take 30,000 data points (since the integration time of the 3S1 amplifier is 350 psec). This is a clear disadvantage since the emission signal is obtained each time the spark fires, while to recreate the signal with the sampling approach would require 30,000 spark firings. A gated analog integration procedure was therefore devised to make maximum use of the signal information and thereby enhance the precision of the measurements.

2. The Gated Integrator and the Related Timing Circuitry

A circuit diagram of the gated, synchronous integrator and the timing signals that trigger it are shown in Figure 24. The complete circuit was housed in a Heath model EU-801 Analog Digital Designer (ADD). Monostable multivibrators (N74121, Signetics Corp.) were placed on printed circuit boards and these boards were housed in the ADD. The operational amplifiers were Burr-Brown model 3308/12C. A Heath Company model EU-900-JA Analog Switch card was

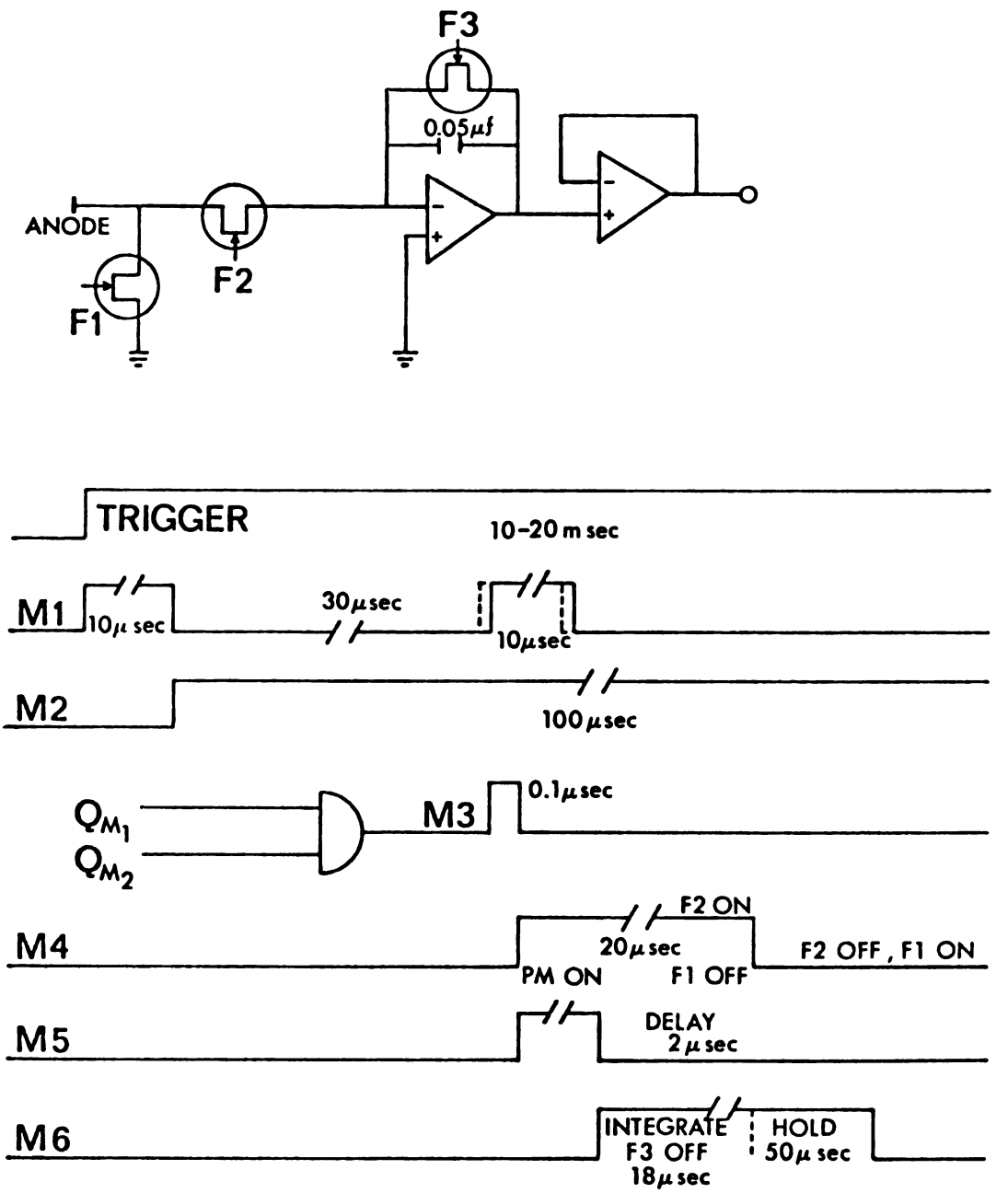

Figure 24. Schematic diagram of the gated integrator and its triggering signals.

used for the field effect transistor (FET) switches. The tranistor drivers on the Heath analog switch card were replaced with 2N4121 transistors to provide a slightly faster switching speed.

The anode of the PMT is connected to the integrator through FET 2 (F2) during some portion of the spark's lifetime. While the spark is off, F2 is open, the anode is connected to ground through F1, and the capacitor is shorted by F3. When the spark is commanded to fire by the function generator (see Part I), a signal from the sync. line of the function generator triggers a monostable multivibrator (M1). The falling edge of the output signal from M1 triggers M2.

The spark, however, fires with a time-jitter of about 2 μsec after a 30 μsec delay relative to the sync. trigger. When the spark fires, high frequency oscillations (ringing) occur in the power supply. The ringing from the power supply couples through the function generator and retriggers M1. The second pulse from M1 therefore arises from the actual spark initiation. Monostable M3 is then triggered on the rise of the output signal from M2 by the logical addition of the signals from M2 and M1.

The function of M3 is to provide a 0.1 μsec delay, relative to spark formation, which allows electrical interference to decay. M3 also functions to protect the FETs (see next section). At the end of the 0.1 μsec delay time, M4 and M5 are triggered.

The driver transistors which operate FETs F1 and F2 are under the control of M4. Once the output of M4 goes to the high state, the photocurrent is diverted from ground to the inverting

input of the operational amplifier (OA). Integration of the photocurrent does not occur at this time because FET F3 still shorts-out the capacitor. After a preset delay time, determined by the output pulse width of M5, M6 is triggered by the trailing edge of the pulse from M5. The leading edge of the pulse from M6 opens F3, and photocurrent integration begins. The integrating period is determined by the difference in time determined by the pulse widths of M4 and M5 (i.e., in the case shown in Figure 24, the integration time would be 18 μsec).

Integration is halted when the output of M4 returns to the low state, which diverts the photocurrent back to ground. The voltage on the capacitor, a value related to the integrated photocurrent, is held on the capacitor. The voltage on the capacitor is tracked by an OA voltage follower. The follower OA was sometimes wired as a follower with gain (145).

Twenty microseconds after the integration period, the output voltage from the OA follower is converted to a digital signal by the analog-to-digital converter of the PDP-Lab 8/e computer, and the capacitor is discharged shortly afterwards. This then completes one measurement cycle.

All pulse widths are variable by adjusting trimming potentiometers which vary the time constant of the monostables. Time resolution can be obtained by controlling the pulse widths of M4 and M5, and a minimum integration time of 0.1 μsec can be obtained. Under normal operation, 1000 time-integrated emission points are obtained and averaged by the computer during a 12 sec acquisition

time. The 1000 point average is called a run. Five such runs are taken and averaged, and the computer then reports the average of the runs together with the SD and the RSD. Usual integration times were on the order of 10 μsec, and, therefore, the total emission integration time for one run is only 10 msec.

3. Circuitry for Photomultiplier Tube Gating

Since the initial continuum gives rise to high PMT currents (~ 100 mA) it was decided to turn the PMT "off" during the initial portion of the spark, for protection of both the FETs and the PMT, since the PMT might go into saturation (146). Various complex methods of PMT gating have been proposed (126, 127, 147) for obtaining time resolution. Since, time resolution is obtained through the timing circuitry shown in Figure 24, and since gating is only required for protection, a simple circuit was designed for the PMT gating, and it is shown in Figure 25.

The circuit shown in Figure 25 was mounted on a printed circuit board directly in the PMT housing. The circuit was connected at the base of the PMT to the dynode (DY) chain between dynodes DY 2 and DY 4. The mode of operation of the PMT, whether conventional or gated, could be controlled with the use of a toggle switch mounted on the face-plate of the PMT housing.

When operated in the pulsed mode, the circuit is under the control of the inverted output from M4 ($\overline{M4}$). The majority of the time, the output of $\overline{M4}$ is in the high state. In this condition, the

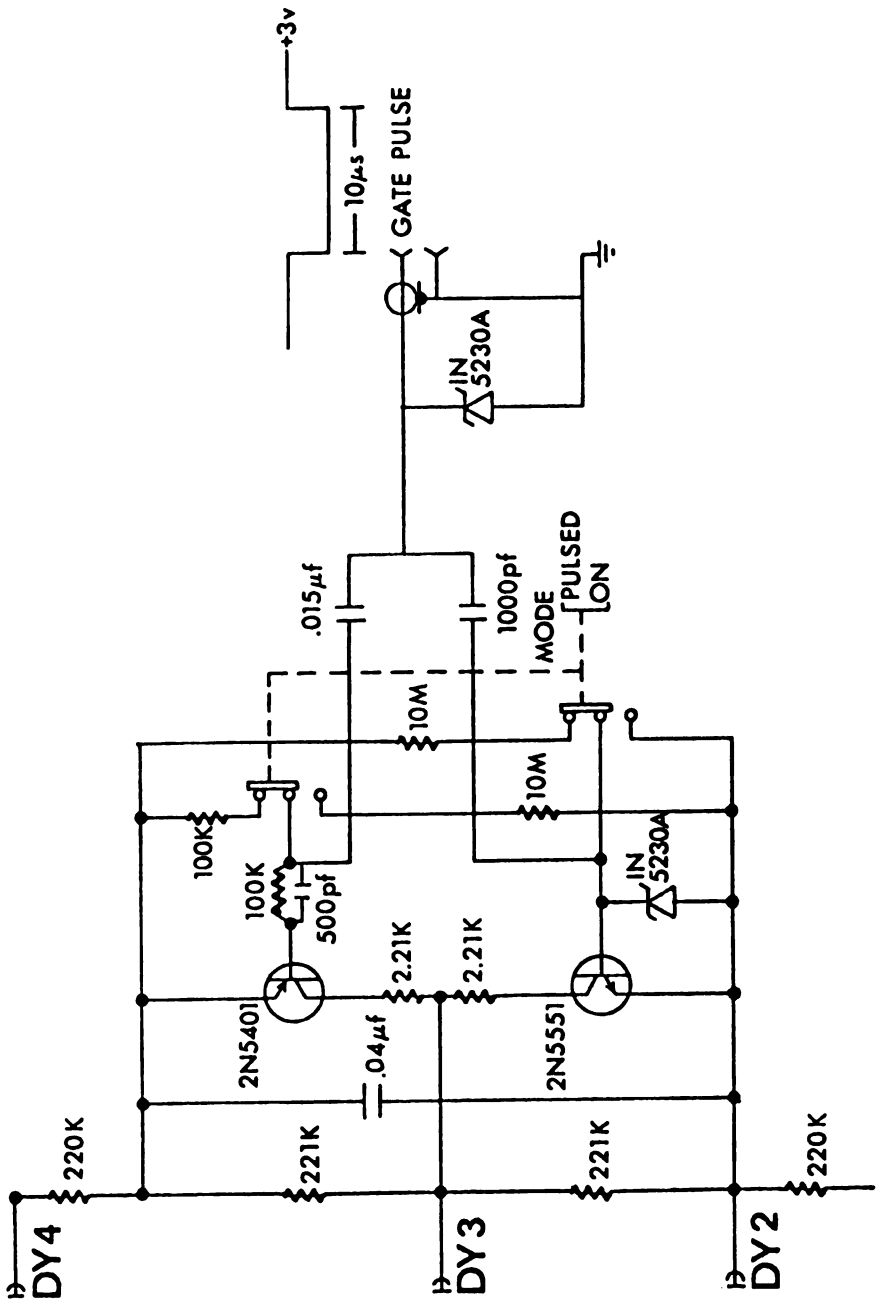

Figure 25. Circuit diagram for photomultiplier tube pulsing.

interelectrode voltage between DY 2 and DY 3 is low (~ 5V) and full electron amplification does not occur. Thus the PMT is essentially "off." After the 0.1 μsec delay, after spark breakdown, introduced by M3, the 221 KΩ "dummy" resistor located between DY 3 and DY 4 is switched into the voltage divider chain and DY 3 then becomes 150 V more positive than DY 2. Under these conditions the PMT is "on." After the photocurrent integration time, determined by M4, the PMT is switched "off." One of the two 221 KΩ resistors is always connected to the dynodes so that the PMT power supply always "sees" a constant resistance, and supplies a constant current. The last three dynodes of the PMT are stabilized with capacitors (see Experimental chapter of Part I). The reduction in gain of the PMT in the "off" state relative to the "on" state is 80%.

The pulsing of the PMT produced no ill effects, with regard to the dark current observed, over long durations. The PMT dark current was measured with a Heath model EU-703-31 photometric readout module at an anode to cathode supply voltage of 1130 V under static and pulsed conditions, and was found to be 3×10^{-9} and 1×10^{-9} A, respectively. The turn-on time of the PMT is determined by the rise times of the complimentary transistors (shown in Figure 25), and was found to be 0.3 μsec. This value was deemed adequate for the analytical determinations that will be presented. The usual operating conditions for the entire system are listed in Table 1.

Table 1. Usual operating parameters for spectrochemical determinations.

Nebulizer Pressure	3.5 kg/cm^2
Argon Flow Rate	3.8 l/min
Solution Uptake Rate	2.5 ml/min
Heating Tape Voltage	115 V
Monochromator Slit Width	75 μ m (0.15 nm bandpass)
Photomultiplier Tube Supply Voltage	1130 V
Sparking Frequency	80 Hz
Number of Sparks per Run	1000
Integration Time per Run	Variable (5-100 msec)
Total Time per Run	12 seconds
Number of Runs per Analysis	5

IV. TIME-RESOLVED CHARACTERIZATION OF THE SPARK SOURCE

Since the spark is a transitory plasma, all attempts at characterization should be made through the use of time-resolved spectroscopy. Walters (126) using nsec time resolution studied the plasma formation in a spark discharge in an argon atmosphere. His data conclusively and elegantly show that ionization of metastable argon atoms results in initial plasma production. In the spark described in this work, it has been shown that the analytical region occurs after current ceasation on the μsec time scale. It was decided, therefore, that the spark plasma should be characterized, through its optical emission, on a μsec time-resolved basis.

To obtain time-resolved, signal averaged spectra, the interface shown in Figure 5 was modified. The 3T2 time base and the 3S1 amplifier were replaced with the monostable timing circuit and the gated integrator described in the previous section. The computer was not triggered by the function generator, but rather by the high-to-low transistions of monostable M4 (Figure 24). The program and the remainder of the hardware were identical to that discussed in Part I.

As has been shown earlier in Figures 22 and 23, time resolution is required for maximum precision and sensitivity. The time-resolved emission spectra of the spark source obtained for

various integration times are shown in Figures 26-28. Spectra A-E shows the time course of the emission while spectrum F shows the total emission integrated from 2-100 μsec. In spectrum F continuum emission, emission from neutral argon (emission lines mostly around 400 nm), emission from the Balmer series of hydrogen (α - γ), and emission from the hydroxyl radical can be seen.

From the spectra shown and from similar spectra with better wavelength resolution, the plasma is characterized, in the sections that follow, according to its electron concentration, the nature and extent of processes governing the continuum emission, and its spectroscopic temperature.

A. General Spectral Observations

If one looks at the time-resolved spectra (A-E) sequentially, the following changes in the spectra are noted: the continuum decreases with time, the intensity of the argon lines diminish, the hydroxyl band emission appears late in time (spectrum C) and begins to dominate the emission observed (spectra D and E), and the emission from the H_α, H_β, and H_γ lines diminish in intensity and their widths decrease.

In spectrum A, the steep rise in emission beginning at 200 nm can be observed. This is attributed to the spectral response of the PMT (S5) and, therefore, the continuum emission probably extends into the vacuum-uv. The spectrum is continuous to about 600 nm. The cause of the continuous emission is discussed in a subsequent section.

Figure 26. Time-resolved emission of the spark source integrated from 0.5-2 μsec (curve A) and from 2-5 μsec (curve B).

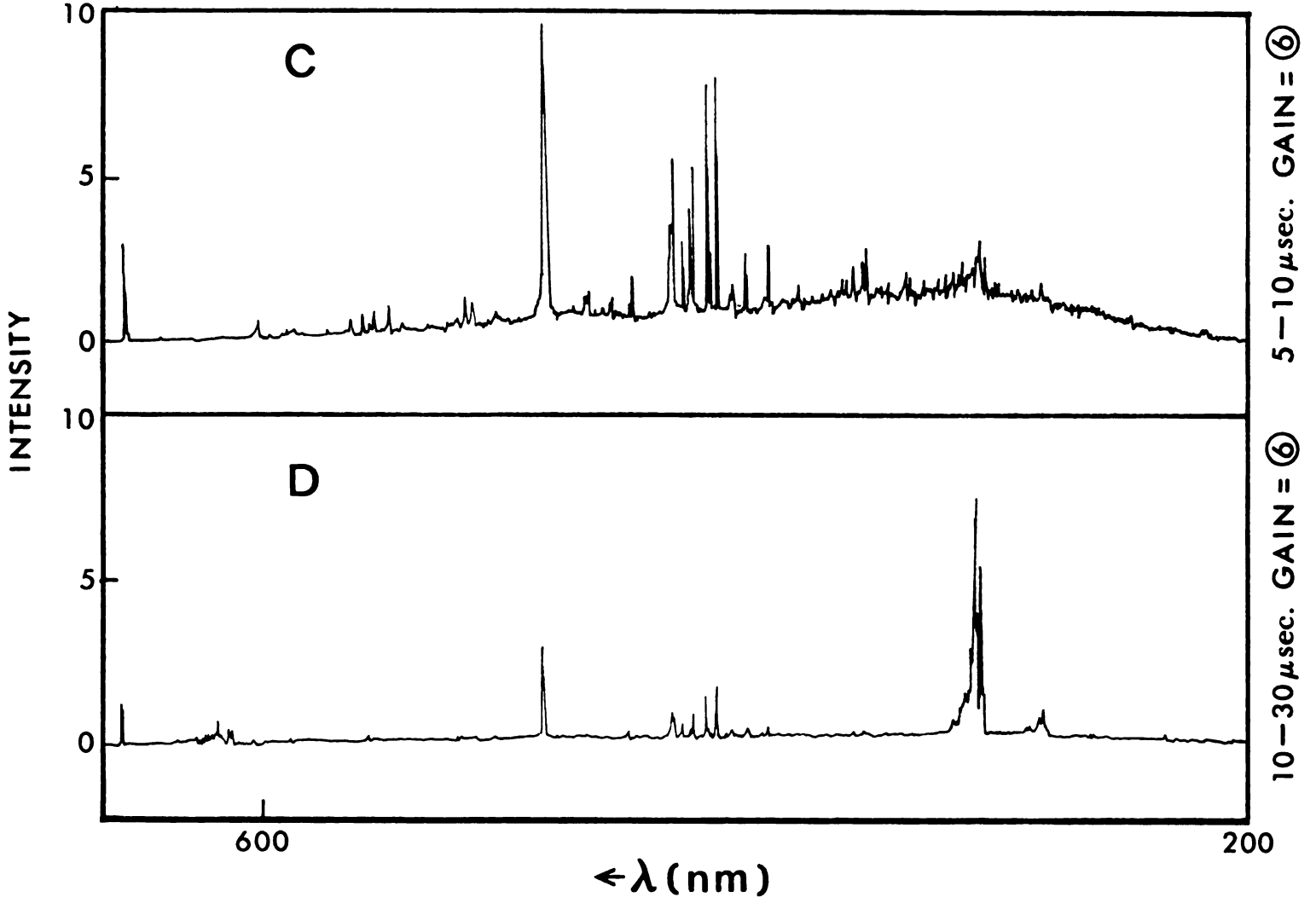

Figure 27. Time-resolved emission integrated from 5-10 μsec (curve C) and from 10-30 μsec (curve D).

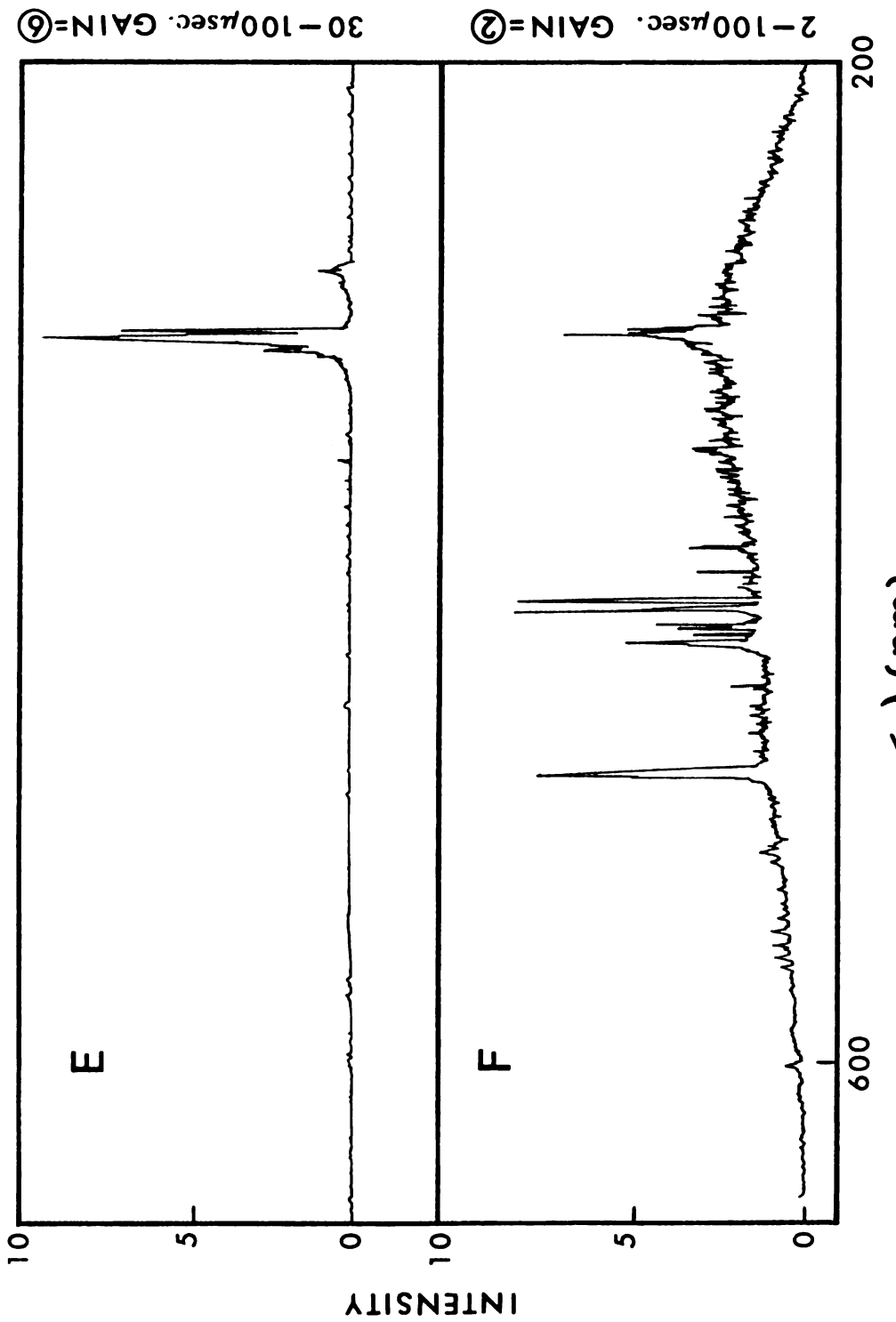

Figure 28. Time-resolved emission integrated from 30-100 μsec (curve E) and time integrated emission from 2-100 μsec (curve F).

The hydrogen lines observed result from the decomposition of the residual water which is carried by the argon into the spark. Hydrogen emission is observed very early in time, while OH bands are observed no earlier than 5 μsec. After this time, the emission from OH radicals, with band heads at 306.4 and 281.1 nm (148), occurs.

Because of the time behavior of the emission from hydrogen and the hydroxyl radical, it appears that the water vapor present in the spark is decomposed immediately at the onset of current. Barnes (64) studied the emission from a spark containing water and he concluded that in a "high energy spark" water is decomposed directly to hydrogen atoms while in a "low energy spark" hydroxyl emission is observed early in time. The spark source used in this work therefore falls into the "high energy spark" classification. This is consistant with the observation made earlier, that in the breakdown portion the spark is of very high energy. But since the on-time is very short, the correct classification for this source is a "high power spark."

The emission from atomic hydrogen is used in the next section to characterize the spark with regard to the electron concentrations. The emission from atomic argon is used in a later chapter to obtain the spectroscopic temperature.

B. Calculation of Electron Density

The dominant line-broadening mechanism in dense plasmas is Stark broadening caused by the electric fields of free electrons and ions which surround the radiating atoms. Because hydrogen is

subject to a linear Stark effect (149), the hydrogen Balmer lines, shown in spectra A-E, undergo pronounced Stark broadening, which depends almost entirely on the charged particle density. Thus, experimentaly obtained Stark-broadened emission profiles of hydrogen are used to obtain a measure of the electron density. For the electron concentration (N_e) determination, the H_β line, with emission at is at 486.1 nm, was chosen. A typical Stark-broadened emission profile of this line, observed from 5-10 μsec after spark breakdown, is shown in Figure 29. Similar profiles were obtained at times of 0.5-2 μsec, 10-15 μsec, and 15-20 μsec, from which the Stark width of the emission was calculated.

Kolb and Griem (150) developed an improved theory of Stark broadening based on the impact approximation. For a hydrogen line, one can relate the Stark width, scaled to the 2/3 power, to N_e directly through a proportionately coefficient. The coefficient's value is slightly temperature dependent. Since the slectron temperature was not known, coefficients tabulated by Griem (149) for various reasonable temperatures were averaged, and this was used to calculate N_e. Also, to increase precision three determinations were made of the H_β emission profile. Table 2 lists the results obtained for N_e at various times, and the percent relative standard deviation (RSD).

Surprisingly, considering the high RSD, the percent decrease in the electron density of 96% over the first 20 μsec agrees to within 2% of the decrease in N_e observed by Steinhaus, et al. (129), during the first 20 μsec of a critically damped spark of less than 0.5 μsec duration. The results shown in Table 2 are used in the next section

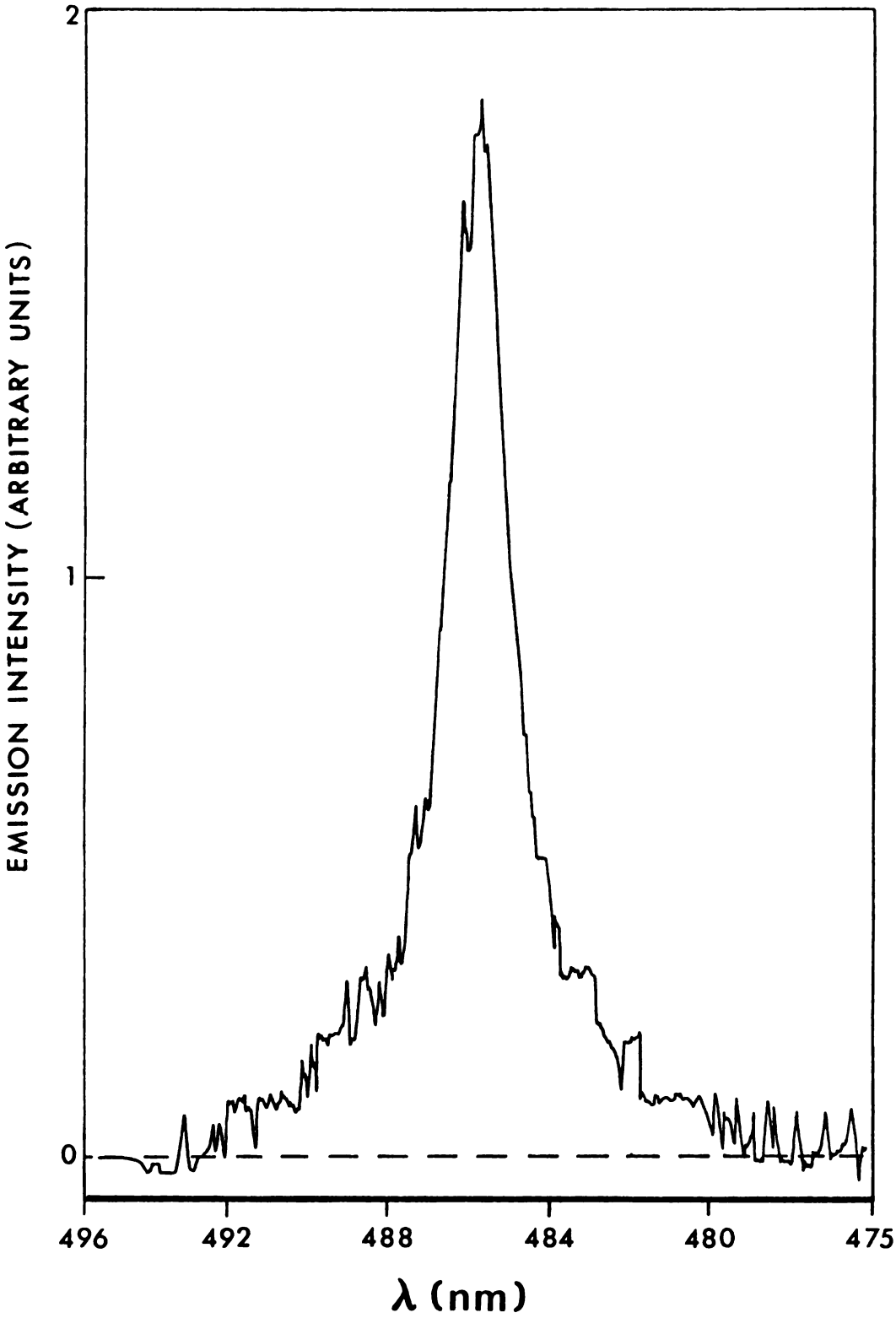

Figure 29. Stark broadened emission profile of the H_β line taken from 5-10 μsec.

Table 2. Electron concentration from Stark profiles of the H_β emission.

Time (μsec)	Stark Width (nm)	N_e(electrons/cc)	RSD
0.5-2	3.07	5.6×10^{16}	44%
2-5	1.75	2.4×10^{16}	10%
5-10	0.68	6.1×10^{15}	20%
10-15	0.43	3.1×10^{15}	20%
15-20	0.28	2.1×10^{15}	26%

in an attempt to discern the mechanisms responsible for the continuum radiation observed.

C. Discussion of the Continuum Emission

According to the theory proposed by Unsöld (152), continuum emission in a decaying plasma can arise from radiative recombination (free-bound transitions), or bremsstrahlung (free-free transitions). Radiative recombination occurs when a free electron combines with an ion into some bound state, with the excess energy being carried off by a photon. Hence the process can be expressed as

$$X^+ + e \rightarrow X^* + h\nu_{cont.} \qquad (30)$$

where X^+ in the argon spark plasma represents an ion and X* represents an excited neutral atomic state of argon, hydrogen, or oxygen. Bremsstrahlung, on the other hand, is a free-free transition in

which a free electron, that is moving inside the electric field of an ion, emits a photon and the electron thereby decays to a lower energy state.

An attempt was made to assess the relative contributions of bremsstrahlung and radiative recombination to the continuum observed from 0.5-20 μsec after spark initiation. If recombination is to play an important role as a mechanism for the production of the continuum, the recombination coefficient (α) should have reasonably large values. In Equation 30, α represents the rate of removal of electrons, or positive ions.

Olsen and Huxford (124) suggest that α can be determined from the slope of a plot of the inverse of the ion concentration as a function of time. Since it is difficult to assess the positive ion density, we can justly assume that the electron density equals the positive ion density. The values obtained for N_e (listed earlier) are used here to determine α. Figure 30 is a plot of $1/N_e$ vs. time, and α, as determined from the slope of the linear portion, is 3.1×10^{-11} cm^3/ion-sec.

Craggs and Meek (153) have discussed mechanisms of afterglows in argon and suggest that the radiation can be due to radiative recombination only if $\alpha \geq 10^{-11} cm^3$/ion-sec. It appears, therefore, that radiative recombination plays the dominant role in the production of the observed continuum emission from 2-100 μsec (spectra B-E of Figures 26-28).

Earlier in time than 2 μsec, spectrum A of Figure 26, the probability of radiative recombination would be much smaller since

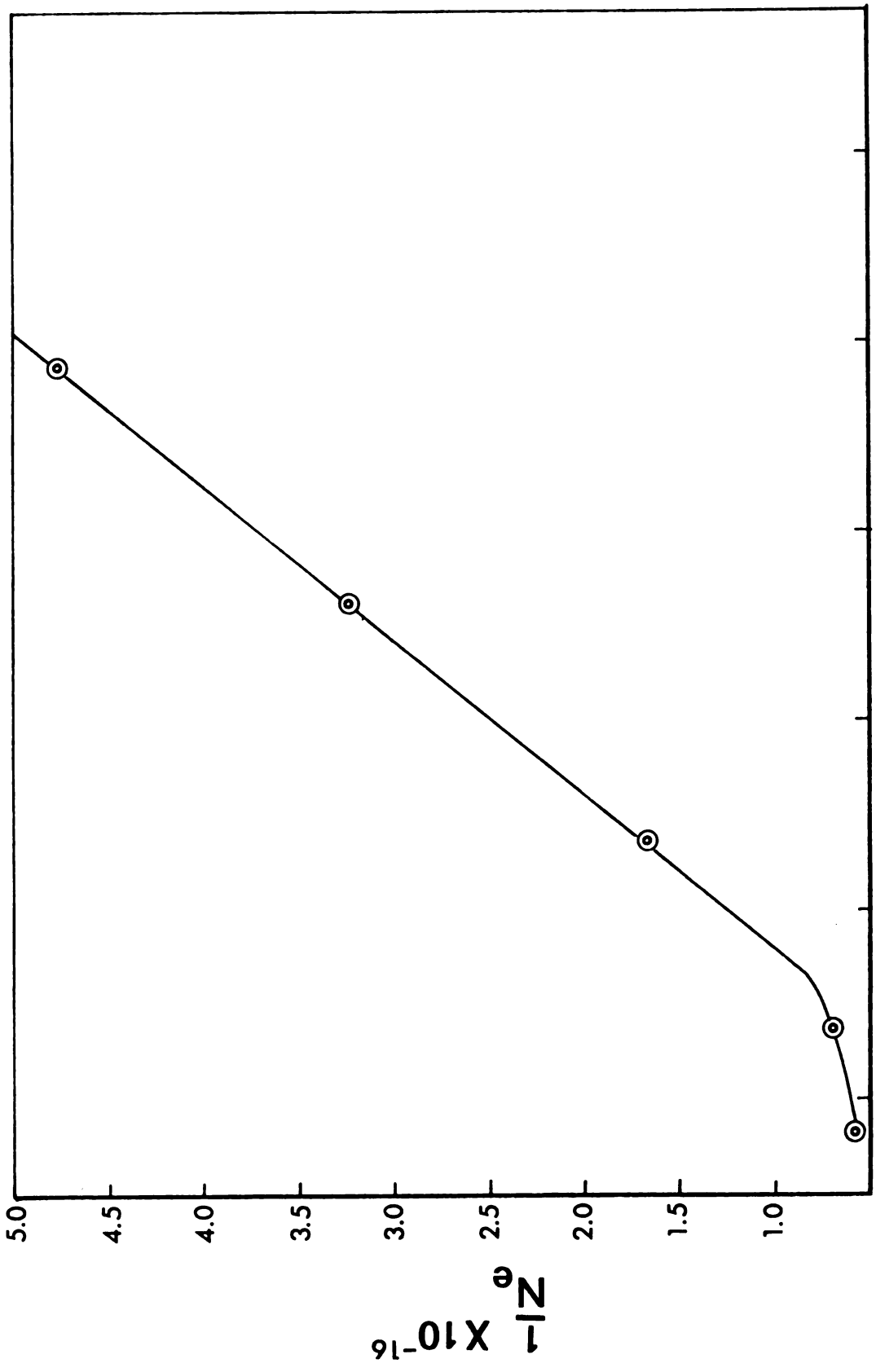

Figure 30. Plot of the inverse of the electron density as a function of time.

the electron velocities would be higher, which would prevent capture of the electron by the ion. On the other hand, the decrease in intensity associated with bremsstrahlung would not be as pronounced. In Figure 26 it is observed that the spectral distribution in the continuum has changed in going from spectrum A in spectrum B, but remains unchanged to spectra B to F (Figures 26-28).

Combining the above arguments, it appears that both bremsstrahlung and radiative recombination mechanisms are active. Both free-free and free-bound transitions appear to contribute to the continuum early in time (Figure 26A). On the other hand, it appears that radiative recombination plays the overwhelming role as the mechanism responsible for the continuum at later times (spectra B-F, Figures 26-28). This then is a plausible, though not conclusive, explanation for the observed continuum emission.

Once radiative recombination has occurred, excited states of neutral argon atoms (Ar*) are formed. These atoms can then undergo radiative transitions to the ground state, as is shown in spectra A to D (Figures 26-27). The argon emission lines are used in the next section to obtain the argon excitation temperatures at various times.

D. The Determination of the Plasma "Temperature"

1. The Spectroscopic (Excitation) Temperature

The intensity I of a spectral line of wavelength λ emitted by a transition from an upper energy level E_2 to a lower energy E_1 is given by:

$$I = \frac{CA_{2\rightarrow 1}N_2}{\lambda} \quad , \tag{31}$$

where C is a proportionately constant, $A_{2\rightarrow 1}$ is the transition probability, and N_2 is the population of state 2. For a Maxwell-Boltzmann distribution, N_2 can be expressed as

$$N_2 = \frac{Ng_2}{Z} \exp\ (-E_2/kT) \quad , \tag{32}$$

where N is total number of atoms of the emitting species, Z is the partition function, g_2 is the statistical weight of state 2, k is the Boltzmann constant, T is the temperature, and E_2 is the energy of state 2 relative to the ground state. Combining Equations 31 and 32, we obtain:

$$I = \frac{C'g_2A_{2\rightarrow 1}}{\lambda} \exp\ (-E_2/kT), \tag{32}$$

where C' = CN/Z. Rearranging Equation 32 and taking the logarithm results in

$$\log\left(\frac{I\lambda}{g_2A_{2\rightarrow 1}}\right) = \log C' - \frac{E_2}{2.303kT} \quad . \tag{33}$$

Equation 33 states that a plot of left hand side of the equation vs. E_2 will result in a straight line whose slope is proportional to the temperature.

Reif and co-workers (154) discussed the validity of the slope method for obtaining the temperature. They concluded that the method yields correct values, if the emission intensity measurements

are not affected by self-absorption, if accurate transitions probabilities are available, and if the wavelength response of the spectrometer is properly calibrated. This latter requirement can be waved if the emission lines are observed over a small wavelength interval. Knopps, et al. (155) and Tourin (156) have stated that an argon plasma is transparent below 650 nm, and the authors therefore found that negligible self-absorption occurs below this wavelength. Accurate transition probabilities for a series of argon lines observed in emission from a plasma were recently published by Adcock and Plumtree (157) and by Malone and Corcoran (158). Malone and Corcoran obtained values of the transition probability for the 5P-4S transitions of neutral argon with a minimum precision of 3.3%. The emissions corresponding to the 5P-4S transitions are observed most prominently in Figures 26-28. It was therefore decided to use a series of seven of these lines, spread over a wavelength interval of 15 nm, for the calculation of the spectroscopic temperature from Equation 33.

The data collection routine involved obtaining emission spectra from 415.0 nm to 430.0 nm. The argon emission intensities were obtained from the spectra after background subtraction. Three such spectra were obtained over each time interval, and the time intervals studied were 2-5 μsec, 5-10 μsec, 10-15 μsec, and 15-20 μsec. The data obtained from the three spectra at one interval in time were averaged,and the logarithm of the average was calculated, together with the variance of the average. Values listed for transitions probabilities were obtained from tables (158), together with the variance of the transition probability. The transition

probabilities were combined with the observed intensities in the proper form and the resulting points were plotted against the energy of the excited state (158). Figure 31 shows such a curve obtained from 5-10 μsec together with the wavelength of the argon lines used to obtain the data. The "bars" on the data points represent standard deviations which were calculated by taking the square root of the sum of the variances in the intensity and $A_{2\rightarrow1}$ (158) values. The best fit of the data points to a straight line was obtained by a computerized least squares routine. The slope, subsequently used to evaluate the temperature, was calculated by the computer. The temperatures obtained, together with the relative standard deviation (RSD) of the measurements, are listed in Table 3. Due to the high RSD (~10%), the temperatures were rounded off to the nearest 50°K.

Table 3. Spectroscopic argon temperatures.

Time (μsec)	Temperature (°K)	RSD
2-5	4300 ± 300	7.0%
5-10	4700 ± 400	8.5%
10-15	4550 ± 400	8.8%
15-20	3800 ± 400	10.5%

From the data presented in Table 3 it appears as though the excitation temperature remains relatively constant at about 4500°K

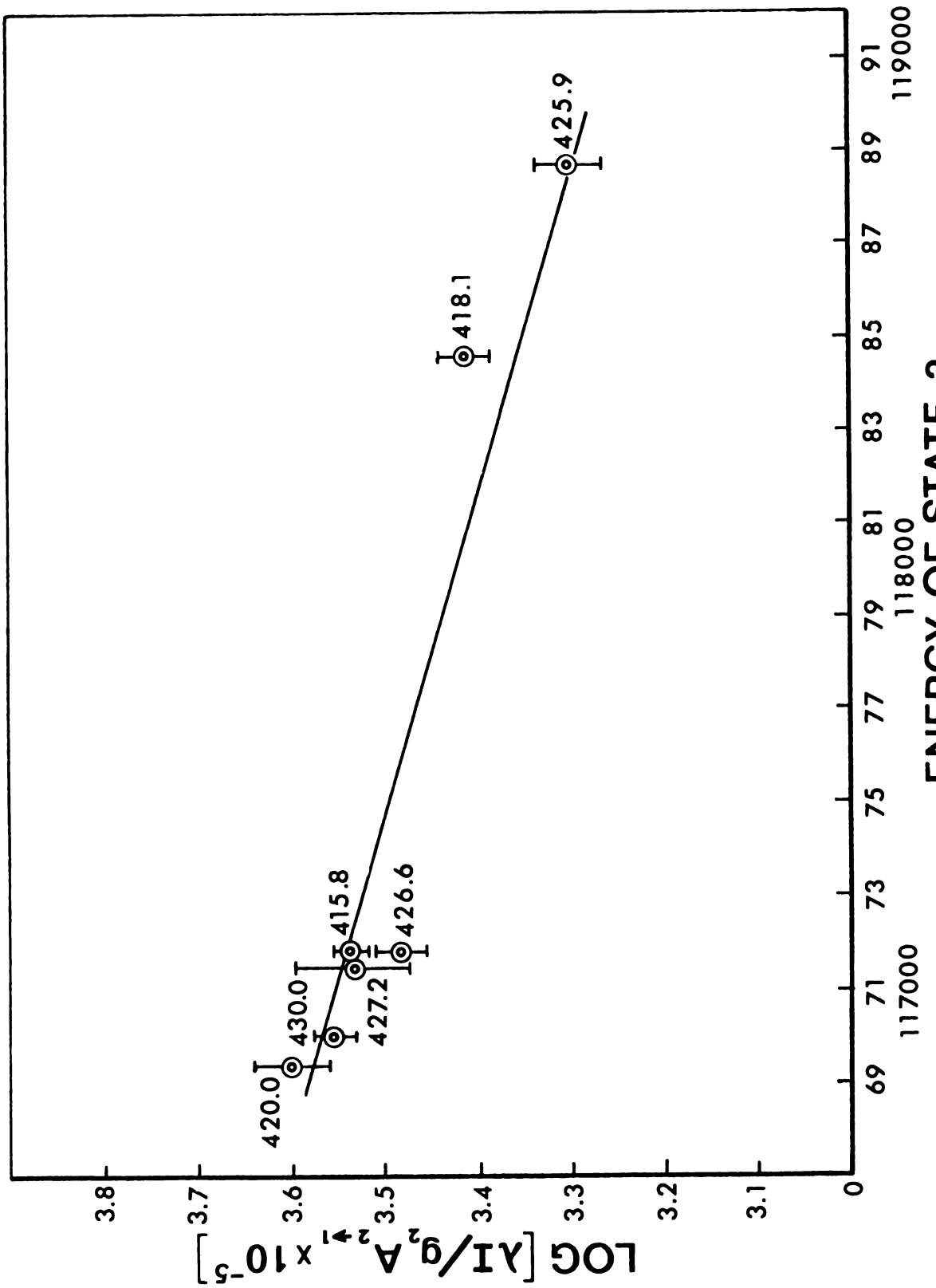

Figure 31. Slope method for various argon emission lines to determine the temperature at 5-10 μsec.

from 2-15 μsec, and then decreases over the next 5 μsec time interval to about 3800°K.

The spectroscopic temperature, observed in the time region (2-15 μsec) where the spark source is used for analyte determinations, appears to be quite similar to the temperatures obtained by workers using a microwave plasma, generated in argon, at atmospheric pressure, as a spectrochemical emission source. Taylor, et al. (159) obtained an excitation temperature of 4850°K, while Fallgatter and co-workers (160) obtained an excitation temperature of 4920°K. These workers (160) also measured the electron concentration and obtained a value of 1.8×10^{15} cm^3. Hence, the spark source described here appears to have an excitation temperature similar to that reported for the microwave plasma, but with a much higher electron density.

For a plasma in a monoatomic gas, four kinds of temperatures exist (161) each of which pertains to a distinct aspect of the physical state of the system. These four temperatures are the electron temperature, the gas temperature, the excitation temperature and the ionization temperature. If all the temperatures have the same value, the plasma is said to be in thermodynamic equilibrium. It was, therefore, decided to obtain another "temperature" to check for plasma equilibrium.

2. The Ionization Temperature

The ionization temperature was measured by obtaining the intensity ratio of the 393.3 nm Ca^+ line and the 422.7 nm Ca^0 line, when a 2 PPM solution of Ca was aspirated into the introduction system.

The parameters used to obtain the intensities are those listed in Table 1.

The degree of ionization, as a function of temperature and electron pressure (P_e), is given by the Saha relationship. Using the notation of Boumans (151), we can write that the intensity of an ion-atom pair is governed by the temperature (T) according to:

$$\log (I^+/I) = -\log P_e + \log \frac{g^+A^+_{2\to1}\lambda}{gA_{2\to1}\lambda^+} - \frac{5040}{T}(V_{ij} + V_q^+ - V_q)$$

$$+ 5/2 \log T - 6.18 , \qquad (34)$$

where the superscript "+" refers to the ions, V_q is the excitation level from which emission occurs, V_{ij} is the apparent ionization potential for the atom (and therefore contains the partition functions (161)), and all other terms have been previously defined. The apparent ionization potential for calcium, 5.83 eV, was obtained from tables of Boumans (161). Using tables complied by Corliss and Bozman (10), the gA values for the atom and ion line were found to be 1.0 and 0.91, respectively. The excited state energy levels were obtained from spectral tables (162), and were given to be 2.93 eV and 3.15 eV for the atom and ion, respectively. The electron pressure is related to the electron density by:

$$P_e = \frac{N_e T}{7.34 \times 10^{21}} , \qquad (35)$$

With time averages of electron densities from Table 2 and the combination of Equations 34 and 35, ionization temperatures were determined at time intervals of 2-15 μsec and 15-30 μsec. The results obtained, averaged for three sets of intensity ratio pairs are listed in Table 4.

Table 4. Ionization temperatures.

Time (μsec)	Temperature °K	RSD
2-15	6600 ± 500	7.5%
15-30	5150 ± 500	9.7%

Since there is a significant difference between the evaluated spectroscopic and ionization temperatures, it is obvious that the spark plasma is not in thermodynamic equilibrium. The agreement found for the excitation temperature between the spark source and the microwave plasma is not found here using the ionization temperature as a criterion (160).

From the discussion presented, it appears that the characterization of the spark plasma is not complete. More extensive work in this area is currently being performed in this laboratory. To summarize the information gained to date, the reader is referred to the spectra shown in Figures 26-28, to Table 4 and to Table 5. In Table 5 the continuum intensity is represented by the time-averaged value of the PMT photocurrent taken at a 0.15 nm bandpass and at 300 nm.

Table 5. Spark source characterization.

Time (μsec)	N_e (cc^{-1})	T Excitation (°K)	Continuum Intensity (μA, see text)
0.5-2	$5.6 \pm 2.5 \times 10^{16}$	---	5500
2-5	$2.4 \pm .20 \times 10^{16}$	4300 ± 300	1800
5-10	$6.1 \pm 1.2 \times 10^{16}$	4700 ± 400	250
10-15	$3.1 \pm .6 \times 10^{15}$	4550 ± 400	---
15-20	$2.1 \pm .6 \times 10^{15}$	3800 ± 400	20
30-100	---	---	3

V. SPARK SOURCE APPLICATION TO SOLUTION ANALYSIS

After characterizing the source and designing the detection system, it was felt that the system could be applied to spectrochemical analysis, since it possesses many desirable characteristics as an emission source. Both the time-sliced and time-resolved forms of emission observation were employed, and these will be described together with data obtained on eight test elements.

The elements chosen were boron, silcon, aluminum, phosphorous, carbon, molybdenum, copper, and calcium. Boron, silcon, phosphorous, carbon, and molybdenum were chosen because these are considered to be "refractory" elements, and are difficult to determine spectroscopically. Copper was chosen to facilitate a comparison of the sensitivity of the source with the sensitivity of conventional techniques used for spectrochemical analysis. Calcium was chosen so that both the ion and the neutral emission could be monitored. Aluminum was chosen in order to observe if there was an interelement interference by aluminum on the emission from calcium. The analytical data obtained for these elements together with interelement effects, will be discussed in the chapters that follow.

The routine precision that is obtained is 2-4%, measured at concentrations one order of magnitude higher than the detection limit. Calibration curves, signal-to-background ratio plots, tables of

sensitivities, and sensitivity comparisons will be presented in the sections that follow.

A. Spectrochemical Determinations Using Time-Slicing

It is obvious, from Figures 22 and 23, that some form of time discrimination technique is needed to minimize the initial spark background. However, the optimum position in time to begin integration was not initially known. An optimization procedure was, therefore, developed that employs the gated-integration detection system, and the parameters listed in Table 1. The test element was Mo, and a 2 PPM solution of Mo (as Na_2MoO_4) was prepared.

First a delay time of 0.5 μsec was used and the signal was integrated to 100 μsec. Then, the delay time was increased to 1.0 μsec and the signal was again integrated to 100 μsec. In this manner the initial spark background could be "blanked out." The experiment was continued for decay times up to 2.0 μsec, and the resulting data are shown in Figure 32. It is clearly shown that the extent of signal emission observed from 0.5-2.0 μsec is quite small, while the amount of background emission observed in this time interval is quite large.

The line used for the above test was a resonance line of very low energy (3.26 eV). It can be argued that the signal-time profile shown in Figure 32 might be peculiar to low energy lines, and if a transistion were observed from a relatively high energy state, the emission might be observed to decrease quickly with time. To

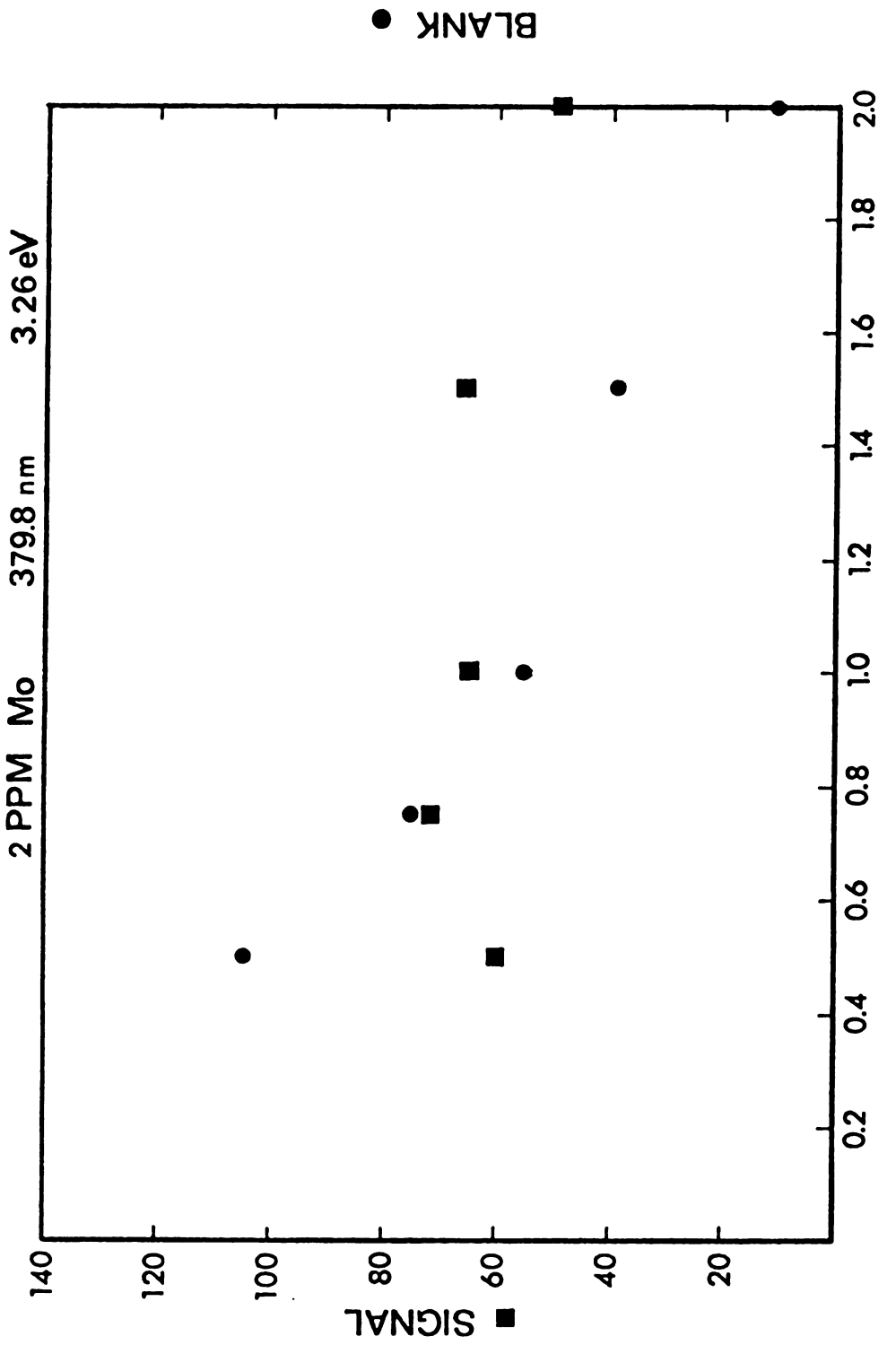

Figure 32. Signal and background plots for a 2 PPM Mo solution from 0.5 to 2.0 μsec.

check the validity of this argument, a curve similar to Figure 32 must be obtained for a high energy transition.

The 247.8 nm emission line of carbon is a nonresonance line which is produced by a transistion from the $^1P_1$ state, whose energy is 7.68 eV above the ground state (163), to the $^1S_0$ state. To obtain the emission-time profile of a high energy line, emission from the $^1P_1$ state of C was monitored. The most convenient, controlled source of carbon is the trace impurity (~50PPM) of carbon containing species in the argon tank and this was used to obtain the data. Figure 33 is a plot of the signal emission observed at 247.8 nm. The data shown in Figure 33 were obtained under conditions similar to those used to obtain Figure 32 except that the introduction system was by-passed and the argon flow rate was reduced to 1.7 l/min.

It can be seen by a comparison of Figures 32 and 33, that the rate of decay of the sample's emission signal is never larger than the rate of decay from the background during the initial 2 μsec period. One will also observe that the carbon line has decreased a proportionally larger amount than the Mo line in the 1.0-2.0 μsec time interval. Data similar to that shown in Figures 32 and 33 were obtained for the Cu 324.7 nm line, the Al 396.1 nm line, the Ca 422.7 nm line, and the Ca^+ 393.3 nm line. From all the data, it was found that the rate of decay of the background was always larger than the rate of decay of the signal, over the first 2 μsec. It must be stressed, however, that the emission from each element, and for that matter each line of each element, has its own characteristic decay rate. The decay rate of the emission appears to be directly related

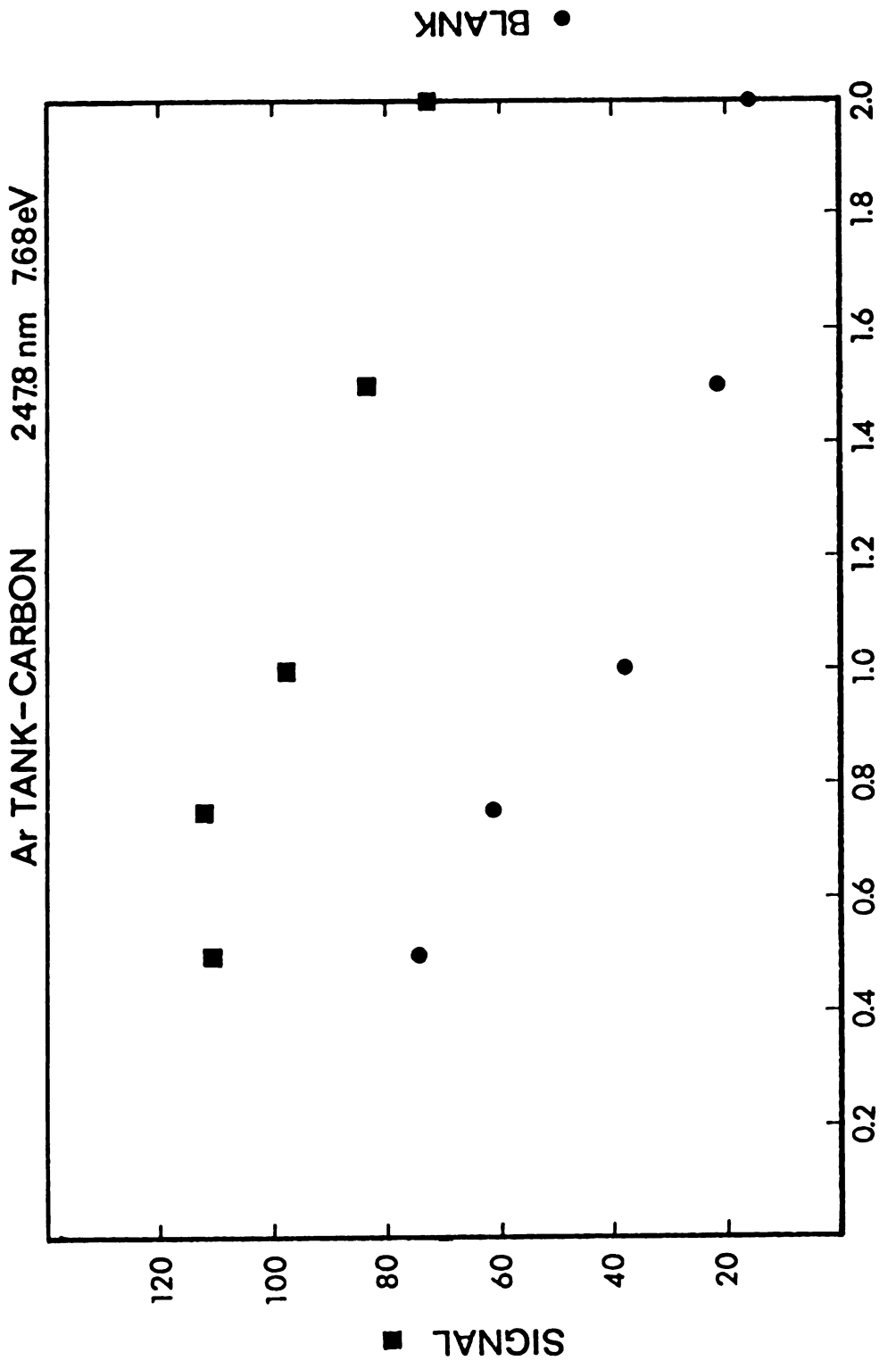

Figure 33. Signal and background plots for the trace residual carbon in the argon supply from 0.5 to 2.0 μsec.

to the upper excitation energy level and also directly related to the dissociation energy of the monoxide of the element, although no conclusive data has as yet been obtained. It, therefore, seems clear that the optimum delay time for observation depends on the element under study, but certainly is no less than 2.0 μsec.

With a 2.0 μsec time delay, working curves and detection limits were obtained for the eight elements. For convenience, the end of the integration period was chosen as 100 μsec and the data that are presented in this section were, therefore, obtained in the time-sliced mode of observation.

For the data that are presented in this work, the detection limit (DL) is defined as that sample concentration which produces a signal-to-noise ratio (S/N) equal to two. Since five pairs of sample-background measurements were made (see Table 1), the definition of DL as S/N = 2 corresponds to a confidence level of 99.7% (164). The S/N is calculated by:

$$S/N = \frac{\bar{T} - \bar{B}}{(\sigma^2_{\bar{T}} + \sigma^2_{\bar{B}})^{1/2}} = \frac{\bar{S}}{(\sigma^2_{\bar{S}} + 2\sigma^2_{\bar{B}})^{1/2}} , \qquad (36)$$

where $\bar{T}$ is the average of total observed emission (signal + blank), $\bar{B}$ is the average background emission, $\bar{S}$ is the average signal emission ($\bar{T} - \bar{B}$), and $\sigma^2_{\bar{T}}$ and $\sigma^2_{\bar{B}}$ are the variances of $\bar{T}$ and $\bar{B}$, respectively. At the detection limit, the signal emission is quite low relative to the background, and hence $\sigma^2_B > \sigma^2_S$. The detection limit is therefore defined by

$$S/N = 2 = \frac{\bar{S}}{(2)^{1/2}\sigma_{\bar{B}}} , \qquad (37)$$

where $\sigma_{\bar{B}}$ is the standard deviation of the average of the background emission.

Figure 34 shows a typical working curve obtained for silicon (Na_2SiO_3). A 2.0 μsec delay time was used with a 98 μsec integration time. Three sets of data were obtained at two hour intervals, with each set obtained according to conditions listed in Table 1. The analytically useful information from Figure 34 is summarized in Table 6. Figure 34 shows the actual data points obtained over this six hour time period, and this shows the extreme long-term stability of the system. When only two data points are shown, the emission intensities overlapped.

To further check the stability of the system, a 2 PPM Cu solution ($Cu(NO_3)_2$) was run over a period of one hour. In this one hour, 100 pairs of sample and background measurements, each averaging 1000 firings were made, and the spark was fired 10^5 times to obtain the data. The relative standard deviation of the 100 data points was 3.9%. The 100 points has a fairly true Gaussian distribution in that 38% of the points were outside one standard deviation units, while 2% of the points were over two standard deviation units from the 100 point average.

The eight elements chosen to show the utility of the system for spectrochemical analysis were Si(Na_2SiO_3), Mo(Na_2MoO_4), Al($Al(NO_3)_3$), C($Ca(C_2H_3O_2)_2$), Ca($Ca(C_2H_3O_2)_2$), P(NaH_2PO_4), Cu($Cu(NO_3)_2$), and

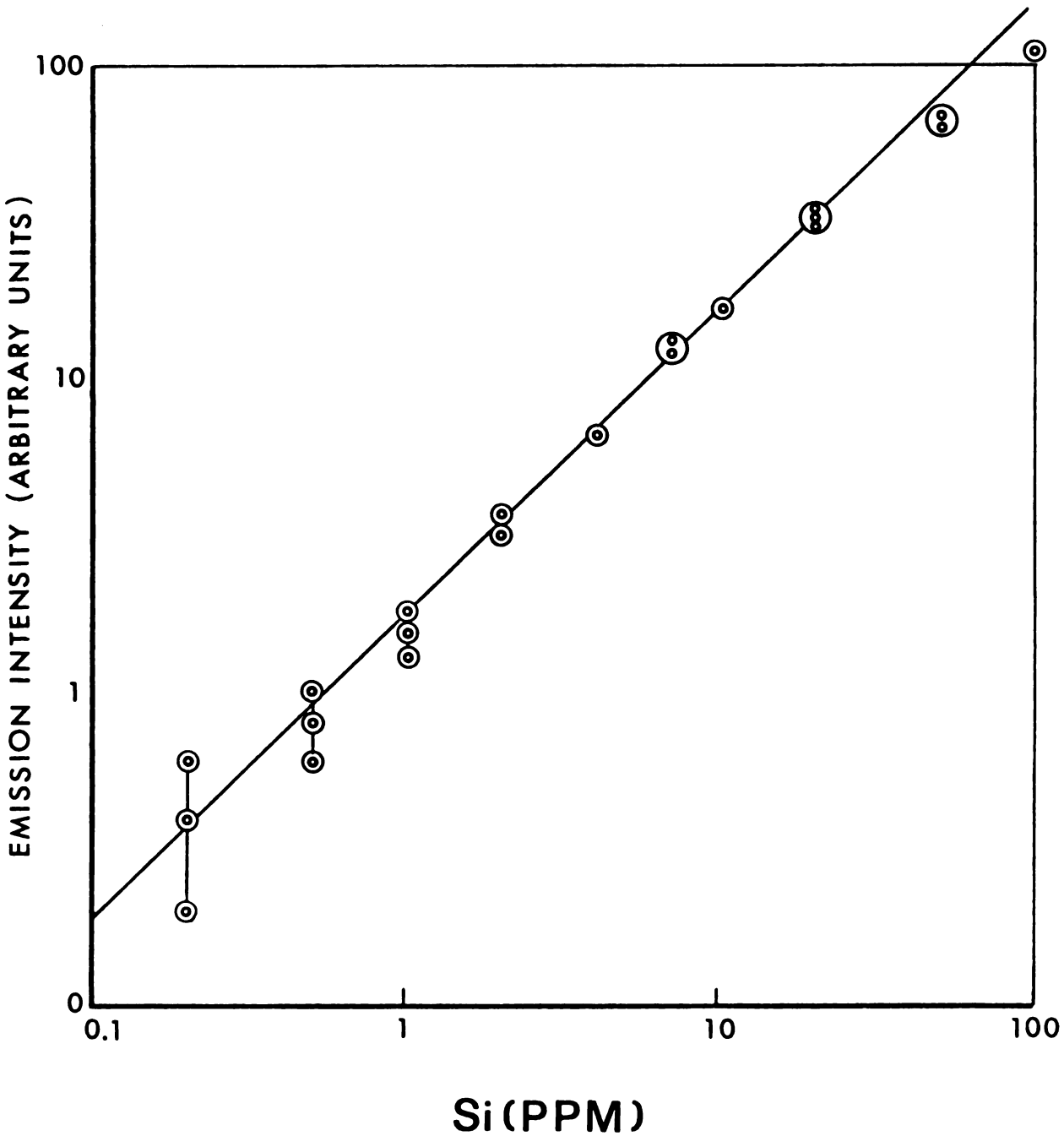

Figure 34. Analytical curve for silicon obtained over a six hour period.

$B(Na_2B_4O_7)$. For these eight elements, detection limits (DL), upper linear concentration ranges (C_u), slopes (M) of the working curves over the linear concentration region, and the emission lines that were used to obtain the information in the time-sliced mode, are listed in Table 6.

The data presented in Table 6 are indeed attractive. One obtains linear working curves, with usual unity slopes. While being attractive, the data presented in Table 6 are not the optimum that the system is capable of producing.

The data presented in Table 6 were obtained by time-sliced observation of the emission. Recall, however, that every element has its own characteristic emission-time profile, while the emission from the background decreases constantly with time. The detection limit is defined as the signal divided by the standard deviation of the background. If the standard deviation of the background is directly proportional to the background, and if the background decreases at a rate faster than the signal, there will be an optimum observation time at which the S/N is a maximum. From the above discussion, the instant in time at which the S/N is a maximum will be identical to the time at which the S/B is a maximum. Hence, to obtain the maximum sensitivity from the system, the interval in time at which the analyte gives a maximum signal-to-background ratio must be found. Integration of the emission signal must then be performed over this time period. In other words, the emission must be observed by using time resolution, rather than time slicing.

Table 6. Analytical information in time-sliced mode of operation.

Element	Emission Line (nm)	DL(PPM)	C_u(PPM)	M
Si	288.1	0.2	40	0.99
Si	251.6	0.08	40	1.01
Mo	379.8	0.4	25	1.00
Al	396.1	0.5	50	1.01
C	247.8	2.0[a]	100	1.01
Ca	393.3[b]	0.05	50	1.15[d]
Ca	422.7	0.1	50	1.13[d]
P	253.5	2.0	40	1.02
Cu	324.7	0.07	50	1.00
B	249.7[c]	0.2	40	1.05

[a]Influenced by residual carbon in the argon.

[b]Ion line.

[c]Combination of the 249.77 and 249.68 nm lines.

[d]See next chapter for discussion.

B. Spectrochemical Analysis with Time-Resolved Spectrometry

It was found that the easiest method for obtaining the emission intensity over a particular time interval was to control only the delay time monostable. The end of the integration was held at a fixed time of 100 μsec, the delay time set at 2 μsec, and the emission was integrated from 2-100 μsec.

The delay time was then increased by 1 μsec and the emission obtained in this manner was subtracted from the emission obtained from 2-100 μsec. The difference then corresponds to the integrated emission from 2-3 μsec after spark initiation. Therefore, increasing the delay time by 1 or 2 μsec steps would give the corresponding integrated time-resolved emission. This was done for both the sample emission S and the background emission B. In Figure 35 the signal-to-background ratio obtained in the time-resolved mode ($\Delta S/\Delta B$), and the signal-to-background ratio obtained in the time-sliced mode (S/B) are plotted for a 25 PPM B sample as a function of time. Note that $\Delta S/\Delta B$ has a maximum of about 30 at about 8 μsec, while S/B has a value of about 6 at 2 μsec and a maximum of 10 at about 4 μsec. This data would indicate that an improvement in sensitivity of about five over that listed in Table 6 should be obtained using time-resolved observation of the emission.

Because the switching speed of the field effect transistors, which control the integration period, is only 100 nsec, it was decided that attempts at integrating a 1 μsec time interval would lead to large errors. Therefore, a 5 μsec time interval bounding the observed

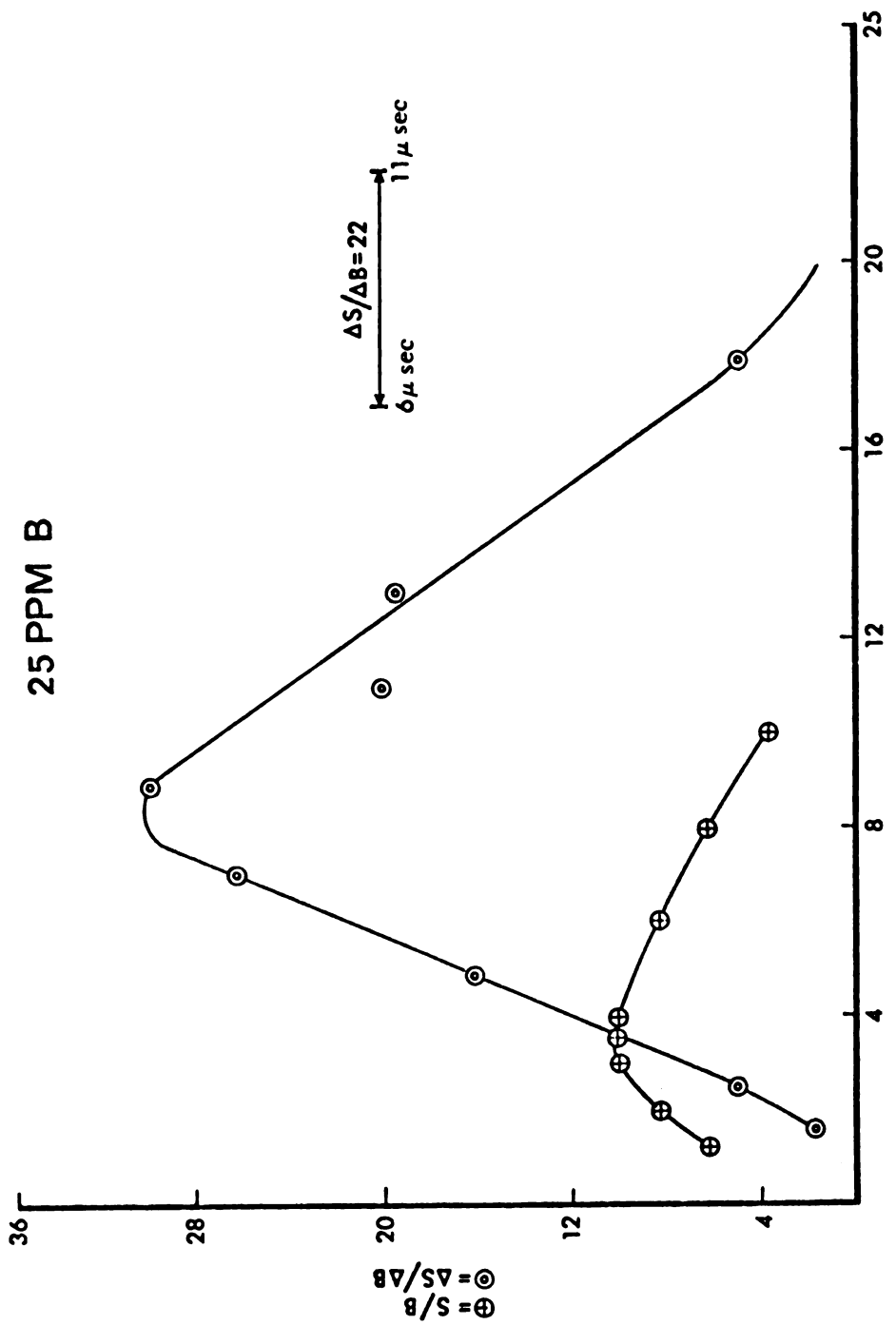

Figure 35. Signal-to-background ratios for a 25 PPM B solution in time-sliced and time-resolved modes.

$\Delta S/\Delta B$ maximum was selected as the minimum integration period. In Figure 35 for boron, this corresponds to integration from 6-11 μsec with an observed $\Delta S/\Delta B = 22$ for the 25 PPM B sample. Hence, a predicted increase of about a factor of four in the sensitivity should result.

Similarly for calcium, Figure 36 results when the time-resolved, signal-to-background ratio is plotted. Hence, an integration time period of 15 μsec, between 15 and 30 μsec, was selected. The improvement in the signal-to-background ratio in this time period over that used to obtain the data for Table 6, is a factor of 12.

The calibration curves obtained for boron and calcium are shown in Figures 37 and 38, respectively. To obtain the working curve for boron, the integrate monostable was set at 11 μsec, and the delay monostable was set at 6 μsec. For the calcium data, the integrate time was set to 30 μsec, while the delay was set at 15 μsec. The boron growth curve is linear over three orders of magnitude with a detection limit of 70 PPB, and unity slope. The calcium calibration curve is linear over four orders of magnitude with a detection limit of 8 PPB, and a slope of 1.1. The reasons for the bending observed in the working curves at higher concentrations, have not been investigated but it is assumed that it is due to self-absorption.

All the analytical data contained in Figures 37 and 38 are summarized in Table 7. Optimum time intervals and calibration curves were also obtained for aluminum and phosphorous, and these are also listed in Table 7 together with the detection limits, the improvement

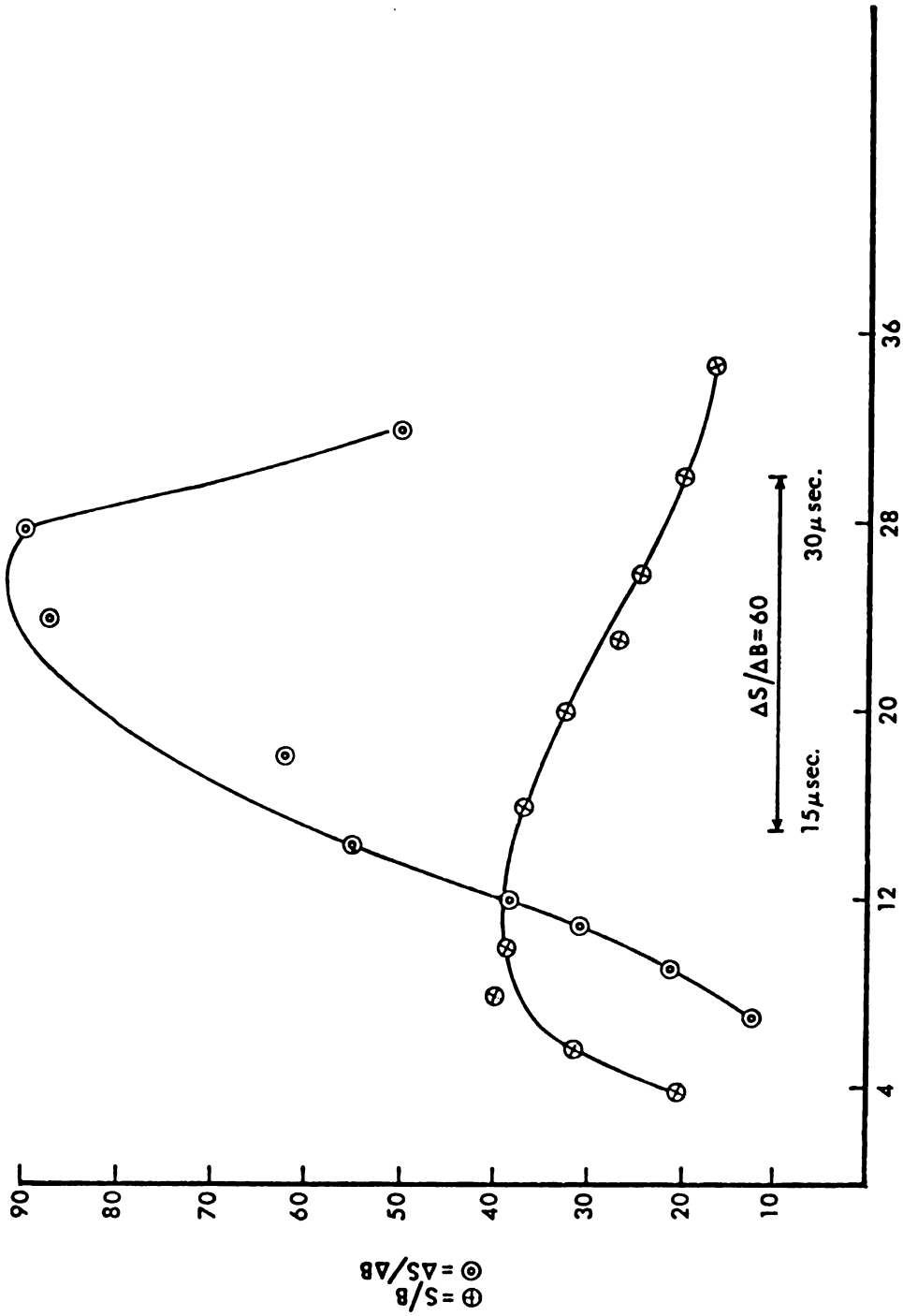

Figure 36. Signal-to-background ratios for a 2 PPM Ca solution in time-sliced and time-resolved modes.

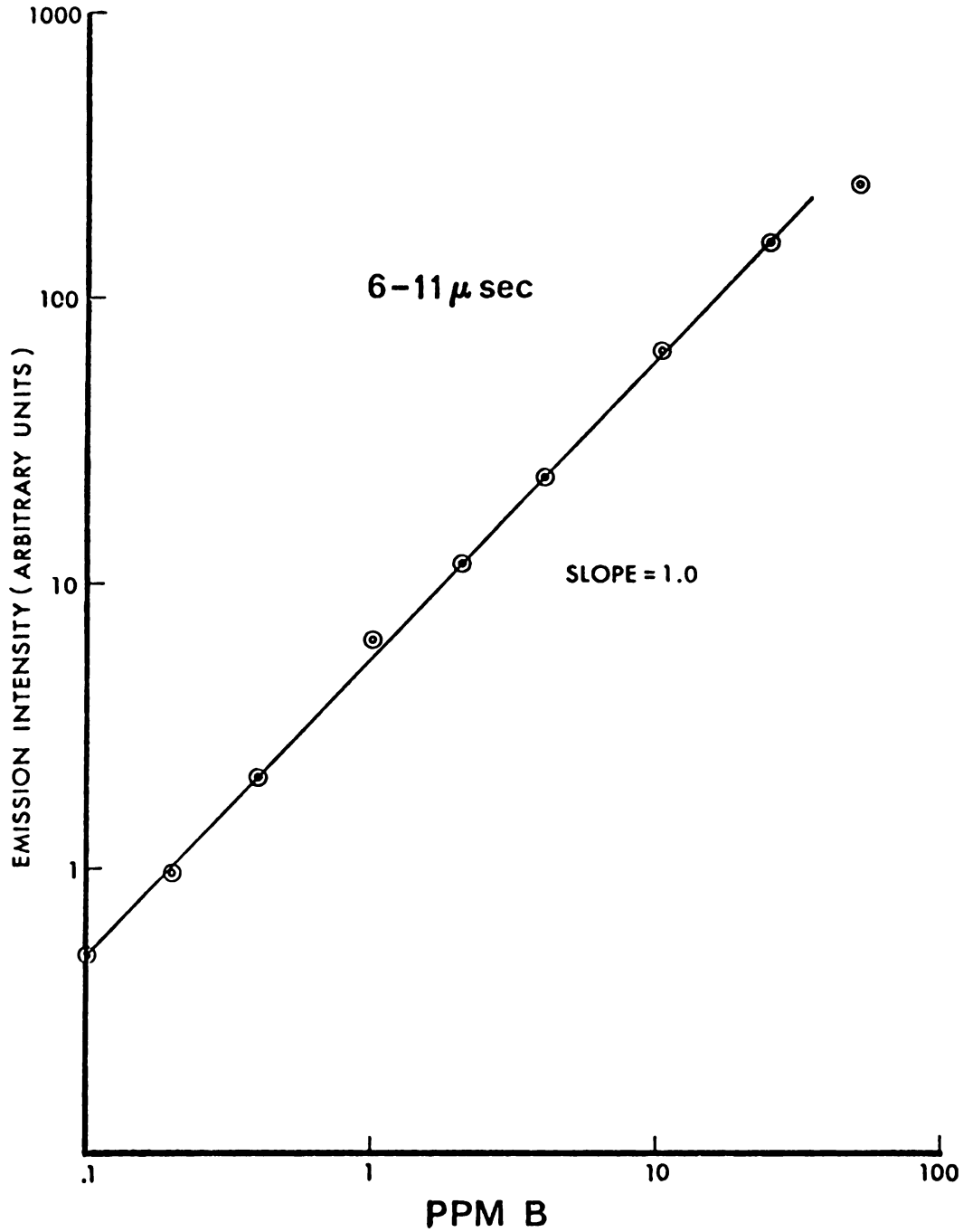

Figure 37. Calibration curve for boron integrating from 6-11 μsec.

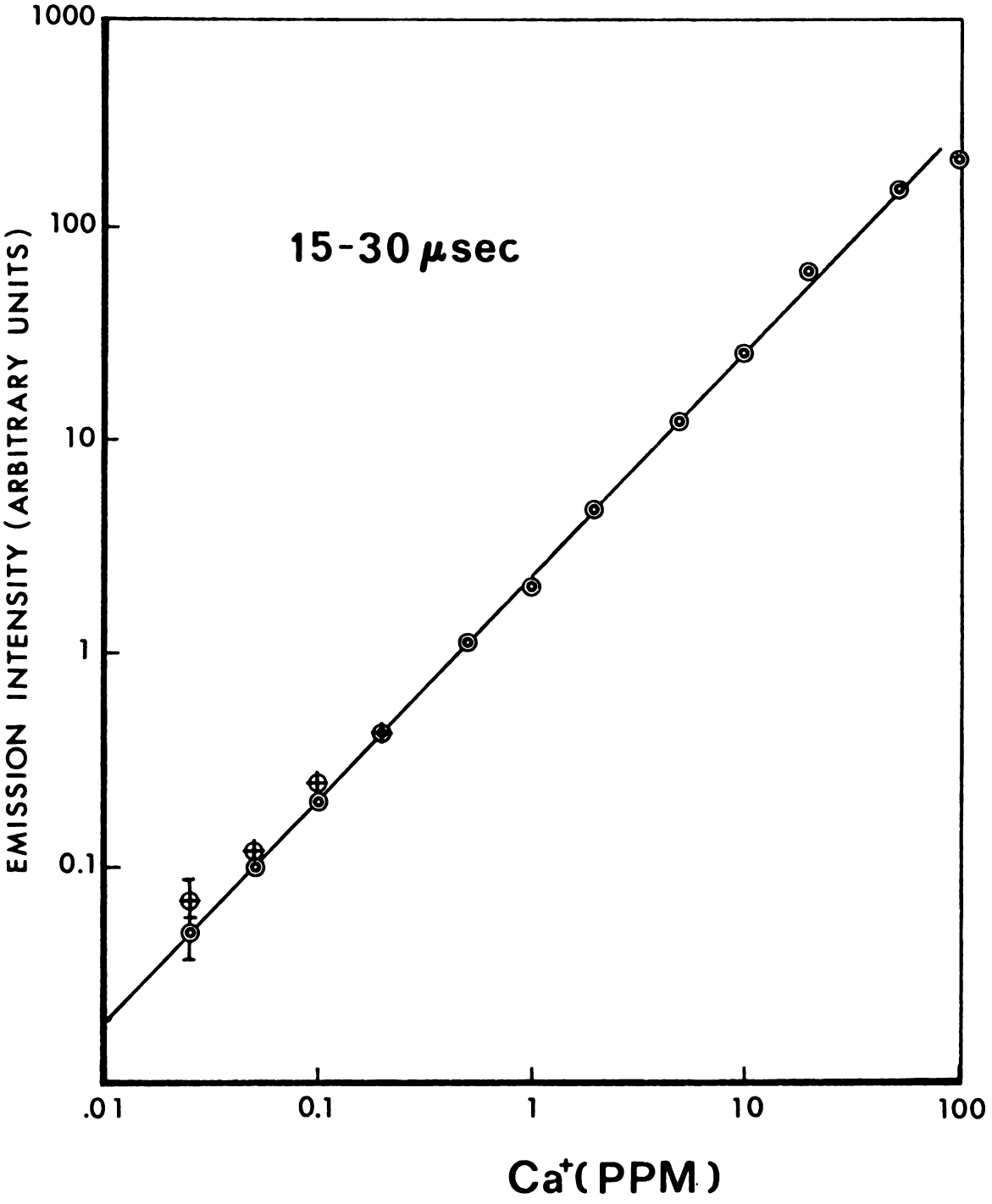

Figure 38. Calibration curve for calcium integrating from 15-30 μsec.

Table 7. Analytical parameters obtained under time-resolution.

Element	Emission Line (nm)	Time Interval (μsec)	DL(PPM)	S	S'/B'	C_u(PPM)	M
B	249.7[a]	6-11	0.07	2.9	3.7	40	1.04
Ca	393.3	15-30	0.008	6.2	12	50	1.10
Al	396.1	10-15	0.32	1.6	3.1	50	1.06
P	253.5	8-13	0.50	4.0	6.5	40	1.01

[a]Combination of 249.77 and 249.68 nm lines.

in sensitivity (S) relative to time slicing, the improvement in signal-to-background ratio (S'/B') observed over time slicing, and other parameters of analytical importance.

The comparison of Table 6 with Table 7 shows the effect of time resolution. It is obvious that lower detection limits can be obtained for the time-resolved mode. However, the total improvement obtained in S/B did not manifest itself in the improvement in sensitivity. This can arise from the switching errors of the FETs, which would be more pronounced over a short integration period. In fact, in a 5 μsec integration period, a 2% error is introduced in the switching alone. Or, it is also possible that the standard deviation of the background emission is not directly related to the magnitude of the background. In any event, a definite improvement in sensitivity results from time resolution over time slicing.

C. Comparisons with Other Analytical Techniques

A comparison of the sensitivities, for the eight elements studied, between the spark source described in this work, and other electrical discharges for spectrochemical solution analysis, is made in Table 8. Although the table is not complete, it appears that the spark source described in this work gives much better sensitivity than either the pourous-cup, the rotating disc, or the vacuum-cup techniques.

Table 9 shows a comparison of sensitivities obtained in flame spectroscopy, plasma excitation, and the present work. Both

Table 8. Comparison of sensitivities (PPM) obtained by electronic excitation for solution analysis.

Element	Emission Line (nm)	Arc Excitation	Spark Excitation		
		Vacuum-Cup (166)	Porous-Cup (85, 87)	Rotating-Disc (85, 86)	Present System
B	249.7[b]	0.6	0.5	0.1	0.07
Si	251.6	--	1.0	--	0.08[a]
Mo	379.8	--	--	--	0.4[a]
	313.2	--	0.1	0.3	--
Al	396.1	6	0.3	0.3	0.32
C	247.8	--	--	--	2.0[a]
Cu	324.7	1	0.2	0.25	0.07[a]
P	253.5	--	--	4.0	0.5
Ca	393.3	--	0.01	--	0.008

[a]Not time optimized.

[b]Combination of 249.77 and 249.68 nm lines.

Table 9. Comparison with sensitivities (PPM) obtained in flame and plasma spectroscopy.

Element	Analysis Line (nm)	Flame		Plasma (106, 108, 169)	Present System
		AAS (166)	AES (76, 167, 168)		
B	249.7[d]	3	30	0.04	0.07
Si	251.6	0.2	5	0.2	0.08[a]
Mo	379.8	0.03	0.03	0.45	0.4[a]
Al	396.1	0.03	0.2	0.03	0.32
C	247.8	--	--	--	2.0[a]
Cu	324.7	0.005	0.01	0.001	0.07[a]
P	253.5	--	3.0(PO)	3.0	0.5
Ca	393.3[b]	--	--	0.01	0.008
	422.7	0.002	0.0001[c]		

[a]Not optimized in time.
[b]Ion Line.
[c]Using an ionization suppressent.
[d]Combination of 249.77 and 249.68 nm lines.

atomic absorption spectroscopy (AAS) and atomic emission spectroscopy (AES) are listed under flame techniques. Both forms of plasmas, microwave and induction-coupled radio-frequency have been combined, and the best detection limit obtained by either form of plasma has been listed. All the detection limits reported in the literature have been modified to conform with the definition of the detection limit represented by Equation 37 ($S/\sigma_B \approx 3$).

The data presented in Table 9 are quite satisfying. The miniature spark source is more sensitive than the flame for the determination of boron, silcon, carbon and phosphorous. In this comparison all flames (air/C_2H_2, N_2O/C_2H_2, etc.) have been considered. For the remainder of the elements (molybdenum, aluminum, copper and calcium) the sensitivity of the spark source is within an order of magnitude of the sensitivity observed in AAS.

A comparison between the spark source and the plasma (both microwave and induction-coupled radio-frequency) shows that the high power spark source is more sensitive for the determination of silicon, molybdenum, phosphorous and calcium. Its sensitivity is within an order of magnitude of the plasma for boron, aluminum and copper.

Summarizing the information presented for the elements studied, we see that silcon and phosphorous have the <u>best</u> sensitivities in the miniature spark source (better than either flame or plasma techniques). For the remainder of the elements, the sensitivity of the spark source, at the present time, is within one order of magnitude of the best detection limits reported in the literature. It must be recognized that four of the detection limits presented for the spark

source were obtained under nontime optimized conditions. Recognizing that the system described in this work has been in operation for only about one year, it should be obvious why the words "at the present time" were used in the sentence above.

VI. INTERELEMENT STUDIES AND MULTIELEMENT APPLICATIONS

In this chapter, the interelement effects that have been observed in emission spectrochemical analysis with the miniature spark source are discussed. A strong enhancement of calcium emission has been observed when cesium is present in the sample. This is discussed, and possible mechanisms are considered based on time-resolved spectral observations. The slopes of calcium working curves in the presence of cesium are shown to decrease to unity.

A depression of the calcium emission in the presence of aluminum has been observed. In the time-integrated mode of observation, the depression is appreciable. In the time-resolved mode, the depression can be nearly eliminated when observations are made in the first few microseconds. It is shown that, while the time range of maximum sensitivity, the "analytical region," is between 5-30 μsec, the range for maximum qualitative information is between 1-3 μsec.

A. Effects of Cesium on Calcium Emission

The data presented in Tables 6 and 7, show that slopes greater than unity were consistently obtained for the Ca analytical curves. At first it was believed that this was caused by a direct ionization interference which would produce linear growth curves,

with greater than unity slopes, if the logarithm of the emission intensity were plotted as a function of the logarithm of the concentration (170). This would be due to the well-established fact (171) that the percentage of atoms ionized varies inversely with their concentration. Hence, the addition of an ionization suppressant should depress ionization and thereby enhance sensitivity. An ionization suppressant should also produce growth curves with unity slopes. The addition of an ionization suppressant such as potassium or cesium is common practice in flame atomic spectrometry when easily ionized elements are to be analyzed in high temperature flames (172-174).

To study the influence of an ionization suppressant on the Ca emission, a series of Ca solutions was prepared with varying Ca concentrations and a constant concentration of Cs (200 PPM). The solutions were analyzed by emission with the spark source, using the parameters listed in Table 1. The 422.7 nm Ca resonance line was employed. A series of solutions containing Ca with no added Cs was also measured. Growth curves, which were obtained under the time-sliced mode of operation, are shown in Figure 39, for both sets of samples. Two complete determinations were made on each sample, and the "bars" shown in Figure 39 represents the standard deviation of each determination.

Figure 39, shows that the addition of Cs to Ca results in an increase in the sensitivity, and a working curve with unity slope. If the detection limit decrease is actually caused by a suppression of the ionization of the neutral atom, one should be able to observe a decrease in the emission from calcium ions when Cs is present. Workers

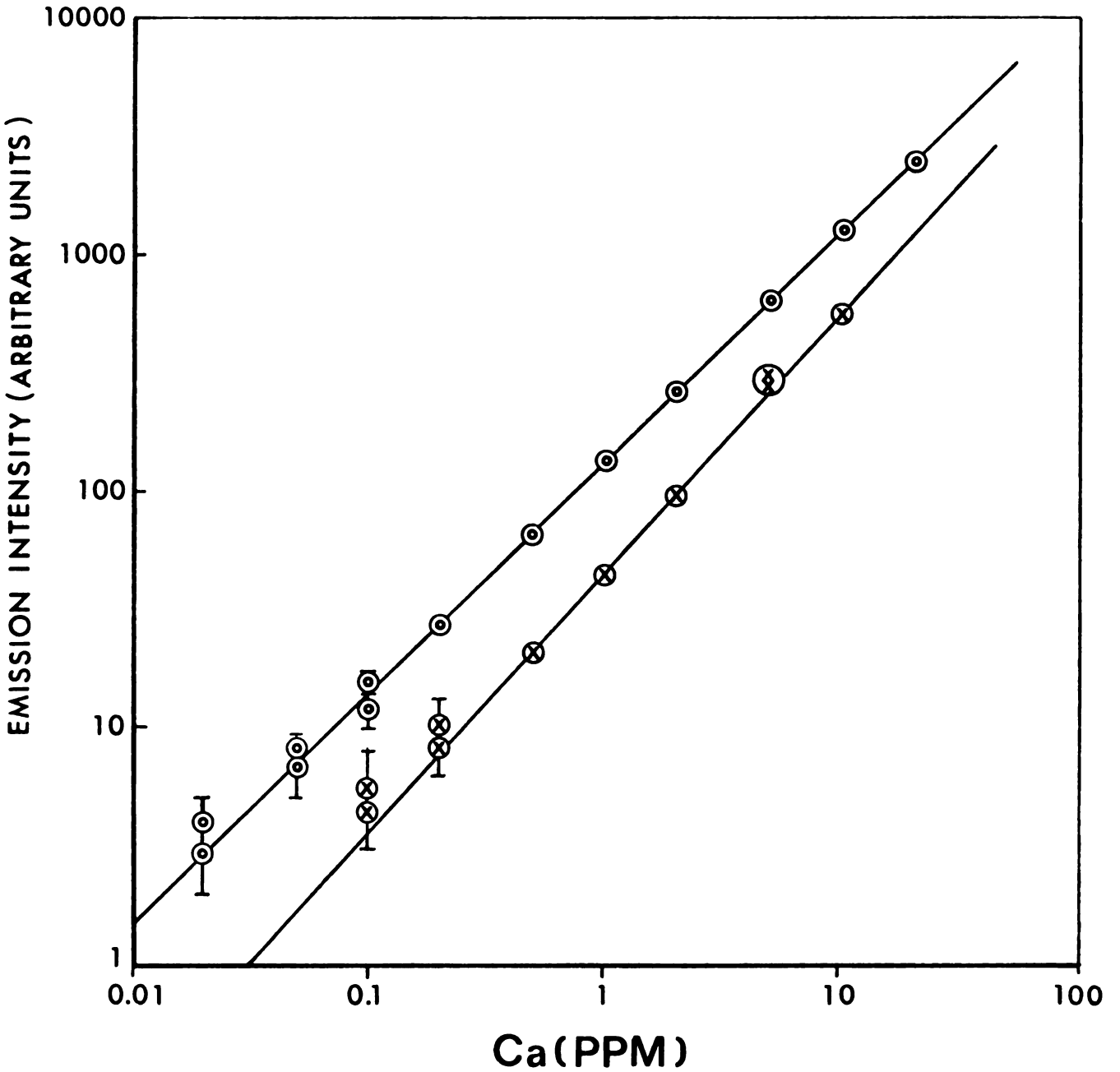

Figure 39. Calibration curves for calcium with and without the addition of 200 PPM Cs.

(74, 175) using N_2O/C_2H_2 flames have observed an enhancement of the calcium neutral atom emission with a simultaneous depression in the calcium ion emission when an ionization suppressant was added to the sample containing Ca.

In this work, however, an enhancement was observed for both the Ca atom emission and the ion emission upon the addition of 200 PPM of Cs. Without time optimization, the detection limits for calcium in the presence of 200 PPM of Cs, were found to be 0.02 PPM at the 422.7 nm atom line and 0.008 PPM at the 393.3 nm ion line. The slopes of the working curves were 0.98 and 0.96 for the calcium atom and ion line, respectively.

The enhancement in the emission intensity for both the atom and the ion lines of alkali earth metals, upon the addition of alkali metals, has recently been observed by workers who used a microwave plasma excitation source (108, 169, 176). These workers, however, offered no explanation for the observed behavior.

To understand the nature of the observed increase in the atom and ion emission intensity, the emission was studied on a time-resolved basis. Solutions were prepared with a variable concentration of cesium (0, 8, 16, 40, 80 and 200 PPM), and two fixed concentrations of calcium (0.4 and 2 PPM). Three time intervals (2-15, 15-30 and 30-100 μsec) were chosen for integration of the emission. When summed, the emission observed in these three time-windows should produce the data previously shown in Figure 39. In Figures 40, 41 and 42, the percent enhancement in the Ca emission intensity due to the Cs, is plotted as a function of the Cs

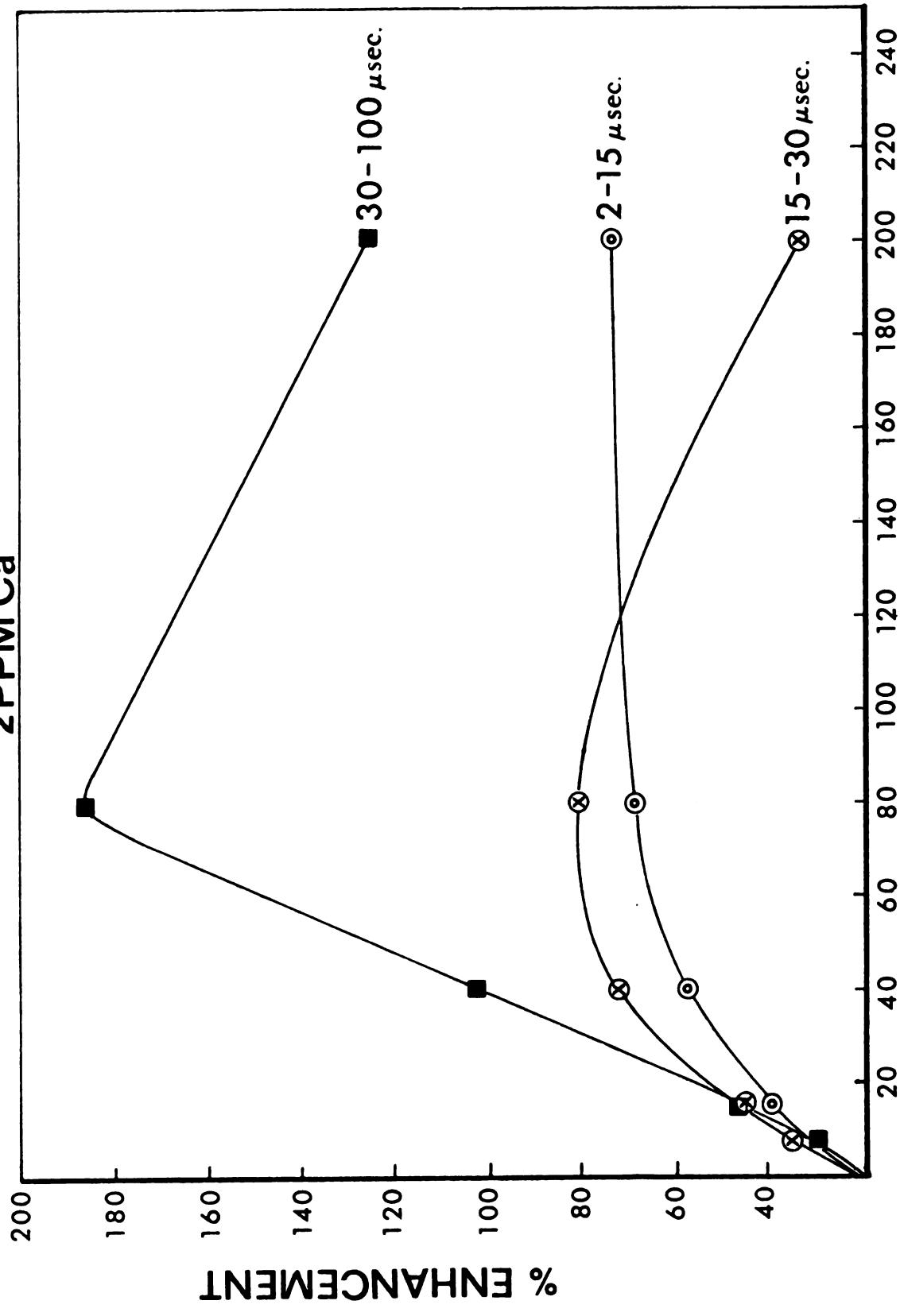

Figure 40. Time-resolved enhancements of Cs on the emission from 2 PPM CaI.

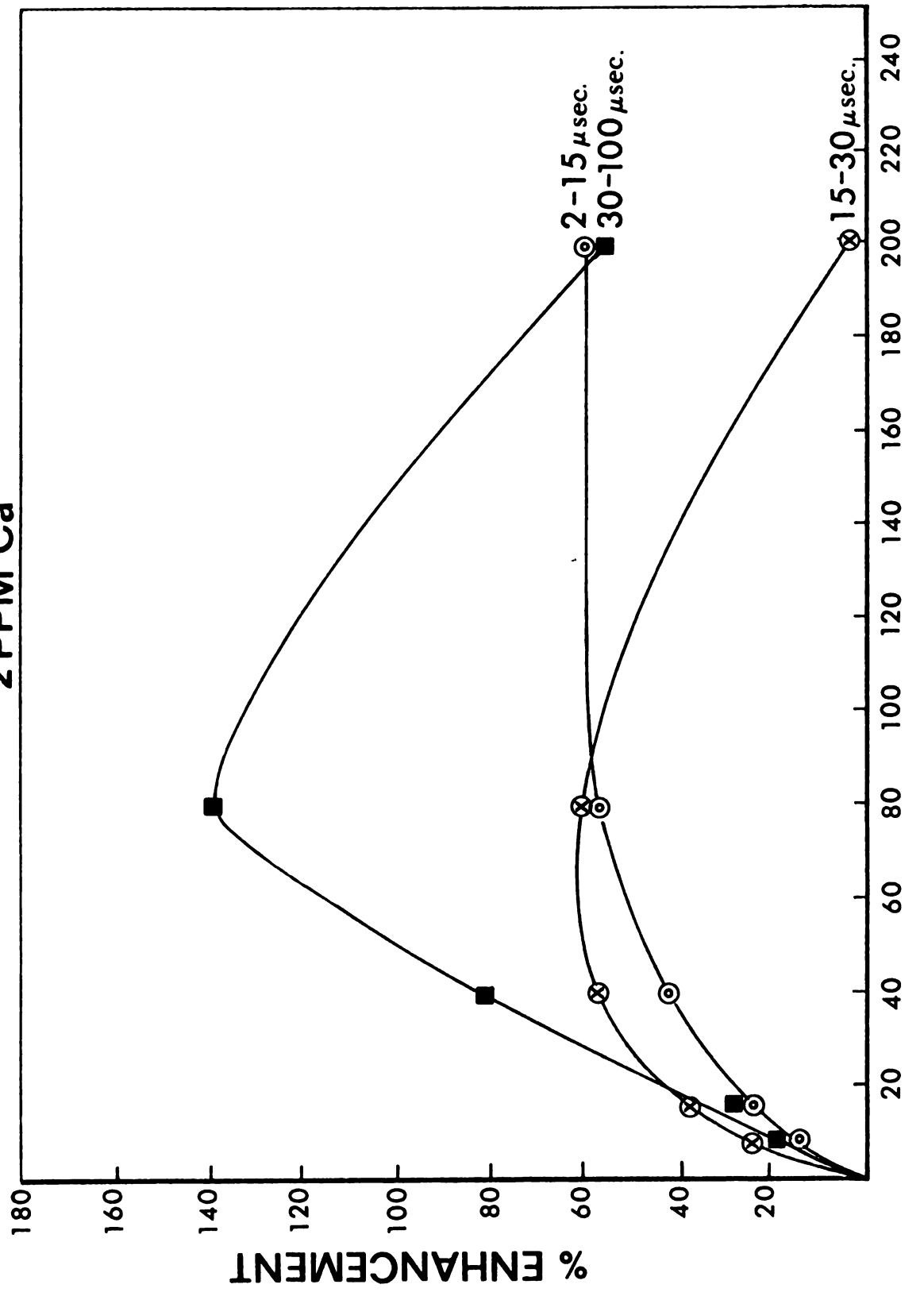

Figure 41. Time-resolved enhancements of Cs on the emission from 2 PPM CaII.

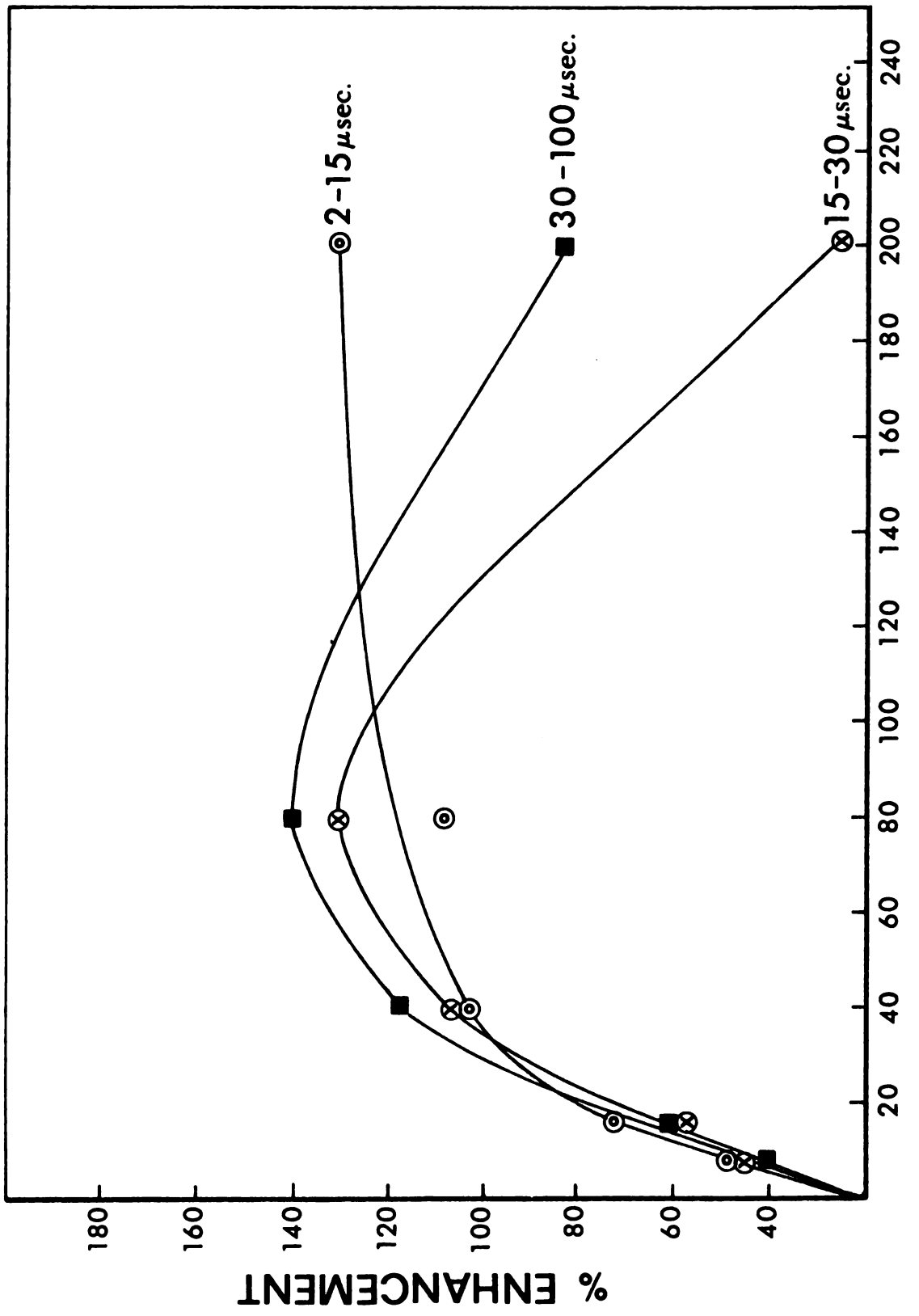

Figure 42. Time-resolved enhancements of Cs on the emission from 0.4 PPM CaII.

concentration for the 2 PPM CaI line and for the 0.4 and 2 PPM CaII line. The enhancements are plotted for the three time intervals chosen, and for both the ion and atom emission of the 2 PPM Ca sample.

Looking at the 2-15 μsec time interval, in Figures 40-42, we see that the emission increases and then becomes independent of the Cs concentration. For the 2 PPM Ca solution, the emission from both the neutral atom and the ion show identical enhancement patterns in this time period. The ion emission from the 0.4 PPM Ca solution shows the leveling off of the enhancements observed for the 2 PPM solutions, but as a much higher percent enhancement. Hence, it appears that in this time interval, the percent enhancement is not only dependent on the Cs concentration, but also on the Ca concentration. Since the extent of the enhancement is dependent upon the Ca concentration, and since ionization is proportional to the inverse of the concentration, it appears that the Cs acts as an ionization suppressent for Ca. However, since the emission from the CaII is actually enhanced by the presence of Cs, it would indicate that Cs is suppressing the ionization of CaII to CaIII. This would account for the linear, unity slope, working curve shown in Figure 39.

In the 15-30 μsec time interval, we again see the same behavior for the 2 PPM solutions, and that the emission from the lower concentration of Ca is enhanced to a greater extent, relative to the higher concentration. These observations can be explained by the above discussion.

The behavior of all the curves taken in the 15-30 μsec interval are not similar to the corresponding 2-15 μsec interval, in that they show a much more pronounced dependence on the Cs concentration. Each curve shows that the enhancement reaches a maximum at about 80 PPM of Cs, and that percent enhancement decreases at higher concentrations. This decrease can be due to an alkali volatization interference (174) on the salt particles that contain the Ca by the high concentration of Cs. Hence, in this time period the enhancement of Cs on the emission from Ca is dependent on the Ca concentration, and is also strongly dependent on the concentration of Cs.

In the last time period, 30-100 μsec, note that the 0.4 PPM and the 2 PPM CaII emissions have identical enhancement characteristics. In the 30-100 μsec time interval, it appears that the ionization of CaII has been completely halted. This is due not only to the effects of Cs, but also to the fact that the "temperature" of the spark has diminished greatly. Also in this time period, we finally observe that the emission from the CaI is enhanced to a greater extent than the CaII emission. Therefore, in this time interval the Cs finally begins to suppress the ionization of CaI.

The enhancement caused by the alkali elements on the emission of the alkali earths is, therefore, a quite complex process. Not only is the process dependent on the concentration of both elements, but also the observed enhancement is strongly a function of time.

B. Effects of Aluminum on Calcium Emission

Workers (163, 177) in the area of flame spectroscopy have shown that Al exhibits a marked depression on the emission of Ca in normal flames such as the O_2/H_2, air/H_2 and air/C_2H_2 flames. This depression is believed to be caused by the formation of an Al-O-Ca agregate which cannot be dissociated in the flame. Workers (74), using high temperature N_2O/C_2H_2 flames, have observed slight enhancements of the emission from Ca in the presence of Al. With microwave plasmas, workers (108) have reported a pronounced depression of Ca emission by Al.

To see if the miniature spark source exhibits this well-known interference, solutions containing 2 PPM Ca were prepared with varying concentrations of Al (0, 2, 4, 10, 20, 40 and 80 PPM). The emission was measured at the 422.7 and the 393.3 nm Ca lines, and time-slicing (2-100 μsec integration) was used. Both lines of Ca exhibit the same effect, and the results obtained for the ion line are plotted in Figure 43. It can be seen that the Ca emission intensity decreases as a function of the Al concentration. Although the depression is not as pronounced as in flame spectroscopy (163), it is nonetheless appreciable.

To observe the depression as a function of time, solutions containing 2 PPM of Ca with varying concentrations of Al (0, 8, 20 PPM) were prepared. Time-resolved data were obtained with the method of successive subtractions described earlier, for various time intervals (0.6-1.0, 1.0-1.5, 2.2-3.0, 3.0-5.0 and 5.0-7.0 μsec). The

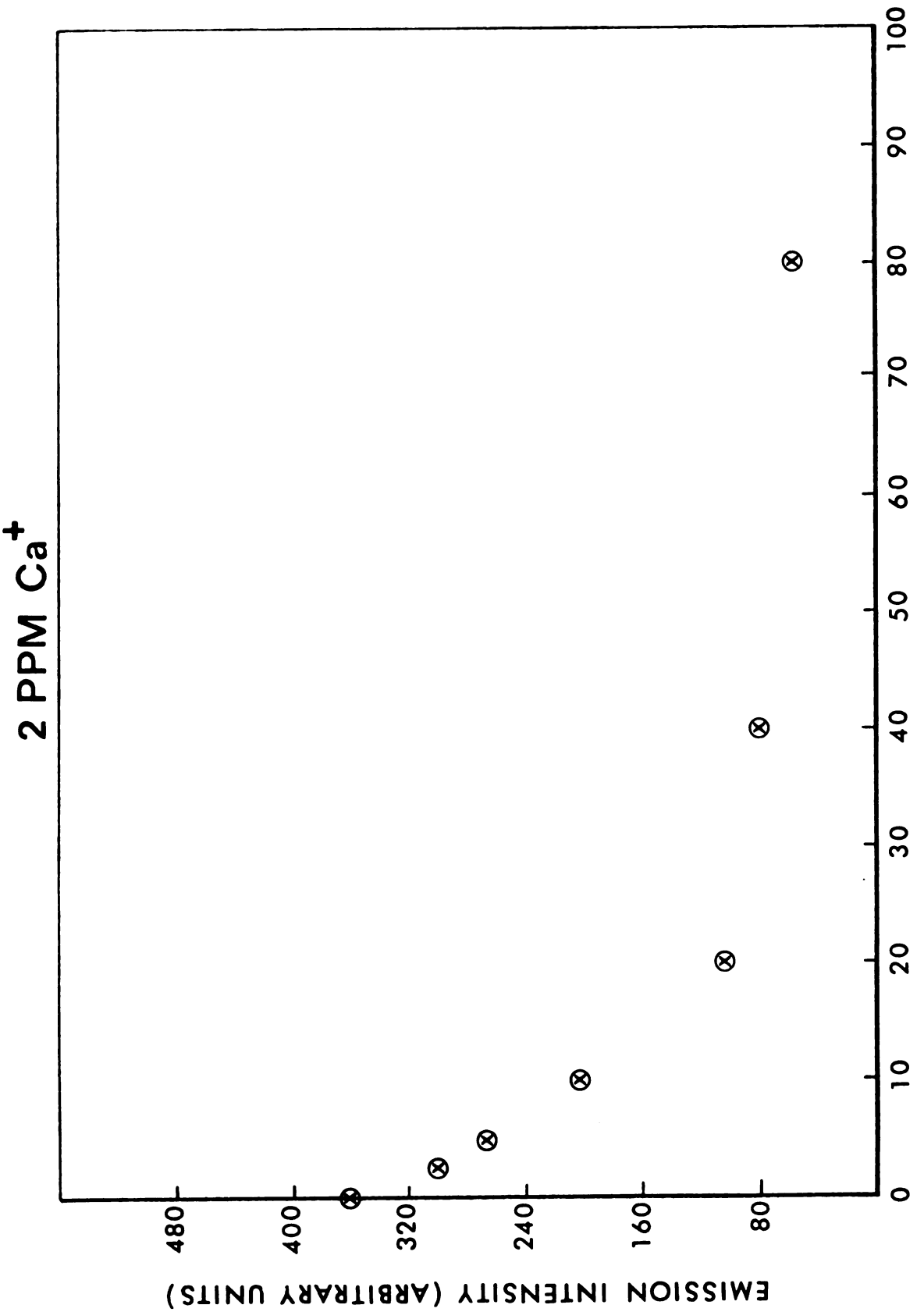

Figure 43. Depression of various concentrations of Al on the time-integrated emission of 2 PPM Ca.

percent depression of the two concentrations of Al on the 2 PPM Ca emission, relative to the emission of the pure 2 PPM Ca is shown in Figure 44. The percent depression, over the various time intervals, is plotted at the midpoint of that time interval. From Figure 44 we can see that Al produces a depression in the Ca emission at all times, except for the 8 PPM Al solution in the 0.6-1.0 μsec interval.

The extent of the depression is very much a function of time. Observation of the emission from Ca in the 0.6-1.0 μsec time scale results in a zero percent depression from the 8 PPM Al solution, and only an eight percent depression from the 20 PPM Al solution. This should be compared to the 30% and the 68% depressions, from the 8 and 20 PPM Al, respectively, later in time.

From the data presented in the previous chapter, dealing with the signal-to-background ratio as a function of time, one would not want to make quantitative determinations in this (0.6-2.0 μsec) early time interval because the sensitivity would be very low. However, it appears that interelement effects are at a minimum in this time interval. Therefore, for qualitative and semi-quantitative information, it is suggested that observations be made early in time. Once it has been ascertained whether an enhancement or a depression exists, the experimenter can shift the integration time into the "analytical region" (5-30 μsec) to obtain increased sensitivity.

C. Multielement Analysis Capability

To demonstrate the multielement capability of the miniature spark source, a solution containing 5 PPM of Ca, B, Si, P, and Cu was

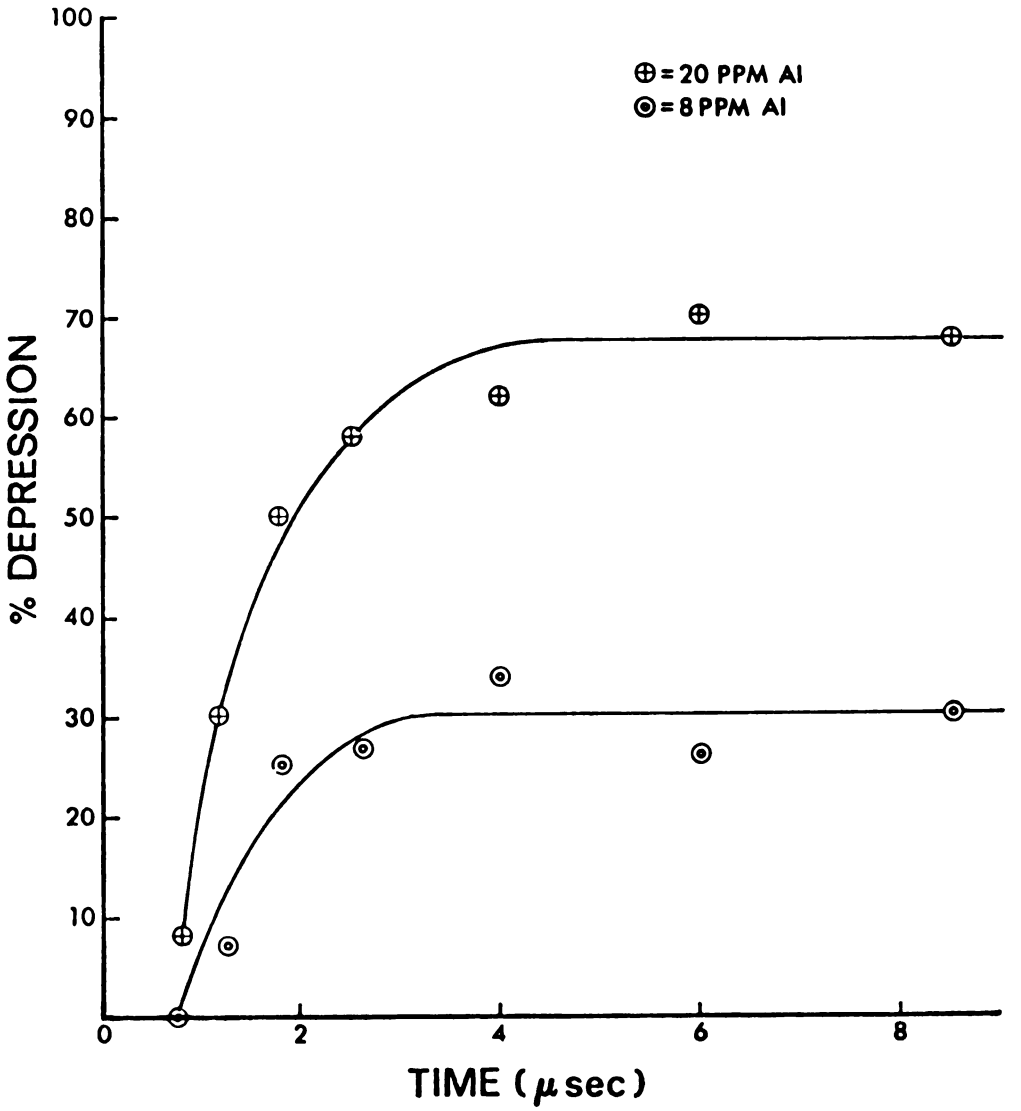

Figure 44. Time-resolved observation of the depression of Al on the emission of 2 PPM Ca.

prepared. This solution was aspirated into the desolvation system, and thereby introduced into the spark. A spectrum was obtained of the emission (see Experimental chapter), over the 6-11 μsec time interval, and it is shown in Figure 45. The inset shown represents an increase of five in the gain. In the inset one can clearly see the high signal-to-background obtained for the emission lines of Si, B, P, and C (introduced as $Ca(C_2H_3O_2)_2$ and as an impurity in the argon tank). Shown in the remainder of the spectrum are the emission lines of Ca, Cu, and the 288.1 nm line of Si. Although this spectrum was obtained using a monochromator, the simultaneous multielement capabilities of the miniature spark source are obvious.

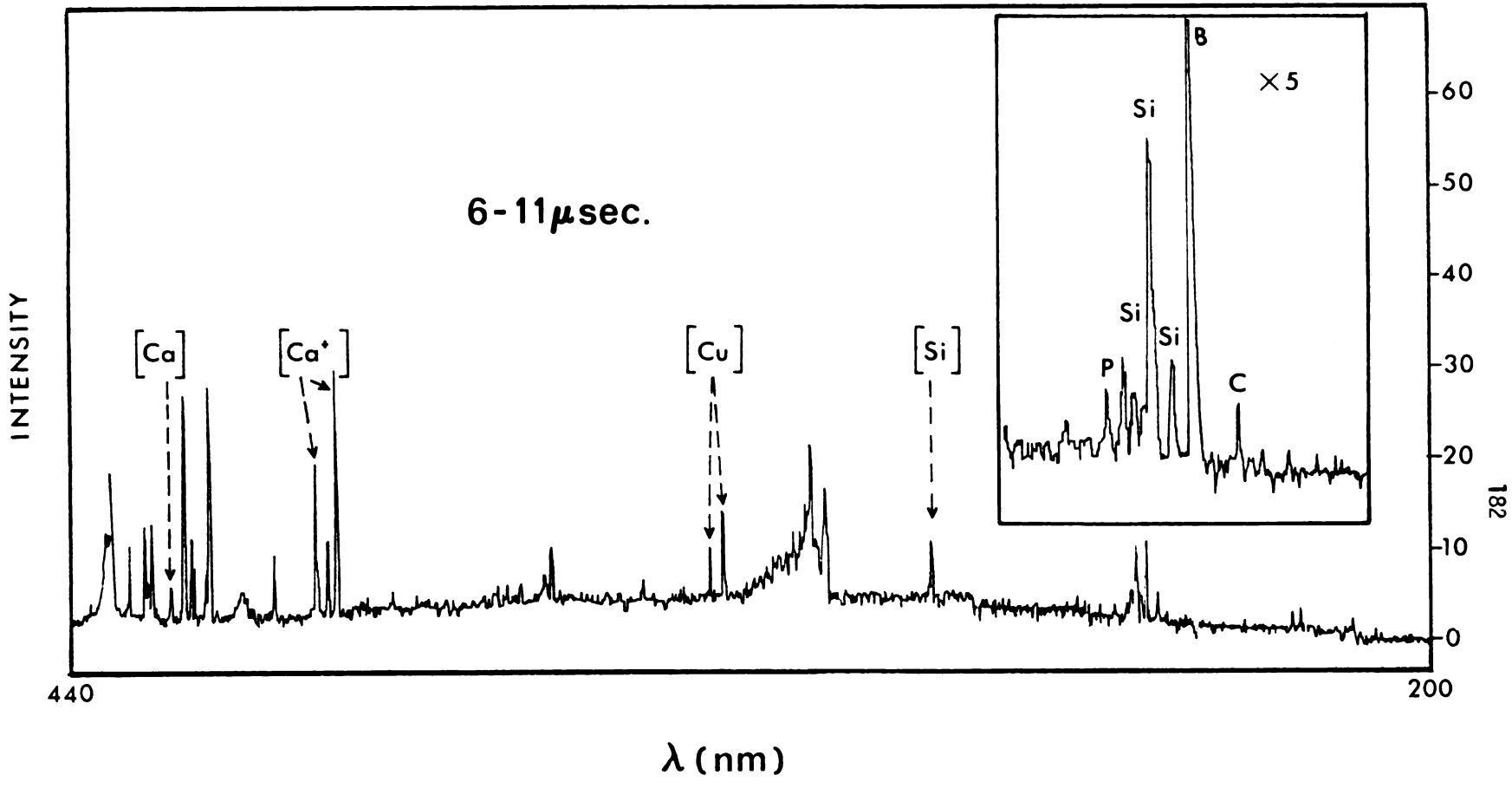

Figure 45. Time-resolved emission spectrum of a multielement sample.

VII. FUTURE PROSPECTIVES

A. Improvements in Instrumentation

Perhaps the major improvement to be made in the system described, is in the introduction system. Workers (106) in plasma spectroscopy have found that the introduction efficiency could be increased by a factor of four through the use of ultrasonic rather than pneumatic nebulization. Hence, using an ultrasonic nebulizer will result in an improvement in the detection limits reported in this work, by a factor of four. Also, with the use of ultrasonic nebulization, the experimenter could control the size of the droplets formed (178). A study could then be performed in order to determine whether the high power spark source shows an optimum in its sensitivity, with regard to the size of the particles introduced.

Various improvements can also be made in the electronics. Better FETs should be obtained, if possible, so that the switching speed would not limit the width of the integration time. The experimenter could then integrate the emission signal over a 1 μsec interval at the optimum S/B, as opposed to the 5 μsec integration time bounding the optimum S/B used in this work. The increased resolving time obtained would surely result in an increase in the sensitivity.

Another possible improvement, would be the replacement of the pulsed high voltage power supply now being used, with a high voltage DC supply. The spark source could then be operated as a free-running, relaxation oscillator (see Part I) with a repetition rate determined by the current limit of the power supply obtained. With a typical power supply, repetition rates of 1 kHz could be obtained. This would decrease the analysis time, over that used in this work, by 1/12. A complete analytical growth curve could then be obtained in less than two minutes.

B. Future Applications

It is obvious from the work presented here that the spark source should prove to be an ideal source for multielement determinations. The experimenter could integrate over the first one or two microseconds, and thereby obtain excellent qualitative information. After the qualitative information is obtained, he could then select the best time interval for obtaining high sensitivity, quantitative information. For simultaneous multielement analysis, this might involve a slight compromise in sensitivity, since each element has its own observation-time optimum. However, even the sensitivities obtained in the time-sliced mode of observation are still very good. Simultaneous multielement determinations would, therefore, only involve a slight reduction in the sensitivity. Work in applying the miniature spark source to the area of multielement analysis of solutions, is currently under investigation in our laboratory by Mr. Edward D. Glass (179).

Another possible application of the spark source is as an on-line gas chromatographic detector, with elemental specificity. Workers (180) have shown that the microwave plasma can be used successfully in this area. The spark source described should be equally useful as a detector for effluents from a gas chromatograph. Work in this application area is currently under investigation in our laboratory by Mr. Robert K. Lantz (181).

Although work in our laboratory is basically concerned with solution analysis, the miniature spark could very easily be applied to the analysis of solids. Since the spark is one of high power with low energy, sampling of the solid sample should be performed external to the spark. An instrument capable of forming very small particles directly from a solid sample, has been recently been described (139). Its application to the miniature spark source described here, should prove to be quite fruitful.

C. Future Studies

The author would like to stress that fundamental studies need to be performed so that a better "picture" can be obtained of the reactions that occur in a spark plasma. The direct interaction of the discharge current with the dry salt crystals needs to be investigated on the nanosecond time scale. The mechanisms of energy transfer from the spark plasma to the salt particles needs to be understood, so that the atomization process can be improved. Changes, if any, in the plasma, upon the addition of water or sample, also need to be studied.

In the present work, only optimization of the time of observation has been performed. Of similar importance should be the optimization in space, wherein different portions of the spark discharge are observed by the detection system. It appears that spacial resolution should also improve the observed sensitivity. Spacial resolution might also lead to a better understanding of the reactions that occur in the spark channel.

The optimum position in time for analytical observation appears to be directly related to the dissociation energy of the monoxide of the element. The optimum time for observation should also depend upon the excitation potential of the emission line observed, the ionization potential of the element, and the matrix of the sample. With sufficient information, it appears that an empirical relationship, which combines all the above properties of the sample, could be obtained. This relationship would then free the experimenter from performing the time-optimization routine.

Even if such a relationship is not found, the computer could be programmed to perform the time-optimization scan. Coupling this with an automated sample delivery system would lead to complete automation of the entire system. The analyst would, however, be required to obtain the sample and present it to the system for a complete elemental analysis.

VIII. COMMENTARY

The spark source (51, 182) described in this work, is a valuable tool for spectrochemical analysis. The precision obtained for quantitative determinations, under routine conditions, is always on the order of 2-4%. The source is not restricted to the analysis of any particular set of elements. Sensitivities obtained in the high power spark source, under completely unoptimized conditions, compare extremely favorably to the best detection limits reported in the literature by a host of workers, using a variety of excitation techniques. Recognizing the fact that the spark source described is a new excitation technique, the detection limits reported in this work only begin to reflect the ultimate obtainable sensitivities.

Interelement effects, which are common to both flame and plasma excitation techniques, are also observed in the miniature spark source. However, interelement interferences can be substantially reduced by making observations at a point in time when the interference is a minimum. This can not be done, of course, using a technique where excitation is continuous.

Another prime attribute of the source is its safety of operation. In flame spectroscopy the laboratory workers are faced with the hazards associated with an open flame. In plasma techniques, the experimenters are exposed to potentially dangerous microwave radiation. The spark source offers no safety hazard. Since

it is completely contained, electrical shock hazards are completely eliminated.

Not only is the spark source safe, but also it is inexpensive to operate. Aside from electrical energy, the entire system requires only a single tank of argon. The spark source requires a minimal amount of maintenance resulting from electrode replacement, which must be performed after about 60 hours of sparking. However, electrode replacement time requires less than a minute.

All the facts presented above together with all the data presented in Part II of this work, lead to the conclusion that the miniature, nanosecond spark source is a valuable tool which should be highly useful in routine, trace elemental analysis.

REFERENCES

REFERENCES

1. A. Einstein, Physik Z. 18, 121 (1917).

2. A. C. G. Mitchell and M. W. Zemansky, "Resonance Radiation and Excited Atoms" (Cambridge University Press, Londong, 1961).

3. G. N. Lewis and M. Kasha, J. Am. Chem. Soc. 67, 994 (1945).

4. S. J. Strickler and R. A. Berg, J. Chem. Phys. 37, 814 (1962).

5. L. E. Bruns, J. Chem. Phys. 52, 1716 (1970).

6. B. P. Kibble, G. Copley and L. Krause, Phys. Rev. 153, 9 (1967).

7. E. Milne, J. London Math. Soc. 1, 1 (1926).

8. J. D. Winefordner and T. J. Vickers, Anal. Chem. 36, 1947 (1964).

9. M. L. Parsons and P. M. McElfresh, Appl. Spectrosc. 26, 472 (1972).

10. C. H. Corliss and W. R. Bozman, "Experimental Transitions Probabilities for Spectral Lines of Seventy Elements" NBS. Monograph 53 (U.S. Gov't Printing Office, Washington, D.C. 1962).

11. K. F. Harbaugh, C. M. O'Donnell and J. D. Winefordner, Anal. Chem. 45, 381 (1973).

12. C. M. O'Donnell, K. F. Harbaugh, R. P. Fisher and J. D. Winefordner, Anal. Chem. 45, 609 (1973).

13. J. B. Birks, D. J. Dyson and T. A. King, Proc. Roy. Soc. A277, 270 (1964).

14. M. Ch. Struder, U. P. Wild and Hs. H. Günthard, J. Phys. E. 3, 847 (1970).

15. C. Füchtbaüer, G. Joos and O. Dinkelacher, Ann. d. Phys. 71, 204 (1923).

16. J. Kuhl, G. Marowsky and R. Torge, Anal. Chem. 44, 375 (1972).

17. E. F. Palermo, "Nondispersive Atomic Absorption and Atomic Fluorescence Spectrometry," Ph.D. Thesis, Mich. State Univ., (1973).

18. E. F. M. van der Held and S. Ornstein, Z. f. Phys. 77, 459 (1932).

19. L. deGalan and J. D. Winefordner, J. Quant. Spectry. Radiative Transfer. 7, 703 (1967).

20. E. Gaviola, Ann. Physik. 81, 681 (1926).

21. W. Z. Kessel, Z. Physik. 103, 125 (1936).

22. A. Müller, R. Lunry and H. Kokubun, Rev. Sci. Instr. 36, 1214 (1965).

23. P. Debye and F. W. Sears, Proc. Natl. Acad. Sci. U.S. 18, 409 (1932).

24. O. Maercks, Z. Physik. 109, 598 (1938).

25. J. B. Birks and I. H. Munro, "Progress in Reaction Kinetics," G. Porter, ed. (Pergamon, Oxford, 1967), Vol. 4, p. 239.

26. E. A. Bailey and G. R. Rollefson, J. Chem. Phys. 21, 1315 (1952).

27. W. L. Butler and K. H. Norris, Biochim. Biophys. Acta, 66, 72 (1963).

28. S. Heron, R. W. P. McWhirter and E. H. Rhoderick, Proc. Roy. Soc. A234, 565 (1956).

29. W. R. Falk and L. Katz, Can. J. Phys. 40, 978 (1962).

30. J. M. Calo, R. C. Axtman and R. G. Persing, Rev. Sci. Instr. 41, 1639 (1970).

31. A. Whetstone, Rev. Sci. Instr. 30, 441 (1959).

32. K. Sakurai, G. Capelle and H. P. Broida, J. Chem. Phys. 54, 1220 (1971).

33. K. Sakurai, G. Capelle and H. P. Broida, J. Chem. Phys. 54, 1412 (1971).

34. J. H. Malmberg, Rev. Sci. Instr. 28, 1027 (1957).

35. S. S. Brody, Rev. Sci. Instr. 28, 1021 (1957).

36. I. B. Berlman, O. J. Steingraber and M. J. Benson, Rev. Sci. Instr. 39, 54 (1968).

37. J. T. D'Alessio, P. K. Ludwig and M. J. Benson, Rev. Sci. Instr. 35, 1015 (1964).

38. J. T. D'Alessio and P. K. Ludwig, IEEE Trans. Nucl. Sci. 12, 351 (1965).

39. J. A. McIntosh, "A Pulse Excitation Method of Determining Nanosecond Fluorescent Lifetimes," M.S. Thesis, Air Force Inst. of Tech., 1967.

40. J. Yguerabide, Rev. Sci Instr. 36, 1734 (1965).

41. R. C. Mackey, S. A. Pollack and R. S. Witte, Rev. Sci. Instr. 36, 1715 (1965).

42. G. A. Morton, Appl. Optics 7, 1 (1968).

43. W. R. Ware, "Fluorescence Lifetime Measurements by Time Correlated Single Photon Counting," Office of Naval Research Tech. Report No. 3 (1968).

44. A. M. Halpern and W. R. Ware, J. Chem. Phys. 54, 1271 (1971).

45. L. M. Bollinger and G. E. Thomas, Rev. Sci. Instr. 32, 1044 (1961).

46. W. J. Nicholson and J. I. Fortoul, Biochim. Biophys. Acta. 143, 577 (1967).

47. Ortec Application Note 35, "The Single Photon Technique for Measuring Light Intensity and Decay Characteristics" (1971).

48. W. J. F. Talbot, Phil. Mag. 34, 73 (1852).

49. J. W. Beams, A. R. Kuhlthau, A. C. Lapsley, J. H. McQueen, L. B. Snoddy, and W. D. Whitehead, Jr., J. Opt. Soc. Am. 37, 868 (1947).

50. D. H. McMahon, A. R. Franklin, and H. R. Carleton, Rev. Sci. Instr. 37, 1142 (1966).

51. J. Zynger and S. R. Crouch, Appl. Spectrosc. 26, 631 (1972).

52. M. L. Boas, "Mathematical Methods in the Physical Sciences" (Wiley, New York, 1966).

53. Handbook of Chemistry and Physics (Chemical Rubber Co., Cleveland, 1969).

54. R. C. A. Photomultiplier Manual Tech. Series PT-61 (1970).

55. Tecktronix Instruction Manual for 3T2 Time Base (1967).

56. Tecktronix Instruction Manual for 3S1 Sampling Amplifier (1967).

57. D. Halliday and R. Resnick, "Physics" (Wiley, New York, 1967).

58. I. A. D. Lewis and F. H. Wells, "Millimicrosecond Pulse Techniques" (McGraw-Hill, New York, 1954).

59. F. B. Frungel, "High Speed Pulse Technology" (Academic Press, New York, 1965), Volume 2.

60. J. M. Meek and J. D. Craggs, "Electrical Breakdown of Gases" (Oxford Press, London, 1953).

61. R. W. B. Pearse and A. G. Gaydon, "The Identification of Molecular Spectra" (Wiley, New York, 1963).

62. J. P. Walters and H. V. Malmstadt, Anal. Chem. 37, 1484 (1965).

63. A. G. Gaydon, "Dissociation Energies and Spectra of Diatomic Molecules" (Chapman and Hall, London, 1968).

64. R. M. Barnes, "Quantitative Analysis of Solutions and Solids and the Identification of Ionization Levels by Submicrosecond Time Resolved Spark Emission Spectroscopy," Ph.D. Thesis, Univ. of Ill., 1966.

65. F. P. Gilmore, "Potential Energy Curves for N_2, NO, O_2 and Corresponding Ions," Rand Corp. Memorandum RM-4034-PR, 1964.

66. R. G. Bennett and F. W. Dalby, J. Chem. Phys. 31, 434 (1959).

67. J. P. Walters, Personal Communication (1972).

68. R. Hultgren, J. Am. Chem. Soc. 54, 2320 (1932).

69. A. Walsh, Spectrochim. Acta. 7, 108 (1955).

70. J. D. Winefordner and T. J. Vickers, Anal. Chem. 36, 161 (1964).

71. B. L. Vallee and A. F. Bartholomay, Anal. Chem. 28, 1753 (1956).

72. G. E. Schmauch and E. J. Serfass, Anal. Chem. 30, 1160 (1958).

73. J. B. Willis, Appl. Optics 7, 1295 (1968).

74. M. D. Amos and J. B. Willis, Spectrochim. Acta. 22, 1325 (1966).

75. G. C. Christian, Anal. Lett. 1, 845 (1968).

76. V. A. Fassell and D. W. Golightly, Anal. Chem. 39, 466 (1967).

77. A. Rivas, Angew. Chem. 50, 903 (1937).

78. M. Fred, N. H. Nachtrieb, and F. S. Tomkins, J. Opt. Soc. Am. 37, 279 (1947).

79. H. A. Slovier and A. Sitkin, J. Opt. Soc. Am. 34, 400 (1944).

80. B. F. Scribner and M. Margoshes, "Treatise on Analytical Chemistry," I. M. Kolthoff and P. J. Elving Eds., Part L, Volume 6 (Wiley, New York, 1965).

81. P. Jolibois and R. Bossuet, Compt. Rend. 204, 1189 (1937).

82. R. Walti, Helv. Chim. Acta. 23, 1446 (1940).

83. F. Twyman, W. Zehden, and E. S. Dreblow, Ind. Eng. Chem., Anal. Ed. 12, 238 (1940).

84. O. S. Duffendack and K. B. Thomson, Am. Soc. Testing Materials, Proc. 36, 301 (1936).

85. W. K. Baer and E. S. Hodge, Appl. Spectrosc. 14, 141 (1960).

86. J. F. Kopp and R. C. Kroner, Appl. Spectrosc. 19, 155 (1965).

87. C. Feldman, Anal. Chem. 21, 1041 (1949).

88. T. H. Zinc, Appl. Spectrosc. 13, 94 (1959).

89. R. A. Mugele and H. D. Evans, Ind. Eng. Chem. 43, 1317 (1951).

90. J. Stupar and J. B. Dawson, Appl. Optics. 7, 1351 (1968).

91. H. Lundegärdth and T. Philipson, Lantbruks-Högshol. Ann. 5, 249 (1938); CA. 32, 6576.

92. Y. Uzumasa and H. Okuno, J. Chem. Soc. Japan. 54, 631 (1933); CA 27, 5022.

93. Y. Uzumasa and H. Okuno, J. Chem. Soc. Japan. 55, 622 (1934); CA 28, 6386.

94. F. W. Lamb, Ind. Eng. Chem., Anal. Ed. 13, 185 (1941).

95. H. V. Malmstadt and R. G. Scholz, Anal. Chem. 27, 881 (1955).

96. S. Kobayashi, Bunseki Kagaku 20, 582 (1971); CA 75, 83808S.

97. N. I. Tarasevich and M. Mohamed, J. Anal. Chem. U.S.S.R. 20, 87 (1965).

98. L. Owen, J. Opt. Soc. Am. 41, 709 (1951).

99. A. L. Schalge, "Emission Spectrochemical Analysis by Spark in Spray Solution Technique," Ph.D. Thesis, Univ. of Ill., 1959; Diss. Abst. 20, 1559 (1959).

100. J. A. Dean and W. J. Carnes, Anal. Chem. 34, 192 (1962).

101. A. Hell, W. F. Ulrich, N. Shifrin, and J. Ramirez-Munoz, Appl. Optics 7, 1317 (1968).

102. A. A. Venghiattis, Appl. Optics 7, 1313 (1968).

103. C. Veillon and M. Margoshes, Spectrochim. Acta 23B, 553 (1968).

104. J. B. Willis, Spectrochim. Acta. 23A, 811 (1967).

105. C. Veillon and M. Margoshes, Spectrochim. Acta 23B, 503 (1968).

106. G. C. Dickinson and V. A. Fassel, Anal. Chem. 41, 1021 (1969).

107. P. W. J. M. Boumans and F. J. DeBoer, Spectrochim. Acta 27B, 391 (1972).

108. H. Kawaguchi, M. Hasegawa, and A. Mizuike, Spectrochim. Acta 27B, 205 (1972).

109. M. Marinkovic and T. J. Vickers, Appl. Spectrosc. 25, 319 (1971).

110. J. W. Robinson, Anal. Chim. Acta 27, 465 (1962).

111. A. Stasheim and H. G. C. Human, Spectrochim. Acta 23B, 265 (1968).

112. D. W. Steinhaus, H. M. Crosswhite, and G. H. Dieke, Spectrochim. Acta 5, 436 (1953).

113. A. Shuster and G. Hemsaleck, Trans. Roy. Soc. 193, 189 (1900).

114. W. L. Dutton, Appl. Spectrosc. 5, 1 (1950).

115. F. Harrington; L. Bovey and A. H. Gabriel, Spectrochim. Acta 18, 631 (1962); Report of a meeting held by the Spectroscopy Group and the Manchester and District Branch of the Institute of Physics and the Physical Society at Manchester on June 16, 1961.

116. J. W. Beams, J. Opt. Soc. Am. 13, 597 (1926).

117. P. A. Kendall, Appl. Spectrosc. 22, 274 (1968).

118. A. Bardóczy, Appl. Spectrosc. 21, 100 (1967).

119. A. Bardóczy and F. Varsányi, Nature 177, 222 (1956).

120. A. Bardóczy, Appl. Spectrosc. 4, 167 (1957).

121. J. P. Walters, Anal. Chem. 40, 1540 (1968).

122. R. D. Sachs and J. P. Walters, Anal. Chem. 42, 61 (1970).

123. J. P. Walters, Appl. Spectrosc. 26, 17 (1972).

124. H. N. Olsen and W. S. Huxford, Phys. Rev. 87, 922 (1952).

125. Tsui-Fanh, C. M. Crandall, and J. D. Craggs, Spectrochim. Acta. 5, 452 (1953).

126. J. P. Walters, Appl. Spectrosc. 26, 323 (1972).

127. H. M. Crosswhite, D. W. Steinhaus, and G. H. Dieke, J. Opt. Soc. Am. 41, 299 (1951).

128. W. W. Schroeder; See reference 113.

129. D. W. Steinhaus, H. M. Crosswhite, and G. H. Dieke, J. Opt. Soc. Am. 43, 257 (1953).

130. J. P. Walters, Appl. Spectrosc. 23, 317 (1969).

131. J. P. Walters, Anal. Chem. 39, 771 (1967).

132. H. van der Piepen and W. W. Schroeder, Spectrochim. Acta 26B, 471 (1971).

133. W. W. Schroeder, J. J. van Niekerk, L. Dicks, A. Strasheim, and H. van der Piepen, Spectrochim. Acta 26B, 331 (1971).

134. R. H. Scott and A. Strasheim, Spectrochim. Acta 26B, 707 (1971).

135. A. Strasheim and F. Blum, Spectrochim. Acta 26B, 685 (1971).

136. G. H. Morrison and A. T. Kashuba, Anal. Chem. 41, 1842 (1969).

137. G. H. Morrison and A. M. Rothenberg, Anal. Chem. 44, 515 (1972).

138. B. N. Colby and G. H. Morrison, Anal. Chem. 44, 1263 (1972).

139. J. J. Jones, R. L. Dahlquist, and R. E. Hoyt, Appl. Spectrosc. 25, 628 (1971).

140. R. K. Winge, V. A. Fassel, R. N. Kniseley, Appl. Spectrosc. 25, 636 (1971).

141. G. Andermann and J. W. Kemp, ASTM Special Technical Publication #259 (American Society for Testing and Materials, Philadelphia, 1959).

142. B. F. Scribner, Pure Appl. Chem. 10, 579 (1965).

143. S. Nakiyama and Y. Tanasawa, Trans. Soc. Mech. Eng. Japan 5, 62 (1939).

144. E. D. Glass, Personal Communication (1973).

145. H. V. Malmstadt and C. G. Enke, "Digital Electronics for Scientists" (Benjamin, New York, 1969).

146. U. Farinelli and R. Malvano, Rev. Sci. Instr. 29, 699 (1958).

147. C. F. Hendee and W. B. Brown, Philips Tech. Rev. 19, 50 (1957).

148. G. H. Dieke and H. M. Crosswhite, J. Quant. Spectry. Radiative Transfer 2, 97 (1962).

149. H. R. Griem, "Plasma Spectroscopy" (McGraw-Hill, New York, 1964).

150. A. C. Kolb and H. R. Griem, Phys. Rev. 111, 514 (1958).

151. P. W. J. M. Boumans, "Theory of Spectrochemical Excitation" (Plenum Press, New York, 1966).

152. A. Unsöld, Ann. Physik. 33, 607 (1938).

153. J. D. Craggs and J. M. Meek, Proc. Roy. Soc. A186, 241 (1946).

154. I. Reif, V. A. Fassel, and R. N. Kniseley, Spectrochim. Acta 28B, 105 (1973).

155. C. F. Knopp, C. F. Gottschlich, and A. B. Cambel, J. Quant. Spectry. Radiative Transfer 2, 297 (1962).

156. R. H. Tourin, J. Quant. Spectry. Radiative Transfer 3, 89 (1963).

157. B. D. Adcock and W. E. G. Plumtree, J. Quant. Spectry. Radiative Transfer 4, 29 (1964).

158. B. S. Malone and W. H. Corcoran, J. Quant. Spectry. Radiative Transfer 6, 443 (1966).

159. H. E. Taylor, J. H. Gibson, and R. K. Skogerboe, Anal. Chem. 42, 1569 (1970).

160. K. Fallgatter, V. Svoboda, and J. D. Winefordner, Appl. Spectrosc. 25, 347 (1971).

161. P. W. J. M. Boumans, "Analytical Emission Spectroscopy," Part II, ed. E. L. Grove (Mercel Decker, New York, 1972).

162. A. N. Zaidel', V. K. Prokof'ev, S. M. Raiskii, V. A. Slavnyi, and E. Ya. Shreider, "Tables of Spectral Lines" (IFI/Plenum, New York, 1970).

163. R. Mavrodineau, "Flame Spectroscopy" (Wiley, New York, 1965).

164. T. J. Vickers and J. D. Winefordner, "Analytical Emission Spectroscopy," Part II, Ed. E. L. Grove (Mercel Decker, New York, 1972).

165. E. E. Bevege and R. E. Gallion, Appl. Spectrosc. 21, 20 (1967).

166. Detection Limits for Model AA-6 Atomic Absorption Spectrophotometer, Varian Techtron Palo Alto,Calif. (1973).

167. A. Syty and J. A. Dean, Appl. Optics 7, 1331 (1968).

168. R. M. Dagnall, G. F. Kirkbright, T. S. West, and R. Wood, Anal. Chim. Acta 47, 407 (1969).

169. S. Murayama, H. Matsuno, and M. Yamamoto, Spectrochim. Acta 23B, 513 (1968).

170. E. F. Bulewicz and P. J. Padley, Spectrochim. Acta 28B, 125 (1973).

171. D. C. Manning and L. Capacho-Delgato, Anal. Chim. Acta 36, 312 (1966).

172. J. A. Bowman and J. B. Willis, Anal. Chem. 39, 1210 (1967).

173. H. D. Fleming, Spectrochim. Acta 23B, 207 (1967).

174. G. R. Kornblum and L. deGalan, Spectrochim. Acta 28B, 139 (1973).

175. T. Maruta, T. Takeuchi, and M. Suzuki, Anal. Chim. Acta 58, 452 (1972).

176. K. Kitagawa and T. Takeuchi, Anal. Chim. Acta 60, 309 (1972).

177. R. M. Dagnall, G. F. Kirkbright, T. S. West, and R. Wood, Anal. Chem. 43, 1765 (1971).

178. J. Spitz and G. Uny, Appl. Optics 7, 1345 (1968).

179. E. D. Glass, J. Zynger, and S. R. Crouch, Current Research (1973).

180. A. J. McCormack, S. C. Tong, and W. D. Cooke, Anal. Chem. 37, 1470 (1965).

181. R. K. Lantz, J. Zynger, and S. R. Crouch, Current Research (1973).

182. J. Zynger and S. R. Crouch, In Preparation (1973).

APPENDIX

TIME-RESOLVED SPECTRA OBTAINED AT A SPARK GAP OF 2.5 mm AND AT VARIOUS TIMES AFTER BREAKDOWN

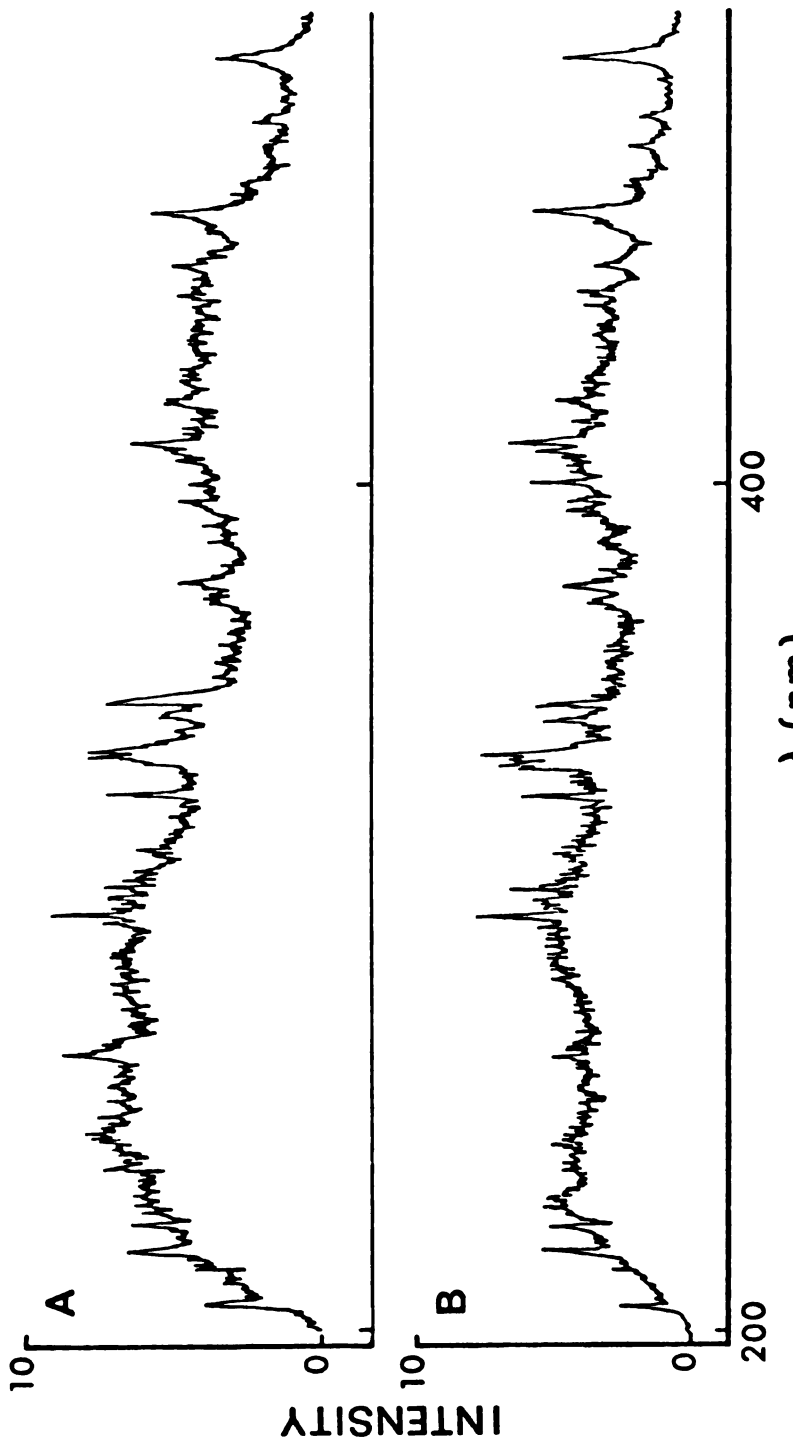

Figure A1. Post breakdown time-resolved spectra in air taken at 10 nsec (spectrum A) and 20 nsec (spectrum B) after t_m.

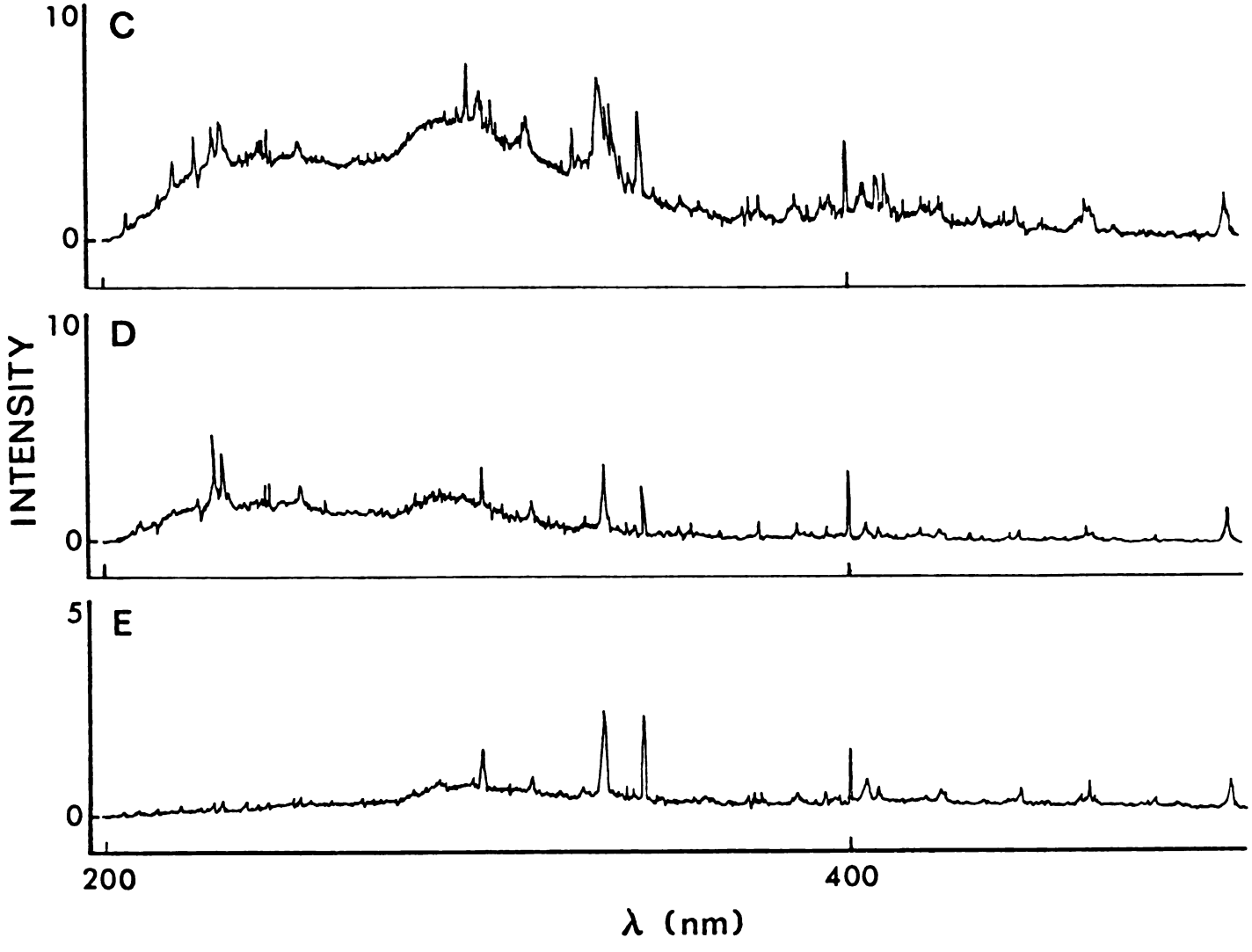

Figure A2. Post breakdown time-resolved spectra in air taken at 40 nsec (spectrum C), 80 nsec (spectrum D) and 120 nsec (spectrum E) after t_m.

VITA

Jacob Zynger was born on November 1, 1948 in Hofgeismer, Germany and he lived there until 1954. He then immigrated with his family, in 1954, to the United States and settled in Brooklyn, New York.

He attended George W. Wingate High School, and was awarded a New York State Regents Scholarship when he entered Brooklyn College of The City University of New York. He received his B.S. degree, with a major in chemistry, in June, 1969. In September of 1969 he entered Michigan State University and studied analytical chemistry under the direction of Dr. Stanley R. Crouch. He will receive his Ph.D. in chemistry, and will be commencing employment as a research analytical chemist with Eli Lilly and Co. in Indianapolis, Indiana in October of 1973.

He is a member of the American Chemical Society and the Society for Applied Spectroscopy.